Conceptual Design of Nuclear-Geothermal Energy Storage Systems for Variable Electricity Production
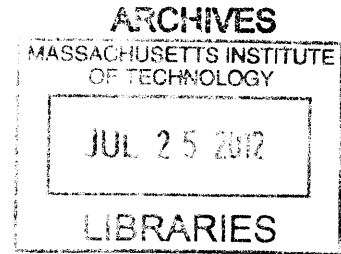
By

Youho Lee

B.S, Nuclear and Quantum Engineering (2009)

Korea Advanced Institute of Science and Technology

SUBMITTED TO THE DEPARTMENT OF NUCLEAR SCIENCE
AND ENGINEERING
IN PARTIAL FULFILLMENT OF THE REQUIREMENTS FOR THE DEGREE OF

MASTER OF SCIENCE IN NUCLEAR SCIENCE AND ENGINEERING
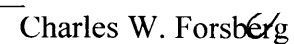AT THE
MASSACHUSETTS INSTITUTE OF TECHNOLOGY

JUNE 2011

Author _____

Youho Lee
Department of Nuclear Science and Engineering
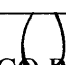2011.5.13

Certified by _____

Charles W. Forsberg
Professor of Nuclear Science and Engineering
Thesis Supervisor

Certified by _____

Michael J. Driscoll
Professor Emeritus of Nuclear Science and Engineering
Thesis Reader

Accepted by _____

Mujid S. Kazimi
TEPCO Professor of Nuclear Engineering
Chair, Department Committee on Graduate Students

ACKNOWLEDGEMENTS

I would like to thank my advisor, Prof. Forsberg, for his guidance and support throughout this study. His creative ideas and initiatives have inspired my learning at MIT. I feel very fortunate to have had a chance to work with Prof. Driscoll who has greatly supported and helped this study. From him, I learned attitudes for lifelong learning. I appreciate Dr. Bernard of the MIT Reactor for giving me valuable advice and help for my graduate studies in general. I am also grateful for my undergraduate advisor Prof. Hee Cheon No, Prof. Jeong Ik Lee and Dr. Sung Joong Kim for giving me advice to successfully make a transition from my undergraduate studies in Korea to graduate studies in the USA. Although I cannot list the names of everyone who helped my studies in this limited space, I do remember and appreciate every single help and advice I have received.

I would like to thank my parents for their unconditional love and support throughout my life. No amount of success in my life would be possible if not for them. Finally, I thank God for becoming the meaning of my academic endeavor.

TABLE OF CONTENTS

List of Figures

List of Tables

Nomenclature

Abbreviations

BWR   Boiling Water Reactor

CFD   Computational Fluid Dynamics

EC   Energy Conversion

EGS   Enhanced Geothermal System

HTR   High Temperature Reactor

LWR   Light Water Reactor

MIT   Massachusetts Institute of Technology

NE   New England

PWR   Pressurized Water Reactor

ISO   Independent System Operator

Engineering Terms

L, Length [m]

t, Time [sec]

k, Thermal conductivity [w/m °C]

T, Temperature [°C or K]

A, Area [m]

$\dot{m}$, Mass flow rate [kg/sec]

η, Efficiency [-]

v, Fluid velocity [m/sec]

P, Pressure [Pa]

μ, Viscosity [Pa.s]

d, Diameter [m]

D, Burial depth [m]

ψ, Fractional Energy Loss [-]

V, Volume [m^3]

M, Mass [kg]

Bi, Biot number [-]

K, Permeability [Darcy[1]]

H, Enthalpy [J/kg]

C_p, Specific heat [J/kg°C]

h, Heat transfer coefficient [w/m^2 °C]

u, Thermal front velocity [m/sec]

ΔP, Pressure drop [Pa]

α, Thermal diffusivity [m^2/sec]

R, Radius [m]

E, Energy [J]

τ, Cycle time [sec]

---

[1] 1Darcy =9.869233E-13 m^2

Δt, time interval [sec]

Economic Terms[2]

L, Plant Capacity [-]

τ, Tax Fraction [-]

r_s, Rate of Return on Equity [-]

$\left(\frac{I}{K}\right)_{-c}$ Overnight Specfic Captial Cost of Plant [$/kW]

c Time required to construct plant [year]

$\left(\frac{O}{K}\right)_{0}$ Specific Operating and Maintenance Cost as of Start of Operation [$/kW/Year]

f_0 Fossil Fuel Cost [$/mmBTU]

φ, Annual Fixed Charge Rate [1/year]

r_b, Rate of Return on Bonds [-]

b, Debt Fraction [-]

y Annual Rate of Monetary Inflation [1/year]

T Prescribed useful life of plant [year]

Subscript [3]

c characteristic

f fluid

∞ bulk

surr surrounding

avg average

mag magnitude

ref reference

in inlet

s sold, or surface[4]

sup superficial

res reservoir

hyd hydraulic static

eff effective

Superscript

- average

$\rightarrow$ vector

---

[2] Distinctions be made with the engineering terms. The economic terms restrictively appear in Chapter 5.
[3] Subscripts for a complete word are not listed here
[4] Distinctions be made based on contents

CHAPTER 1
INTRODUCTION

1.1 Implications of Electricity Storage

The need for energy storage is ubiquitous. Spanning from a small battery in a cell phone to a gigantic dam, energy storage technologies vary as much in their size as their applicability. Nevertheless, electricity storage technologies have one thing in common: potential for significant environmental, economic and energy diversity benefits. In general, the benefits of energy storage can be specifically divided into the following four categories: matching electricity supply to load demand, providing backup power to prevent outages, enabling renewable technologies, and power quality control.

Among the benefits listed above, the most significant one would be matching electricity supply to load demand. Consumer demand for power varies throughout the day as well as seasonally as illustrated in Fig.1-1 for the New England (NE) electricity grid [1]. As will be seen, coping with the seasonal variation is the principal focus of the present work.
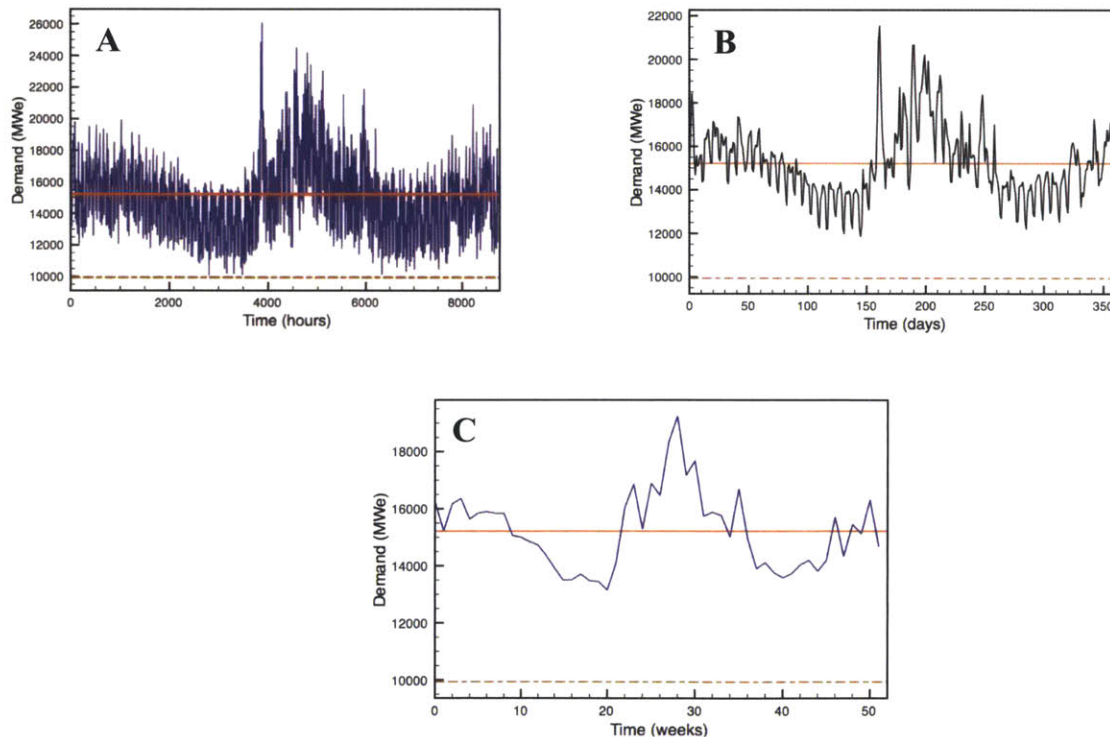
Fig.1-1 New England Electricity Demand Variation: A: Hourly B: Daily C: Weekly (Seasonal)

However, many power plants have limited ability to make rapid changes in their outputs in response to such demand fluctuations. The cost to construct and maintain the additional power plants solely for the purpose of meeting peak demand is high as they sit idle during times of low electricity demand. Hence, a well-designed storage system can improve the overall economics of the generating system by filling in demand valleys and shaving demand peaks using existing power plants more efficiently [2].

In addition, energy storage technologies can provide an environmentally advantageous method of responding to daily fluctuations in demand. Fossil fuel electricity generating power plants are used today to match electricity generation with variable electricity demand. Storing fossil fuels is easy and inexpensive. The capital costs of fossil fuel and gas turbine plants are relatively low; thus, there are not large economic penalties if the plants operate at partial capacity. However, the costs of fossil fuels and concerns about climate change may restrict this use of fossil fuels. The other electricity generating technologies (nuclear, solar, wind, fossil combustion with carbon sequestration) have high capital costs and low operating costs. These characteristics are not suitable for varying electricity production to match demand because total cost remains almost independent of power level [3]. Thus, as long as the storage system is not charged by energy generated from fossil fuel, electricity demand of a grid would be satisfied with lower carbon emissions through the increased use of carbon-free power technologies.

Among the future capital intensive power technologies that emit no carbon dioxide, nuclear energy is the only technology that is deployed on a large scale today. A number of countries are reaching the point at which nuclear reactors operate at part load during the night, weekend and seasonally. For those countries having excess nuclear capacity beyond base load, efficient utilization of nuclear energy during the time when electricity production exceeds demand, is of prime interest. An efficient storage system that can effectively store excess energy at times of low electrical demand will accelerate the deployment of nuclear power reactors and enable nuclear reactors to economically meet intermediate and peak electricity demands.

1.2 Current Status of Energy Storage & Need for Seasonal Storage

Currently the following six energy storage technologies are regarded promising [2]: pumped hydropower, compressed air energy storage, batteries, flywheels, superconducting magnetic energy storage, and electrochemical capacitors. Only pumped hydropower is deployed on a significant scale. The technologies are able to meet the daily or weekly swings in electricity demand as well as the other requirements such as power quality control etc, but do not address the seasonal variations in electricity demand, which

requires storing large amounts of energy. Fig.1-2 summarizes system power rating and discharge time for each of the technologies listed above [2].
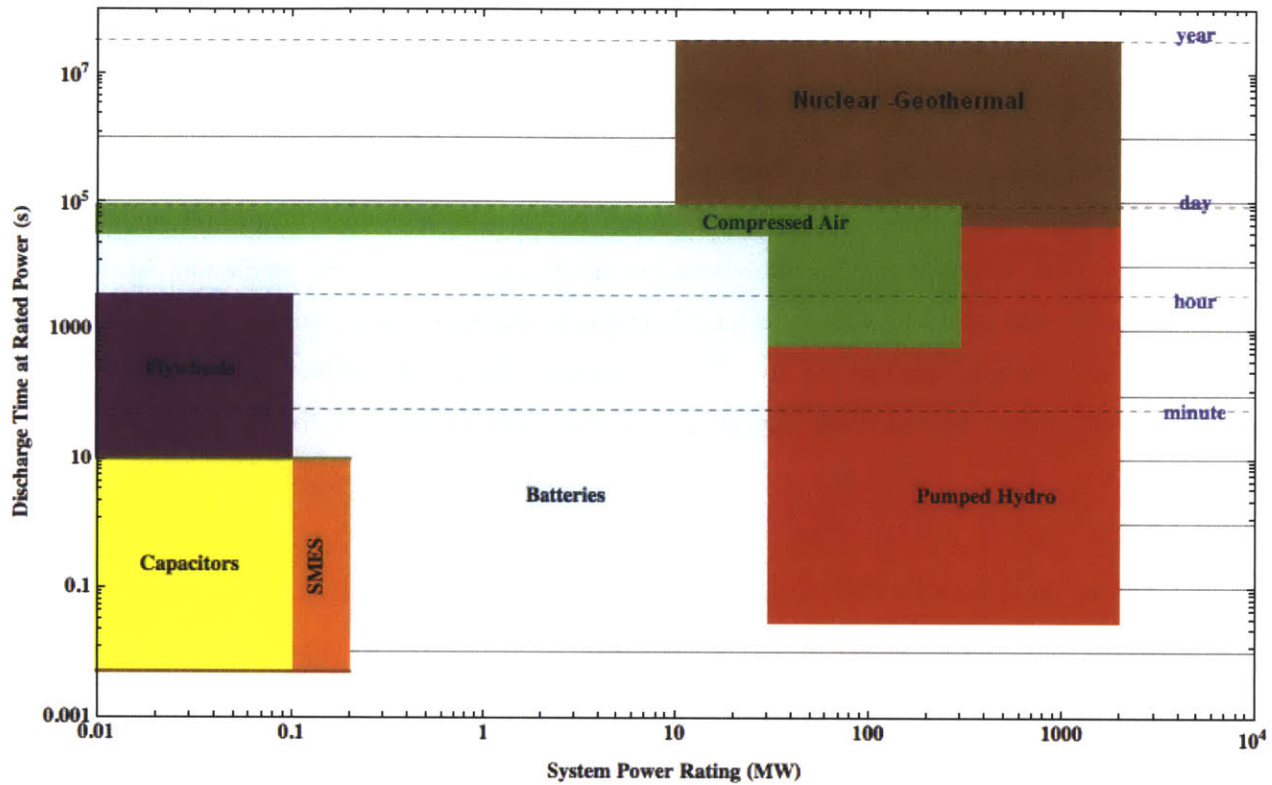
Fig.1-2 Capabilities of Energy Storage Technologies (adapted from ref [4])[5]

As indicated in Fig.1-2, the current energy storage technologies are unable to address the seasonal variations in electricity demand as their discharge time does not exceed a day. This is because their storage capacity is orders of magnitude less than what is required for seasonal storage.

1.3 Objective of the Thesis

In this study, we propose and assess a novel electricity storage option: the "Nuclear-Geothermal Energy Storage System". If the nuclear geothermal energy storage system is shown to be practical, it adds a factor of 100 to the vertical axis of Fig.1-2. That is a different world, where we divide storage into three categories--short term stabilization, daily (including smart grid), and seasonal. The scale of nuclear reactors and the scale of the storage requirements implies storage facilities of a GW(th)-year each.

---

[5] Reference 4 was modified to include the nuclear-geothermal area

1.4 Organization of the Thesis

The chapters which comprise this thesis address relevant topics in the following sequence.

1.4.1 Chapter 2: The Concept of a Nuclear-EGS [6]Storage System

This research proposes a new electricity storage concept. The concept is introduced from the viewpoints of engineering and economics, respectively. Engineering concepts-including integration of existing technologies, system interface and operation-are proposed, along with system operation, to achieve economic benefits. The research explores technical options for nuclear-geothermal systems –i.e. the types of individual technologies one can use to achieve a feasible nuclear-geothermal system. The options include types of geology, heating fluids, power cycle, underground fracturing methods, reservoir size and system operation.

1.4.2 Chapter 3: Nuclear-EGS System Models

With the options identified, relevant modeling of a nuclear-EGS system was conducted as an essential prerequisite to conduct a design study. Results of reservoir engineering studies reveal such essential findings as storage size, transient temperature distribution, heat loss, water leakage and pressure drops. Analysis was then done to understand coupling of the nuclear power plant-heat storage-geothermal power plant with power cycle studies and reveal operational characteristics (efficiency, operating conditions, etc.) of the system as a whole.

1.4.3 Chapter 4: Design of Nuclear EGS System

The individual models from Chapter 3 were considered to identify a possible design space for nuclear-EGS system in terms of design parameters to meet design constraints. Performance metrics of nuclear-EGS system are evaluated and trade-offs between important performance metrics are assessed.

---

[6] EGS stands for Enhanced Geothermal Energy System

1.4.4 Chapter 5: Economic Analysis of Nuclear-EGS System

Economics of the nuclear-geothermal system is addressed based on a sinusoidal approximation to the seasonal demand curve. Electricity cost of nuclear-geothermal is calculated and the effects of the deployment of the system are studied in the context of overall economics of a grid. The economics study not only addresses the feasibility of a nuclear-geothermal system, but also provides directions for the system design in the context of its competitiveness compared to its alternatives. Engineering analysis is combined with economics analysis. The overall system design is addressed for possible system design candidates. In addition, general nuclear-geothermal system design guidelines are proposed. The thesis concludes with a brief summary of findings and recommendations in chapter 6. Appendices to the main report document details in support of the above analysis.

CHAPTER 2

The Concept of a Nuclear-Enhanced Geothermal Power Plant (EGS) Storage System

2.1 Introduction

This chapter is dedicated to introduction of the novel nuclear-geothermal energy storage concept and relevant technical issues. The concept of the system is addressed from the viewpoints of engineering and economics, respectively. Technical options for nuclear-geothermal systems are explored. Qualitative examinations of the identified options scope out the most promising technical features. Reference nuclear geothermal energy system is developed and is further analyzed in the following chapters.

2.2 The System Concept

2.2.1 Engineering Concept: Coupling Between Nuclear Power Plant-Reservoir-Geothermal Power Plant

It is proposed [2] to couple nuclear reactors to thermal heat storage to meet variable electricity demand. The system has two components.

1. A large volume of underground rock is heated with hot water (or steam or carbon dioxide) from a nuclear power plant during periods of low power demand (spring and fall for seasonal storage). A manmade geothermal gigawatt-year heat source is created.

2. The heat is extracted during times of high power demand. The man-made geothermal heat source is used to produce peak electricity-daily, weekly, and seasonally. This uses available geothermal power technology.

When used for seasonal demand, the nuclear plants would input up to 4000MW(th) for 3 months in the spring and fall to store 1Gw(th)-year of energy to meet winter and summer peak power demands. Actual thermal input and output would vary as determined by availability of excess heat or the need for peak electricity. The concept of the nuclear-geothermal system is illustrated in Fig.2-1.

Nuclear-Geothermal System

Thermal Input to Rock

Thermal Output From Rock

Cap Rock

Permeable Rock

Nuclear Plant

Fluid Return

Fluid Input

Nesjavellir Geothermal power plant, Iceland.
120MW(e), Wikimedia Commons (2010)
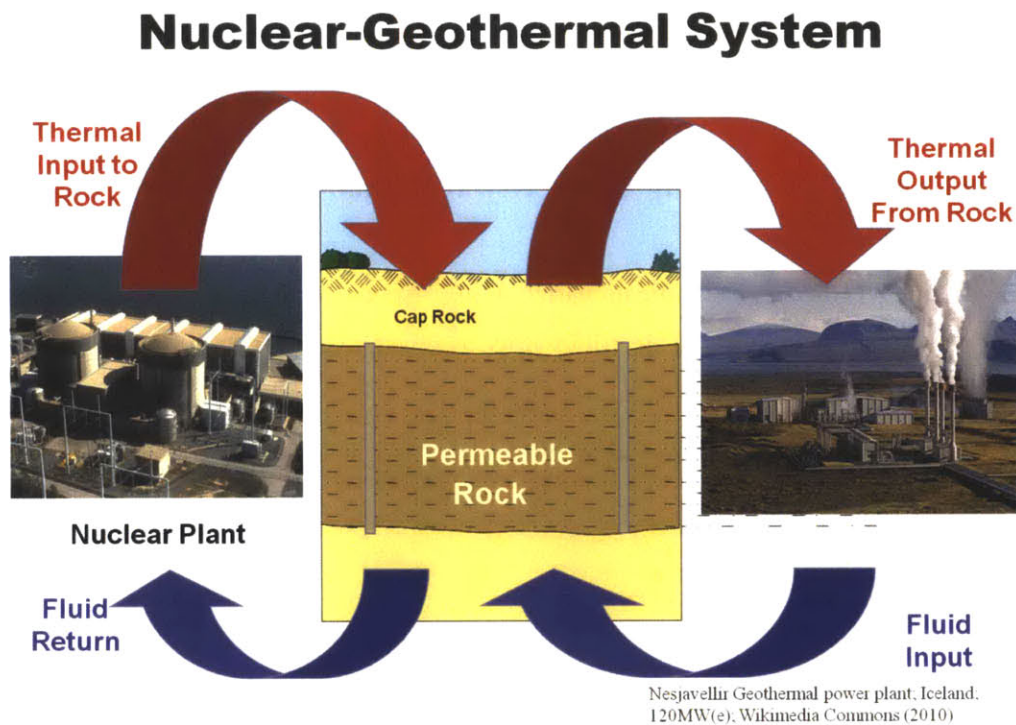
Fig.2-1 Conceptual Diagram of Nuclear-Geothermal Energy Storage System

Each geological storage site is linked to a reactor site that may contain multiple nuclear and geothermal power plants. Considering the fact that each nuclear reactor produces about a gigawatt of electrical power (3gigawatts of thermal power) and electricity demand varies between seasons, a reasonable energy storage capacity to meet seasonal variations in electricity demand with the nuclear-geothermal storage is on the order of a gigawatt (thermal)-year [2].

Since rock cannot be insulated, conductive heat losses depend upon the surface area of the hot zone. The larger the system size, the smaller the surface-to-volume ratio of the storage system. This implies that

fractional heat losses are smaller with a large system, as the surface area (heat loss) of the storage rock increases as the square of the system, while the storage volume (heat capacity) increases as the cube of the system size. Thus, the nuclear geothermal storage system intrinsically works only on a large scale – a characteristic that matches this storage technology with nuclear plants and seasonal storage. In order to limit the heat loss mechanism to conduction, the underground rock may be need to be sealed to minimize convective heat losses due to fluid flow through the geology beyond the boundary of the storage system.

It is worth noting that heat storage avoids the energy inefficiencies in transforming electricity to some other storage media (batteries, hydrogen, etc) and back to electricity. The cost of heat is about a third the cost of electricity and thus heat losses result in a smaller economic impact on storage costs.

2.2.2 Economics Concept – Selling Electricity at Higher Peak Power Prices

As discussed in chapter 1, there is a significant variation in seasonal electricity demand. Such a variation in electricity demand leads to changes in electricity price as illustrated in Fig.2-4 [5].
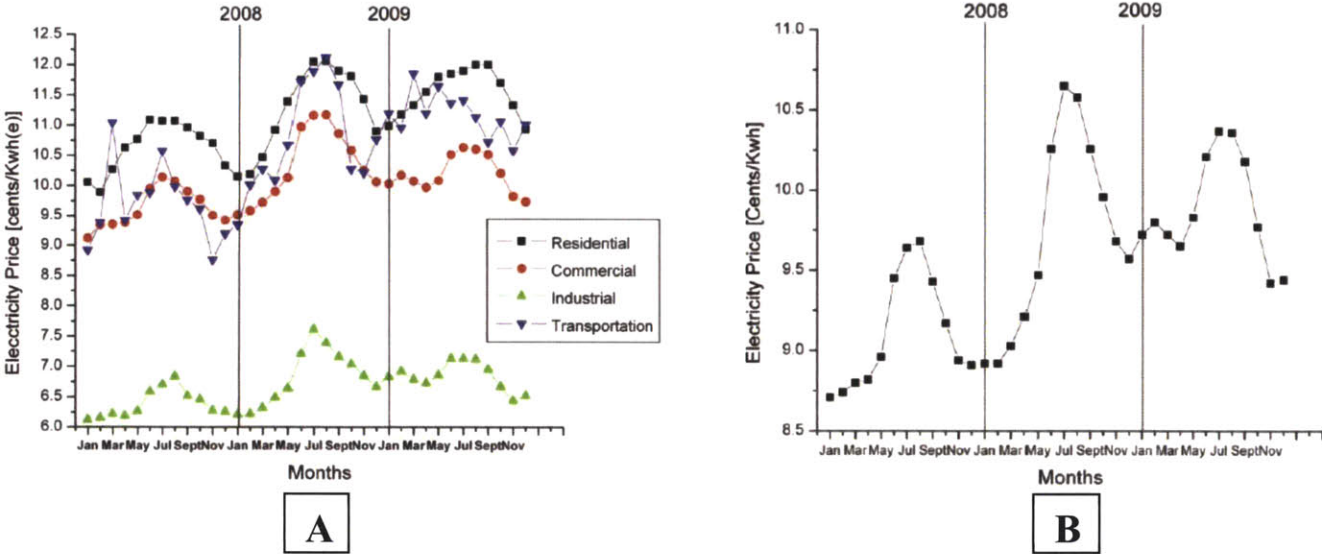
Fig. 2-2 Average Monthly Retail Price of Electricity in the USA, 2007 through 2009
(A: Different Sectors, B: All Sectors Averaged)

Such an electricity price difference between peak power electricity and off-peak power electricity is the economic basis of deployment of the nuclear geothermal system: Store energy when price is low, sell

energy when the price is high. It is important to note that the hourly electricity variation, which is not shown in Fig.2-2, is much more significant because its degree of demand fluctuation is greater and time to cope with such fluctuations is much shorter. Hence a well-planned strategy of seasonal storage – charging at low-price hours during low-price seasons, selling at high-price hours during high price seasons – could take advantage of both hourly and seasonal variations in electricity prices, ultimately leading to justifying the deployment of nuclear-geothermal energy storage systems.

However, basing the economic analysis of the nuclear-geothermal system on the retail price of peak electricity is not appropriate although it helps understand the economic incentive for the deployment of the system. This is because the retail price of electricity is a figure that is determined after taking into account regulations, pricing policy etc. In other words, the instantaneous retail price of electricity is a somewhat skewed or opaque reflection of actual instantaneous electricity demand. Thus, when quantifying economic effects upon the introduction of such a system in a grid, it is recommended to assess changes in electricity generation costs to meet variable electricity demand– not selling price. Hence in this study, economic studies are performed based on quantifying electricity cost.

2.3 Technical Options and Targets

2.3.1 Nuclear Power Plants

The key feature of the nuclear-geothermal electricity storage system is operating a reactor with a constant power output while variably using the power for either producing electricity or storing heat in the underground rock- or possibly doing both. A heat exchanger is needed between the nuclear plant and the fluids used to heat the rock to avoid contamination from the dirt and dissolved materials associated with the rock heat storage system. Due to the possible loss of working fluids underground, an auxiliary make-up fluid line is needed. Such technology is established in the heat mining (geothermal) industry where the same concerns arise.

The choice of the reactor determines the types of fluids to be used. The heat transfer fluid to heat the rock and extract the energy should satisfy three criteria: stability at high temperatures, economy, and chemical compatibility with conditions under the ground.

Many of the individual technologies required for the nuclear-geothermal heat storage system are well established in other industries. The heat transfer fluid options at low temperatures are water and steam. The high-temperature heat transfer option is carbon dioxide. The dividing point is near 300°C—slightly

25

above LWR steam temperatures. Above this temperature there is significant dissolution of silica in hot water with subsequent precipitation of silica when the water is cooled.

LWRs are a commercial technology available today to produce steam or hot water. Injecting steam into underground rock is well established in the petroleum industry, where increasing the rock temperature reduces the viscosity of heavy oil and increases oil recovery. Injecting water underground is practiced in typical hydrothermal and Enhanced-Geothermal-Power plant (EGS) reservoirs as cold water is added to replace hot water that is withdrawn. For nuclear-EGS, using water eliminates some reservoir design complexity. This is because burial depth of the reservoir does not affect hydrodynamics when water is used as long as it is below a certain depth to avoid flashing. This is because water properties are a weak function of pressure. Hence, reservoir depth determination can be practically decoupled with reservoir design.

As opposed to water, use of steam adds complexity in the reservoir design. Heat transfer occurs through condensation when steam is used, meaning that two phase heat transfer, which is far more complex than that of single phase, is involved. Also, reservoir depth determination is more strongly coupled with reservoir design, as depth of reservoir hence pressure significantly affects the velocity of steam due to the compressibility of steam. In addition, steam will induce a greater pressure drop than water because of its faster velocity at the same mass flow rate. Most importantly, such reasons have ruled against use of steam in current hydrothermal or EGS reservoirs. In reality, although we have experience in injecting steam underground in the petroleum industry, we have a very limited experience in circulating steam with the sole purpose of efficient heat transfer underground. Hence, at this point it is concluded that the use of pressurized water in the charging process is more advantageous and justifiable than the use of steam when LWRs are coupled with a reservoir.

High temperature reactors or sodium cooled fast reactors could heat carbon dioxide to high temperature. Carbon dioxide is also injected into some types of oil formations to increase oil recovery and is being injected in a few locations as a method to sequester carbon dioxide. Carbon dioxide appears to have substantial advantages over steam and water at higher temperatures, with better chemical compatibility with most types of geology. Currently studies are being made at the use carbon dioxide as a geo-fluid instead of water in EGS [6]. However, the required high-temperature reactor technology is not yet a commercial technology.

The following table summarizes the nuclear reactor options and the charging fluids

Table 2-1 Summary of Nuclear Reactor Options and Charging Fluids for Nuclear Power Plant-Reservoir Coupling

	Water	Steam	Carbon dioxide
Reactor Type	LWRs	LWRs	SFR, HTR[7]
Temperature	T<300°C	T<300°C	T>300°C
Chemical Compatibility	Moderate	Moderate	Good
System Complexity	Low	Medium	High
Technical Maturity	High	Medium	Low

It appears that modifying existing LWRs to make them suitable for the nuclear-geothermal energy storage system has no serious technical challenges. Sodium fast reactors or high temperature reactors may be able to provide high temperature carbon dioxide for a nuclear geothermal system. However, those advanced nuclear reactors are still under development. Also, it is expected that the near-term deployment of the system, if it is found to be practical, would come with the system coupled with LWRs as long as there is no critical limitation associated with LWRs in the context of integration of the nuclear-geothermal system. In addition, feasibility of the system can be most accurately determined only if we use the known technologies - LWRs. Hence, quantitative analysis of this study consistently assumes the use of LWRs in the system, while qualitatively addressing the broad scope of potential alternative technology options and any possible changes of the system subsequent to introduction.

Looking at the heat injection process using an LWR more in detail, there are two ways we can charge heat to the reservoir, as illustrated in Fig.2-3:

Option A: Using a bypass flow line in the primary hot leg of a LWR to heat up the geo-fluid that is to be injected into a reservoir. The bypass water flows through an intermediate heat exchanger, transferring heat to the geo-fluid of the reservoir, returning to the reactor through the primary cold leg.

Option B: The geofluid is heated in a series of heat exchangers with steam at different temperatures that has been withdrawn from the turbine at different locations. The heating is similar to preheating of feed waters for the steam generator.

---

[7] SFR and HTR stand for Sodium Fast Reactor and High Temperature Reactor, respectively.
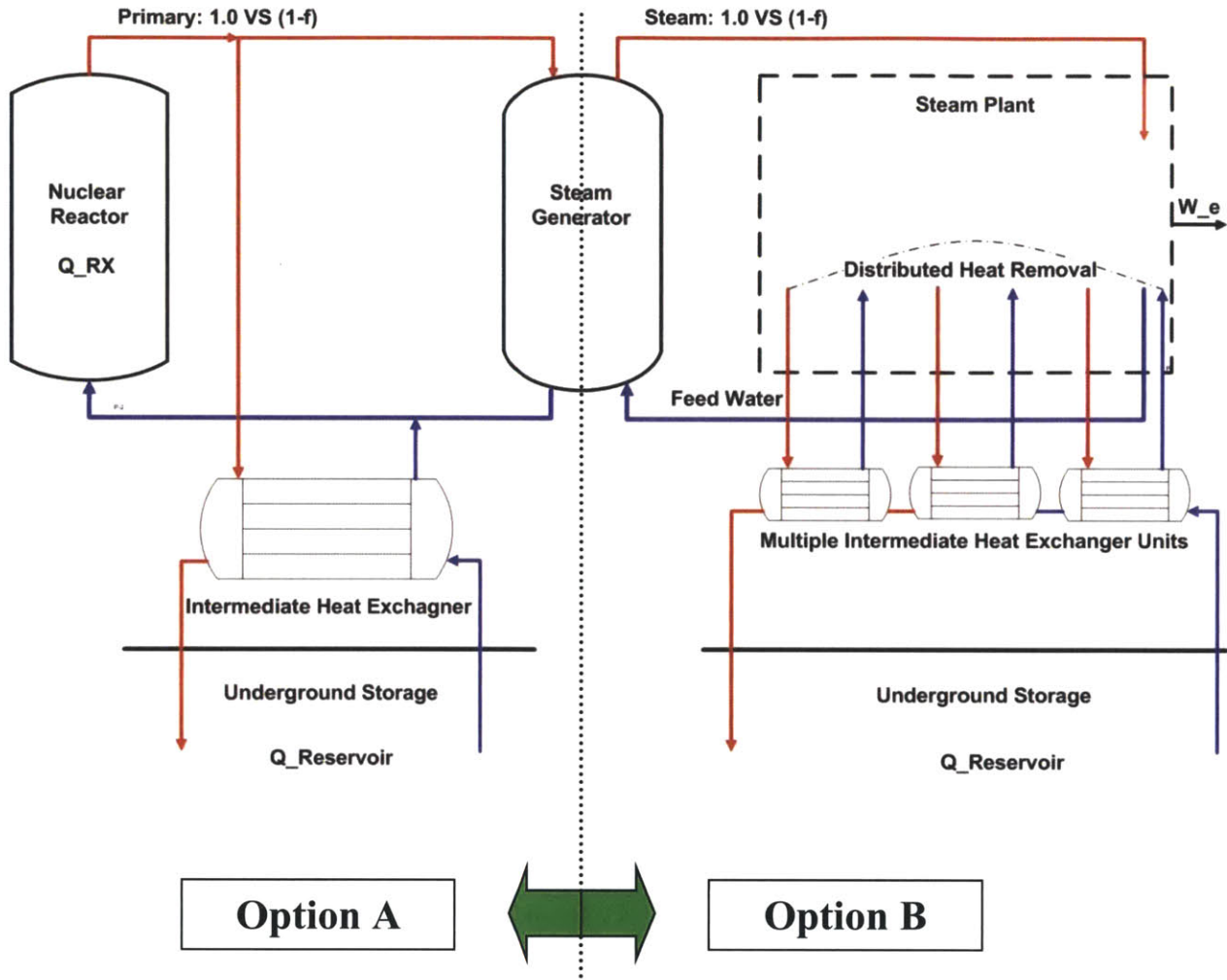
Fig.2-3 Two Different Charging Options for a LWR (PWR)

(*Q_RX, Q_Reservoir, W_e are reactor power, charging power of reservoir, and turbine work, respectively.)

Option A is simple and easy. Also, it can be an efficient way of heating if wants to heat fluid over small temperature range – say 250°C to 300°C- near the reactor temperature. However, if there is a large temperature drop across the heat exchanger with entropy rises, the heat exchange becomes inefficient. Option B is essentially feed water heating system, which is complex and expensive. However, it is a very efficient way of heating if wants to heat water from 50°C to 300°C. Hence, there is a trade-off of high capital cost versus thermodynamic efficiency between the two options.

In a BWR, the intermediate heat exchanger will be a condenser of primary steam. Other than that, the basic coupling scheme would be identical with the option A of the PWR case. The following table summarizes representative temperatures for a typical PWR and BWR [7]:

Table 2-2 Summaries of Representative Temperatures for a PWR and BWR

	PWR[8]	BWR[9]
Outlet temperature	324°C	288°C
Inlet temperature	286°C	278°C
Turbine steam saturation conditions	272.3°C	287.5°C

As shown in Table 2-2, a PWR can heat geofluid temperature higher than a BWR can. Nevertheless, they are more or less the same in the context of operation when coupled with a reservoir.

In sum, the use of water as a geo-fluid during the charging process with thermal withdrawal from the LWR primary side is the most promising option among a number of other technical options in coupling nuclear reactors with a reservoir.

2.3.2 Geothermal Power Plants

Geothermal electric power and heat production from hydrothermal resources has been commercialized since 1904, leading to a large body of experience on what constitutes a good hot water resource. In terms of thermal energy, a kilogram of hot water at temperatures of 150°C to 300°C has a low energy content compared to a kilogram of hydrocarbon liquid. This occurs because only the sensible and latent enthalpy of the geo-fluid can be used, rather than the stored chemical energy released during combustion of a hydrocarbon fuel. Therefore, for a producing geothermal well to be comparable in energy content to an oil well, high mass flow rates of hot water are needed. Typically, 50 to 150 kg/s or more per production well, depending on its temperature, are required to make a geothermal project economical [6].

Hydrothermal projects are based on resources with naturally high well productivity and high temperatures. They rely on having high flow per well to compensate for the capital cost of drilling and completing the system at depth, and they need very high permeability to meet required production and injection flow rates [8].

---

[8] Westinghouse Sequoyah power plant
[9] General Electric BWR/6 power plant

There appear to be five features that are essential to making a hydrothermal geothermal resource commercially viable. They are [9]:

A. a large heat source

B. a permeable reservoir

C. a supply of water

D. an overlying layer of impervious rock

E. a reliable recharge mechanism to replace extracted hot water

If any one of the five features listed above is lacking, the field generally will not be worth exploiting. For example, without a large heat source geofluid temperatures will be relatively low – the thermal energy of the system will be insufficient to support exploitation long enough to make it economic. Without sufficient permeability, the fluid will not be able to move through it – it will not be able to remove much of the stored thermal energy in the rock. Without fluid in the system there is no heat transfer medium and the thermal energy of the reservoir will remain in the reservoir. Without an impermeable cap rock, the geofluids will easily escape to the surface. And lastly, without a reliable and ample recharge to the reservoir, the geofluid will eventually become depleted when it supplies a power plant [9].

In short, a hydrothermal system is a system that heavily relies on the given nature of a reservoir. Such hydrothermal resources are the only geothermal systems that have been developed commercially for electric power generation as of 2007 [9].

There, however, are many geothermal prospects that have high temperature but are lacking fluid in the reservoir or the permeability is too low to support commercial development. These systems can be "enhanced" by engineering the reservoirs through underground stimulation. Such a geothermal system is called an Enhanced Geothermal System (EGS).

The chart below illustrates major kinds of geothermal systems:

Source: SBC summary
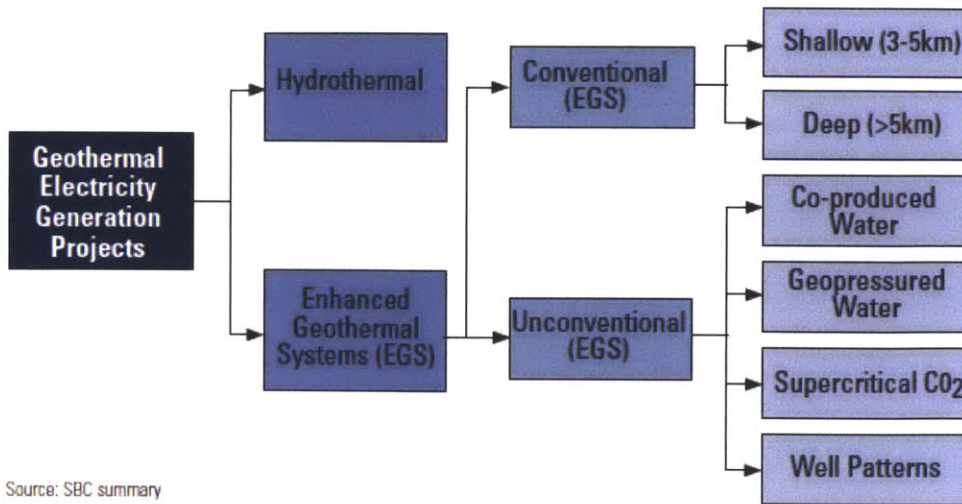
Fig.2-4 Types of Geothermal Energy Generation Projects [10]

In an EGS system, an injection well is drilled into the hot rock to a depth corresponding to the promising zone. Cold water is injected under high pressure to open existing fractures or create new ones. Once the reservoir reaches a state of sufficient volume and permeability, another well (or wells) is drilled to intercept the newly formed reservoir. Ideally, a closed loop is thus created whereby cold water is pumped down the injection well and returned to the surface through the production well. Hot rock is converted into a geothermal energy system The EGS concept is illustrated in Fig.2-5 [8].
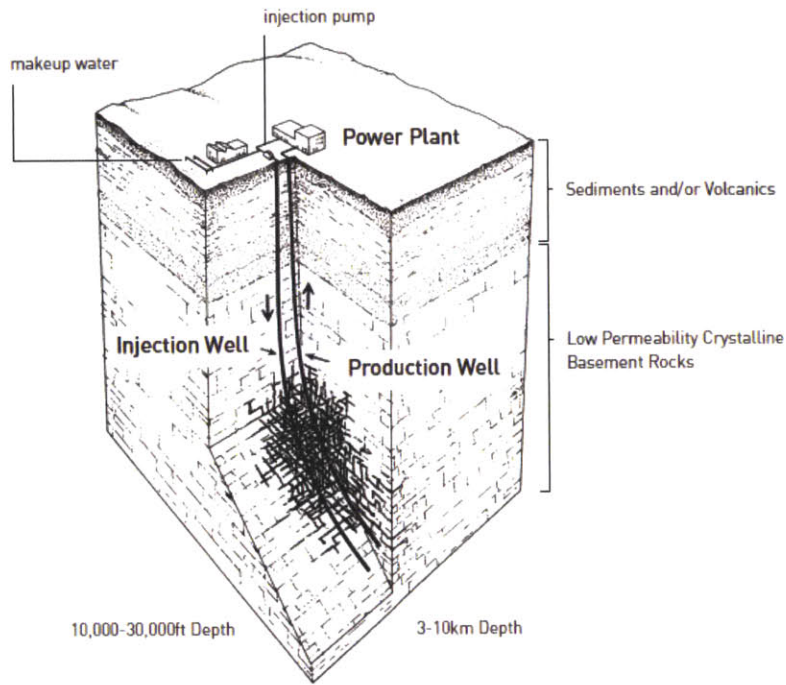
Fig.2-5 EGS Production System Scheme [6]

Such heavy reliance on drilling impacts the economics of EGS significantly, by increasing capital cost. In a simple hydrothermal system, drilling accounts for 40% of a project's capital cost, as indicated in Fig.2-6. In an EGS development, drilling consumes about 60% of the capital cost.
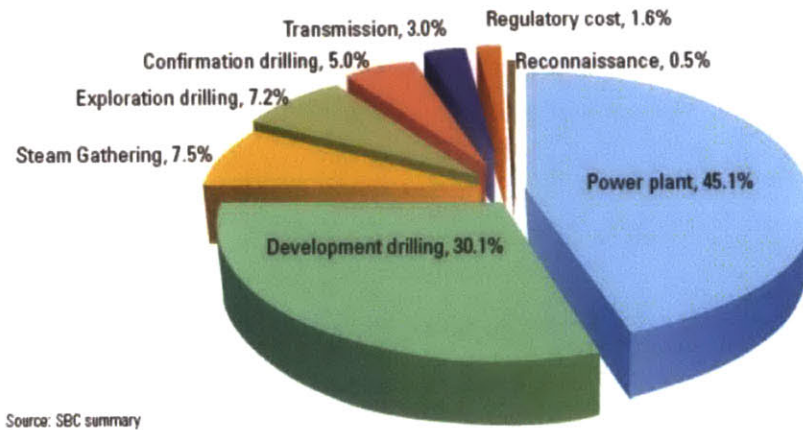
Fig.2-6 Cost Break Down for a 50MW Conventional Flashed Hydrothermal Power Plant [10]

Typically, in a successful hydrothermal reservoir, wells produce 5 MW or more of net electric power through a combination of temperature and flow rate. For instance, a well in a shallow hydrothermal reservoir producing water at 150°C would need to flow at about 125 kg/s (2,000 gpm) to generate about 4.7 MW of net electric power for the grid. Thus, as a starting target for EGS, we assume that the fluid temperature and production flow-rate ranges will need to emulate those in existing hydrothermal systems [8].

The size of geothermal power plants varies: typically between 10~100MW(e), depending on geo-fluid temperature and flow rate. A nuclear-geothermal power system may be larger—but given the lack of industrial experience it would be unreasonable to build a single 1000 MW(e) peak-power plant. Several geothermal peak-power plants will be required to meet peak power demand. This approach can also better match demand.

In a nuclear-geothermal system, where the reservoir is engineered to function as a thermal battery, we need an engineered reservoir. In this study, we assume that we borrow established EGS technologies.

2.3.3 Geothermal Energy Conversion System

This section addresses energy conversion (EC) system options appropriate for fluids obtained from Enhanced Geothermal Systems (EGS). A series of EC systems are given for a variety of EGS fluid conditions; temperature is the primary variable and pressure is the secondary variable. The EC systems used here are either directly adapted from conventional hydrothermal geothermal power plants or involve appropriate modifications. In certain cases, ideas have been borrowed from the fossil-fuel power industry to cope with special conditions that may be encountered in EGS fluids. Several applications are considered. These range from existing "targets-of-opportunity" associated with the coproduction of hot aqueous fluids from oil and gas wells to very hot, ultra-high-pressure geofluids produced from very deep EGS reservoirs. There are four possible energy conversion systems that can be used in a geothermal power plant [6]: binary power plant, single-flash power plant, double-flash power plant and triple-expansion power plant using supercritical EGS fluids. Among the three candidates, the first three are of our interest since their operating temperature range matches that of the nuclear-geothermal system as long as the system is coupled with LWRs. Table 2-3 summarizes EC systems useable with EGS.

33

Table 2-3 Summary of Energy Conversion Systems Usable with Enhanced Geothermal System [6]

Geofluid Temperature °C	Energy Conversion System	Working Fluid	Cooling System
100	Basic binary	R-134a	Water
150	Binary W/recuperator	Isobutane	Air
200	Binary or Single-flash	Isobutane or Geofluid	Air or water
250	Double-flash	Geofluid	Water
400	Single or triple expansion	Geofluid	Water
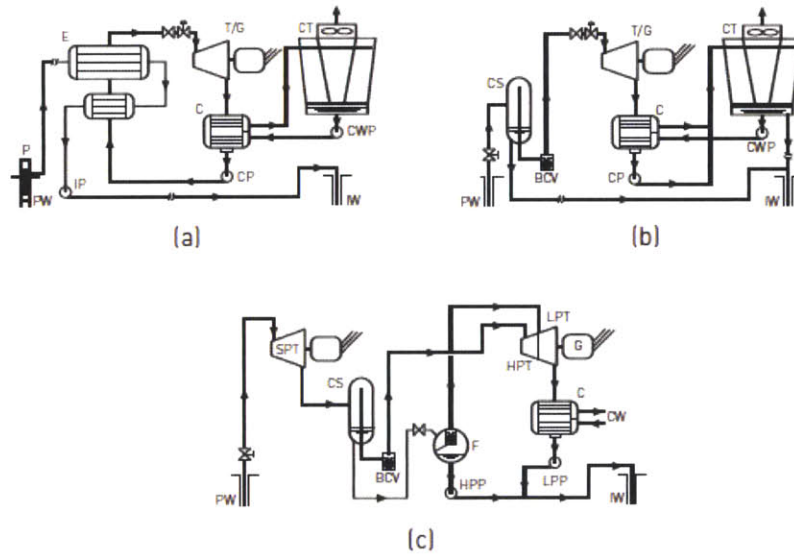
Fig.2-7 Schematics of EGS Power Conversion Systems: (a) a Basic Binary Power Plant; (b) a Single Flash Power Plant; (c) a Triple-Expansion Power Plant for Supercritical EGS Fluids [6]

Assuming the heat loss is small in the reservoir and LWRs are used to charge the reservoir, the reservoir will supply temperature around 200°C ~ 250°C for electricity production when discharged. Depending on the specifications of the reservoir design and operation, a nuclear geothermal system could deploy either binary or flash power cycles, which have the following characteristics:

Option A-Binary cycle: Most geothermal areas contain moderate-temperature water. Energy is extracted from these fluids in binary-cycle power plants. Hot geothermal fluid and a secondary (hence, "binary") fluid with a much lower boiling point than water pass through a heat exchanger. Heat from the geothermal fluid causes the secondary fluid to flash to vapor, which then drives the turbines. Because this is a closed-loop system, virtually nothing is emitted to the atmosphere. Moderate-temperature water is by far the more common geothermal resource, and most geothermal power plants in the future will be binary-cycle plants [11].

Option B-Flash cycle: High temperature geo-fluids can be used in flash plants to make electricity. Fluid is sprayed into a tank held at a lower pressure than the fluid, causing some of the fluid to rapidly vaporize, or "flash." The vapor then drives a turbine, which drives a generator. If the initial temperature is sufficiently high, a double flash system is used. The initial hot water is flahed to provide steam at a particular temperature and the warm water is flashed second time at a lower pressure to create lower pressure steam [11].

This study assumes the use of flash cycles. A detailed electricity conversion study in the context of efficiency with given geo-fluid temperature is conducted in the next chapter.

2.3.4 Geology

Geological conditions vary significantly from place to place, introducing large design differences between sites. The nature of the underground geology is an important consideration in the design of a nuclear geothermal reservoir. Among myriads of different categories of properties, thermal properties and permeability of rock are the most important consideration in the nuclear geothermal heat storage system. The thermal properties – i.e. conductivity, heat capacity etc. – of different rocks are approximately the same. However, permeability – a measure of the ability of a porous material to transmit fluids- differs significantly between rocks as indicated in Fig.2-8. Among the major types of rocks, sandstone has superior permeability relative to other rocks. High natural permeability may cause a decrease in the cost for underground fracturing to achieve the same permeability. Nevertheless, it is not straightforward to conclude that sandstone is the best rock for the nuclear geothermal heat storage system. A greater natural permeability of an underground reservoir could mean greater fluid leakage out of a stimulated reservoir. Also, the structural stability of the geology itself and against a cyclic temperature change, and chemistry of rock at high temperature are crucial items that need to be studied to determine the best geology option among candidates. Additional research on structural and chemistry issues of rock are out of the scope of

this thesis – a first examination of the concept. Rather, it is assumed in this study that as long as an underground storage reservoir operates within the temperature envelope of existing or past reservoirs, the reservoir is structurally and chemically sound. It is important to note that a reservoir of the nuclear geothermal system is an engineered system, meaning that what is more important is the altered characteristics of rock after steps are taken to increase its permeability and hydraulically isolated it from surrounding geology.
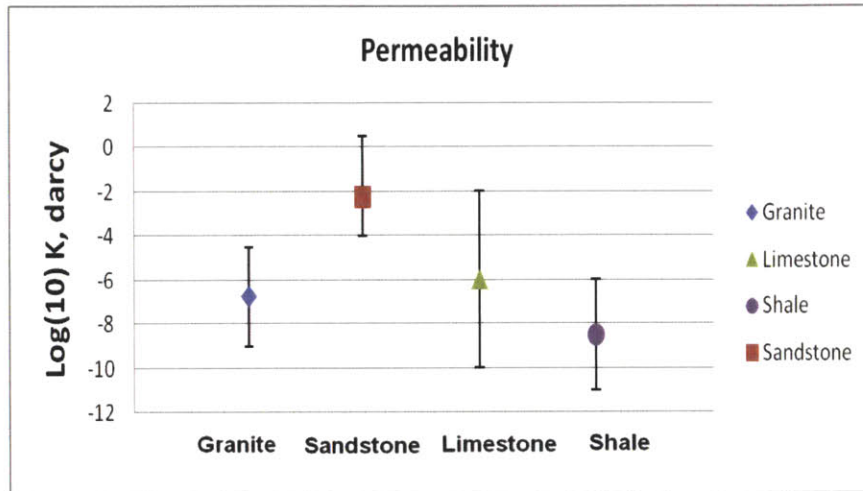
Fig.2-8 Permeability of Different Rocks [12]

2.3.5 Depth

Determining underground storage depth of a nuclear geothermal heat storage system is critical in the context of the system design, underground operating condition, and economics.

In case of using water as the working geofluid, the operating pressure determines the required minimum depth - the top level must be below the depth where the hydrostatic pressure of the ground water exceeds the pressure necessary to maintain the hottest water as a liquid.

The hottest water temperature achievable with a current LWR is 273°C, assuming that the temperature drop across the heat exchanger is negligible. To keep the water saturated liquid at 273°C, 5.7Mpa is needed as a hydrostatic pressure. It was found that a burial depth of 571m is needed to have a hydrostatic pressure of 5.7Mpa. Considering that the vertical depth of the reservoir is 0.5km~1km (the size of the reservoir is determined quantitatively in the next chapter), the heat storage burial depth will be

approximately 1km~1.5 km, which is shallower than the minimum burial depth (>3km) of typical EGS reservoirs.

If steam, rather than pressurized hot water, is the heat transfer fluid, determining the burial depth is more complex than the water case as it bears significance to the design of the system as a whole. The enthalpy change associated with the phase change from vapor to liquid increases as operating pressure decreases. This implies that the required mass flow rate to transfer the same amount of heat decreases as burial depth of the thermal reservoir decreases. Since pressure drop in the porous body is proportional to mass flow rate ($\Delta P \propto \dot{m}$ for laminar, $\Delta P \propto \dot{m}^2$ for turbulent), it might seem that pressure drop decreases as burial depth decreases. However, the density of steam decreases as burial depth decreases ($\rho \propto 1/P$), leading to an increase in velocity for the same mass flow rate. This causes a rise in pressure drop ($\Delta P \propto v$). Hence, there are two competing phenomena that are associated in determining the burial depth, from the view point of pressure drop.

In the case of carbon dioxide, like steam, the depth of the storage geology is related to the density of the fluid. The further underground the storage system, the more dense the fluid becomes, decreasing the velocities of fluids in the underground medium for a given mass flow rate. This is of importance in the design of the system, as velocity of fluids underground is a dominant parameter affecting pressure drop and heat transfer in the rock. For example, pressure drop can be alleviated at the expense of increased drilling cost to increase the burial depth. Therefore, the depth of the energy storage reservoir, in the case of steam and carbon dioxide, affects the design of the nuclear-geothermal storage system as a whole. Hence, it should be determined based on optimizing the system design.

Lithostatic pressure allows the artificial thermal reservoir to operate at shallow depths. However, the rock has to be thoroughly sealed in its upper parts in order to avoid any loss of fluids through the surface.

EGS requires drilling. Drilling costs are a significant fraction of the capital costs of the typical geothermal system, as one has to drill deep holes (Typically>3km) to reach temperatures sufficient for commercial utilization. In a nuclear-geothermal system with water as the working geo fluid, drilling costs are lower because the reservoir is buried at a much shallower depth (1~1.5km). According to the drilling study illustrated by Fig.2-9 [6], drilling cost reduces roughly a factor of four, as the drilling depth decreases from 3km to 1km.
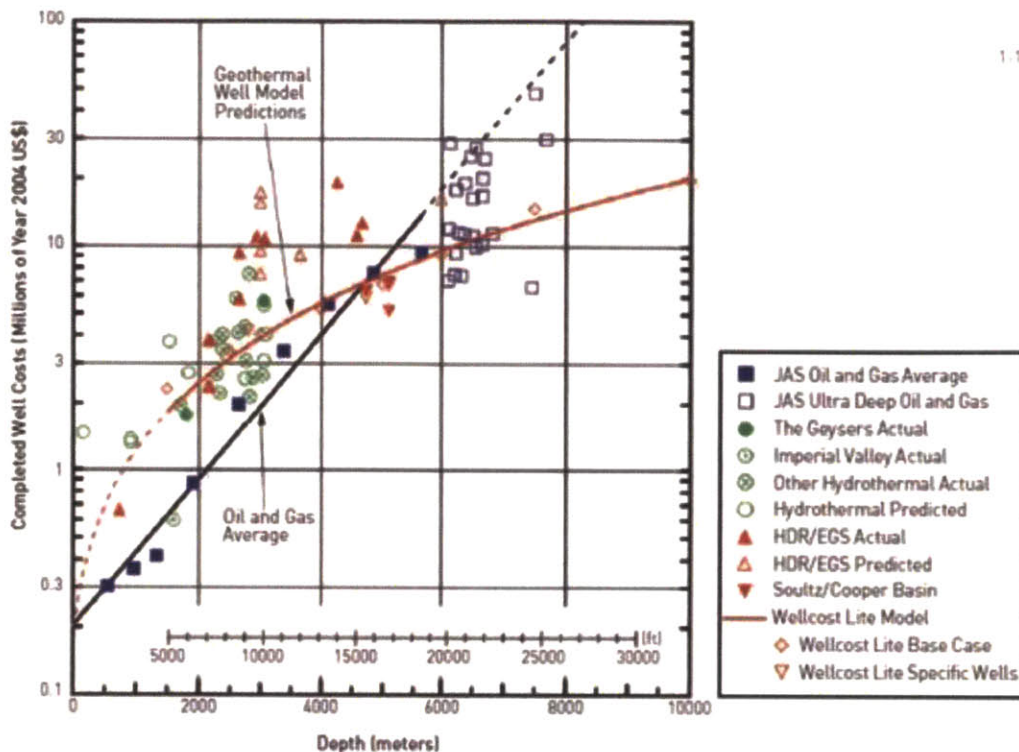
Fig.2-9 Completed Oil, Gas, and Geothermal Well Costs as a Function of Depth in 2004 US $

Therefore, drilling cost – the main constraint on an extensive deployment of EGS- can be significantly reduced by fully leveraging the very system characteristic of the nuclear geothermal system; exploiting heat that is artificially charged at shallower depths.

2.3.6 Underground Stimulation-Increasing Rock Permeability

As stated in the beginning of this chapter, EGS requires a significant underground stimulation to artificially engineer an underground reservoir that otherwise cannot be used for commercial geothermal electricity production. The prime requirement for the design of the artificial heat reservoir is to create artificial permeability to enhance natural permeability to sustain fluid circulation at useful levels for both heat injection and heat extraction. Making underground rock more permeable may be required both to decrease frictional pressure drop during fluid injection and to achieve an efficient recovery of heat with a geothermal power plant. The hydraulic fracture technology to increase the permeability of underground rock is well established in the natural gas and petroleum industries. The alternative is block caving, a

traditional mining technique that can produce underground zones of crushed rock. In addition to these commercial technologies, there are several other options

Option A-Hydraulic fracture:

The first option is drilling wells into a permeable rock. The rock permeability to flow can be increased by hydraulic fracturing. Hydraulic fracturing is injection of high pressure water with proppants into the geology of interest. The high pressure water opens fractures in the rock and the fracture width is maintained after the injection by introducing proppants into the fracture. The proppants prevent the fractures from closing when the injection is stopped. In the oil and gas mining industries, induced rock fracturing using hydraulic fracture is a standard industrial practice. Fig.2-10 illustrates the concept of hydraulic fracture.
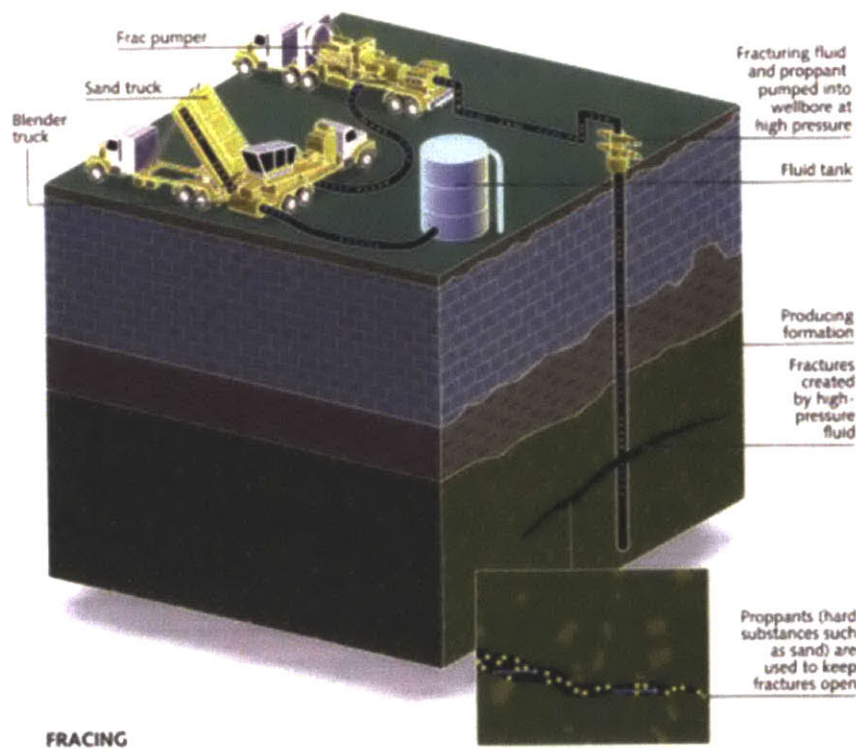
Fig.2-10 Concept of Hydraulic Fracture [13]

From the view point of the designer of the nuclear-geothermal energy storage system, the achievable target permeability after hydraulic fracture is of prime interest. Schlumberger, a major company involved in the business of hydraulic fracturing of oil and gas natural reservoirs, reported that they have achieved

an increase in permeability from 0.1 to 0.3 Darcy [10]. In the Ogachi project in Japan, permeability was increased from $10^{-3} \sim 10^{-4}$ Darcy to $10^{-1} \sim 10^{-2}$ Darcy, which is more than an order of magnitude increase [6]. A two-step-in one fracture stimulation and gravel-pack procedure has created reservoirs with target permeabilities of 2D or greater [10].

It is worth noting that hydraulic fracture has not been developed for nuclear geothermal operations which require higher permeability of the underground reservoir than any other currently existing application including recovery of oil and gas. Very high permeability is not required for recovery of oil and gas applications. It is not currently known how much the technology could increase permeability if there were large incentives for higher permeability.

Option B-Block Caving:

Unlike the well option, where micro-scale fractures provide the permeability, the mining option involves the creation of an underground rubble zone with macroscopic fractures. Conventional mining operations would use mine tunnels at two levels, with the levels separated by 50 to 500 meters. The top level must be below the depth where the hydrostatic pressure of the groundwater exceeds the pressure necessary to maintain the hottest water as a liquid or steam at required pressures. At the lower level, silos would be created (few meters and larger in diameter) upward from the bottom level. The silos would be spaced to prevent rock collapse. Holes for explosives would be drilled between the upper level and the top of the silos. Controlled timed explosives would then create rubble chimneys between the upper and lower level. The mined volume of the original silos is the void space in the final chimneys of broken rock between the two levels. These chimneys would then be the primary heat storage volumes. The rock in the side walls would be secondary heat storage. The tunnels at the top, the bottom, and connecting the two levels are the collector paths for hot and cold water in the heat storage reservoir and thus are sized to meet both mining requirements and nuclear geothermal operational requirements. The alternative to silos would be long linear structures. Structural engineering would determine the minimum supporting rock structure. The following figure is a schematic of the block caving concept.
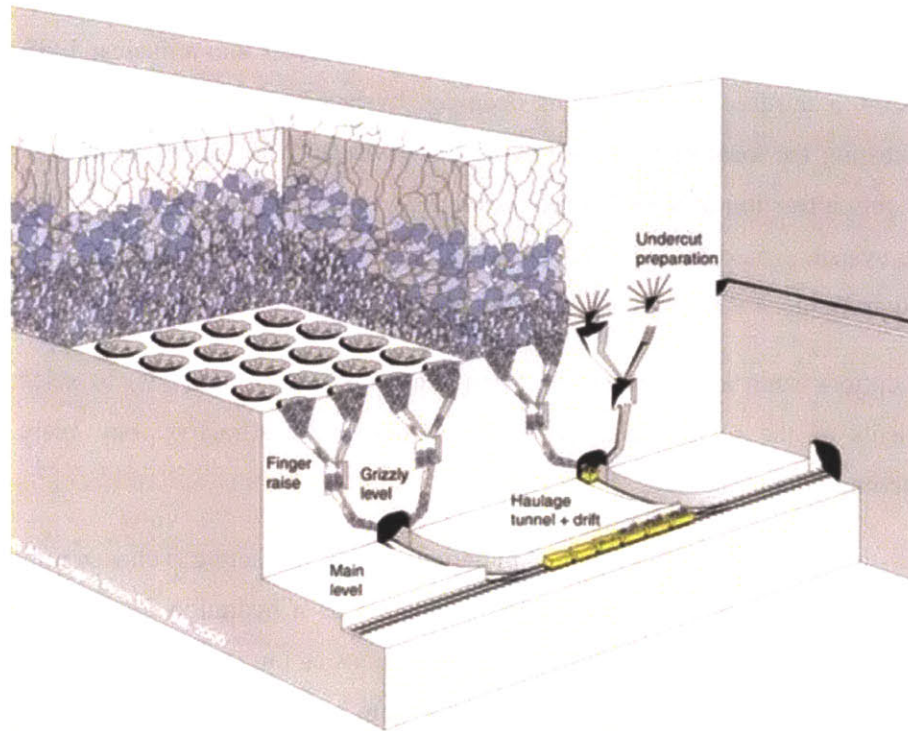
Fig.2-11 Concept of Block Caving [14]

The construction technology is a combination of traditional block caving mining and the underground civil engineering done for facilities such as the Swedish SFR waste disposal facility, geological repository facilities, and the US strategic oil reserves. The distinction between traditional mining operations and underground civil engineering is that the underground civil engineering structures are designed for century lifetimes whereas mines are designed only to last as long as it takes to remove the ore. The access would include a shaft and likely an inclined tunnel to enable high volume rock removal (Swedish granite mining method).

From the viewpoint of the fluid dynamics, the mining option artificially creates flow paths with extremely low hydraulic resistance compared to those inside the rocks. Such an uneven hydraulic resistance between the artificially made paths and the naturally existing paths inside the rock forces the fluid flow towards the low resistance path. Such a phenomenon bears an important implication not only on the pressure drop but also on the heat transfer. Most of the fluid flows through the macroscopic inter-rock conduit and heat transfer no longer occurs at the pore surface of the rock, but rather occurs at the lateral surface of the fractured rocks. Such a reduction in heat transfer area leads to a delay in the heat storing process.

41

Option C-Other:

There are a third set of options – selected removal of a component of the geology to create a high permeability rock. One example is conversion of a heavy oil reservoir into a nuclear-EGS [16]. In some heavy oil reservoirs, a third of the volume is occupied by heavy oil. The heavy oil is recovered by injecting steam, heating the local rock, and allowing lower viscosity hot heavy oil to flow to production wells. Normally, only a fraction of the oil is recovered. However, if such a reservoir was converted into a nuclear-EGS, the system would be expected to operate over time like a washing machine and remove most of the oil. In principle, a very high permeability geology could be created.

There are other options such as injection of various chemicals (such as acids) to selectively remove selected components of the rock. These concepts are potentially attractive; but, there is a lack of experience to determine their viability.

Among the options identified for underground stimulation, hydraulic fracture is chosen to be the reference option. This is because a typical EGS is assumed to operate on a hydraulic fractured reservoir and is regarded as more effective in cases of heat transfer applications as long as associated pumping power is affordable. If pumping power required to maintain fluid-flow in the hydraulic fractured reservoir of the nuclear geothermal is beyond the manageable level, block caved reservoirs deserve more detailed quantitative analysis. A quantitative reservoir study associated with underground stimulation is addressed in chapter 3.

2.4 Conclusion

Many of the individual technologies required for the nuclear-geothermal heat storage system are well established in other industries. Considering the nature of individual technologies that are established in different industries, realization of the nuclear-geothermal heat storage system is dependent upon the efficient synthesis of those existing technologies to meet the requirements of a nuclear geothermal system with competitive economics—storing enough heat and using it to meet daily, weekly, and seasonal variations in electricity demand.

In this chapter, a wide range of technical options to fulfill the functional requirements of the nuclear geothermal system were addressed and the most promising options chosen, based on qualitative analyses. Table 2-3 summarizes the technical options and the chosen ones for further quantitative analyses.

Table 2-3 Summary of Technical Options for Nuclear Geothermal Energy Storage System

Technology	Options	Chosen Option	Constraint Imposed by the Chosen Option
Nuclear Power Plant	· LWRs – PWRs, BWRs · Advanced Reactors	LWRs-PWRs	Maximum geofluid temperature = 273°C
Geo-fluid	· Water · Steam · Carbon Dioxide	Water	Minimum Operating Pressure = 5.7MPa
Nuclear-Reservoir Coupling	· Bypass flow line in the primary side of PWR · Bypass flow line in the secondary side of PWR	Bypass flow line in the primary side of PWR	Need for an intermediate heat exchanger(s)
Geothermal Power Plant	· Hydrothermal · Enhanced Geothermal (EGS)	Enhanced Geothermal (EGS)	Need for underground stimulation
Geothermal Power Cycle	· Flash Power Cycle · Binary Power Cycle	Binary Power Cycle	Efficiency
Geology	· Granite · Sandstone · Shale · Limestone	Sandstone	Rock properties Lithostatic pressure Permeability
Depth	· Ranges of possible depths	1km~1.5km	Adequate hydrostatic pressure; Known drilling cost
Underground Stimulation	· Hydraulic Fracture · Block Caving	Hydraulic Fracture	Maximum permeability of reservoir = 2Darcy

CHAPTER 3

Nuclear-EGS System Models

3.1 Introduction

This chapter is dedicated to the establishment of models that can be used to conduct preliminary design studies as an essential prerequisite. The chapter focuses on the most pivotal design parameters and system performance metrics for the preliminary design study such as storage size, cycle length, heat loss, pressure drop, geothermal power plant performance, etc. The CFD code FLUENT 6.3 is used to capture some reservoir behaviors that analytical models cannot fully describe. Appropriate assumptions are made to simplify models so that they analytically reveal relationships between design parameters and are readily useable for the purpose of preliminary design,

3.2 Principles of Reservoir Modeling

Reservoir modeling is the art of revealing the behavior of fluid and geology interaction in an essentially 'invisible' underground. The inherent limitation characterizing underground reservoir modeling is that no clear picture on underground geology is given. Such an inherent characteristic of reservoir modeling has made the reservoir modeling extremely site-dependent.

Nevertheless, rather than relying on the detailed local pictures of the underground, analysts have consistently used global parameters such as permeability and porosity that characterize the physical representation of the reservoir as a whole. The reservoir working model is a simple model that can capture most of the important reservoir and fluid behaviors with global parameters that characterize a reservoir. Such a reservoir model is a very useful tool to understand the general behavior of a reservoir.

This level of detail is well suited to this study, whose primary focus is the conceptual design of the nuclear-geothermal system. Results obtained from approximate modeling using global parameters will satisfy the purpose of the thesis as long as the model reveals general behavior of a reservoir. Therefore,

the reservoir modeling focuses on coming up with an appropriate reservoir working model – both analytical and computational, depending on the modeling requirements- that can capture the most important behavioral features of underground storage for a nuclear-geothermal system. Results of such modeling will be linked with conceptual design studies to ultimately measure feasibility, understand sensitivities of design parameters, and conceptually optimize the system with respect to cost.

3.3 Analytical Underground Reservoir Model Development

3.3.1 Reservoir Heat Transfer Modes

The way the underground storage of the nuclear-geothermal system is charged and discharged is by heat transfer between rock and fluid. Convection takes place between solid underground rock and geo-fluids and conduction occurs throughout the underground geology. The actual rate of charging and discharging in an underground system is determined by the heat transfer rates of both convection and conduction. If one of the heat transfer modes is exceptionally slower than the other, the heat transfer rate of the underground is limited by the slower mode.

Before starting reservoir modeling, it is worth understanding how the heat transfer in an underground nuclear-geothermal storage system occurs, specifically, figuring out the relative heat transfer rates between convection and conduction. A useful parameter is the Biot number which is defined as follows [15]:

$$\text{Bi} \equiv \frac{hL_c}{k} = \frac{\text{Resistance}_{\text{conduction}}}{\text{Resistance}_{\text{convection}}}$$

Eq.3-1

Where h, L_c, and k are heat transfer coefficient, characteristic length, and conductivity of solid, respectively.

Biot number is a ratio of thermal resistances. If Bi<<1, the resistance of conduction within the solid is much less than the resistance to convection across the fluid boundary layer. Hence, it is reasonable to assume a uniform temperature distribution within a solid at any time during a transient process. Such a fact implies that the temperature gradient in the solid is small and $T(x, t) \approx T(t)$ .For, Bi>>1, the temperature difference across the solid is much larger than that between the surface and the fluid.

45

We can apply the Biot number to the nuclear-geothermal energy storage reservoir. It is customary to define the characteristic length of Eq.3-1 as the ratio of the solid's volume to surface area $L_c = V/A_s$ [15]. It is found that such a value for the pore structure of sandstone is about $\sim 10^{-5}$ m [18]. A typical thermal conductivity of sandstone is 4W/m-k [12]. The heat transfer coefficient, h, is parametrically varied over the possible range of heat transfer coefficients for non-metallic forced convection. The results are summarized in the following Table

Heat Transfer Coefficient (W/m^2k)	Biot Number
1000	0.0025
3000	0.0075
5000	0.0125
7000	0.0175
9000	0.0225
11000	0.0275
13000	0.0325

Table 3-1 Biot Number of a Representative Nuclear-EGS Underground Reservoir

It is clear that the heat transfer in the pore structure of the underground heat storage media of the system is convection limited, as its resistance is orders of magnitude greater than that of conduction. Such a fact implies that solid rock reaches thermal equilibrium with surrounding fluid temperature upon contact with fluids in its pores.

However, there are short-circuits in the flow paths of underground rocks. Hydraulic fracturing artificially creates flow paths with extremely low hydraulic resistance compared to those inside the rocks. Such an uneven hydraulic resistance between the artificially made paths and the naturally existing paths inside the rock forces the fluid flow towards the low resistance path. Such a phenomenon bears an important implication not only on the pressure drop but also on the heat transfer. Most of the fluid flows through the macroscopic inter-rock conduit and heat transfer no longer occurs at the pore surface of the rock, but rather occurs at the lateral surface of the fractured rocks. Such a reduction in heat transfer area leads to a significant delay in the heat transfer process and the temperature.

3.3.2 Reservoir Temperature Modeling

How the temperature of the reservoir changes during charging and discharging processes is the basis of reservoir modeling. The transient temperature profile in the reservoir determines energy storage and reservoir operation. In this section, a 1-D analytical model that gives the transient temperature distribution in the reservoir is developed.

Assume the fluid enters as a liquid (not steam) at a temperature T_{in} greater than the initial temperature of the, T_{rock}. Then do an energy balance for a rock slice of thickness dx, in the direction of the flow:

$$\frac{\partial}{\partial t}\{[\varepsilon\rho_f C_{p,f} + (1-\varepsilon)\rho_s C_{p,s}]TA\,\partial x\} = \dot{m}(x)H(x) - \dot{m}(x+\partial x)H(x+\partial x)$$

Eq. 3-2

Where ρ_f, ρ_s, $C_{p,f}$ and $C_{p,s}$ are the density and specific heat for the fluid and rock, respectively and ε is the rock porosity, H is the enthalpy, A is the projected area of the reservoir and $\dot{m}$ is the mass flow rate of the fluid.

Equation.3-2 assumes that rock and fluid instantaneously come to thermal equilibrium upon contact. Now, $\dot{m}(x) = \dot{m}(x+dx)$ from continuity, and $h(x) = C_{p,f}T$, so Eq.3-2 becomes:

$$[\varepsilon\rho_f C_{p,f} + (1-\varepsilon)\rho_s C_{p,s}]A\frac{\partial T}{\partial t} + \dot{m}C_{p,f}\frac{\partial T}{\partial x} = 0$$

Eq. 3-3

Equation.3-3 is a hyperbolic (wave) equation with a characteristic (wave) velocity equal to:

$$u = \frac{\dot{m}C_{p,f}}{[\varepsilon\rho_f C_{p,f} + (1-\varepsilon)\rho_s C_{p,s}]A}$$

Eq. 3-4

Note that the wave velocity is not equal to the velocity of the fluid($u \neq \frac{\dot{m}}{\varepsilon\rho_f A}$), which makes sense because the thermal inertia of the fluid and rock also control how fast the thermal front moves through the rock. The following figure illustrates the results of the model:
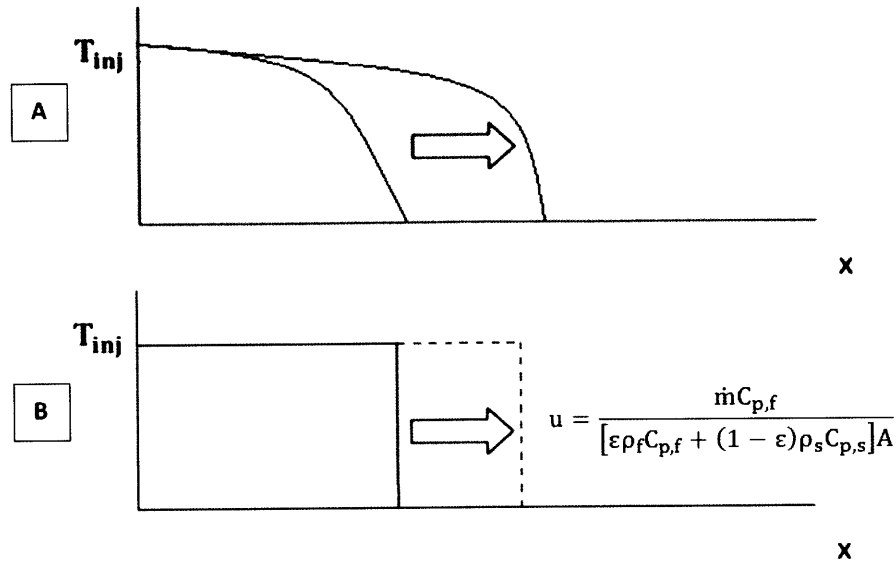
Fig.3-1 1-D Transient Temperature Profile in Underground Storage

A: Reality, B: Model

As illustrated in Fig.3-1, the model essentially assumes step function behavior of temperature propagation in the reservoir. The model is simple to use for preliminary design calculations and the discharging mode is essentially the same as the charging mode. In reality, the reservoir does not necessarily always reach thermal equilibrium with geo-fluids, hence there is a temperature transition distance as illustrated in the case A of Fig.3-1. Such a difference in the temperature profile between the reality and the model may make the model inaccurate. This is because such a temperature tail in reality may alter the energy storage per unit volume in the reservoir, hence significantly affecting the operation scheme of the reservoir. A possible outcome of temperature tailing in the reservoir is the introduction of 'dead-reservoir volume' where the reservoir's temperature is not the desired value. Having identified the possible limitations of the assumptions made for the developed temperature propagation model, for now, we hold off calculating the reservoir charging and discharging rate with the point model until we compare that with a computational simulation which models temperature tailing effects, in Section 3-5.

3.3.3 Reservoir Pressure Drop Modeling

Reservoir pressure drop is one of the most important design considerations. Parasitic pressure loss in the reservoir decreases system efficiency and causes internal reservoir pressure to be above the hydro-static pressure, leading to a number of design implications in the context of loss of water. Such detailed design

48

implications and directions imposed by the pressure drop analysis are discussed in Section 3-6. Reservoir pressure drop can be modeled using Darcy's law:

$$\Delta P = \frac{\mu u_{sup} L}{K} = \frac{\mu \dot{m} L}{\rho A_{superficial} K}$$

Eq. 3-5

where $\Delta P/L, k, \mu, u_{sup}$ are pressure drop per unit distance, permeability, average viscosity, and superficial velocity, respectively. $L, \dot{m}, \rho$ and $A_{superficial}$ are length of reservoir along the direction of fluid flow, mass flow rate, average fluid density, superficial flow area, respectively. Since viscosity and density are dependent on temperature, pressure drop, $\Delta P(t)$, changes as time proceeds. Average pressure drop is approximated assuming that the pressure drop changes linearly with time as follows:

$$\overline{\Delta P} \cong \frac{P_{max} + P_{min}}{2}$$

Eq. 3-6

Where P_{max} and P_{min} represents maximum and minimum pressure drop during a process (charging or discharging).

ΔP_{max} occurs when the reservoir is filled with cold water, where the average viscosity of water in the reservoir is at its maximum.

$$\Delta P_{max} = \frac{\mu_{max} \dot{m} L}{\rho_{max} A_{superficial} K}$$

Eq. 3-7

P_{min} occurs when the reservoir is filled with hot water, where the average viscosity of water in the reservoir is at its minimum.

$$\Delta P_{min} = \frac{\mu_{min} \dot{m} L}{\rho_{min} A_{superficial} K}$$

Eq. 3-8

The pressure drop model does not have as significant limitations in its applicability as the transient reservoir temperature modeling. This is because the permeability of the reservoir, itself, is an empirical parameter that is obtained from experiments for use in Eq.3-5. The only minor detail that may potentially

49

cause the model to deviate from reality is the temperature dependent density and viscosity of the geo-fluid. Pressure drop in a reservoir is evaluated using Eq.3-5 and compared with CFD results in Section 3-5.

3.3.4 Reservoir Heat Loss Modeling

Since rock cannot be insulated, conductive heat losses depend upon the surface area of the hot zone. The larger the system size, the smaller the surface-to-volume ratio of the storage system. This means that heat losses are slower with a large system size, as the surface area of the storage rock increases as the square of the system size while the storage volume increases as the cube of the system size. Thus, the nuclear geothermal storage system intrinsically works only on a large scale – a characteristic suitable for large amounts of energy storage.

Quantifying the amount of heat loss is important in the design process. It essentially imposes a limit on the smallest size of the reservoir and affects the storage efficiency. An analytical model we can use is the transient conduction model for a semi-infinite solid as illustrated in the following figure [15]:
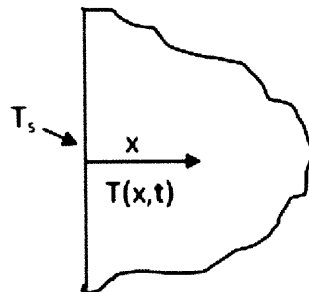
Fig.3-2 Transient Heat Conduction Model for a semi-infinite solid

T_s is the surface temperature of the reservoir. $T(x, t)$ is time and position dependent temperature, which takes into account the heat up and cool down of the surrounding geology. Heat flux at the surface of the reservoir is expressed as follows:

$$q'' = \frac{k(T_s - T_\infty)}{\sqrt{\pi \alpha t}}$$

Eq. 3-9

50

Where α is thermal diffusivity, defined as $\alpha = \frac{k}{\rho c_p}$. T_∞ is the initial temperature (t=0) of the surrounding rock. Eq.3-9 shows that heat flux decreases as $t^{-0.5}$ due to increasing surrounding rock temperature. Cumulative heat loss can be obtained by integrating Eq.3-9 over a time interval of interest as follows:

$$Q''_{cumulative} = \int_0^t q'' dt = \frac{2k(T_s - T_\infty)}{\sqrt{\alpha\pi}}\sqrt{t}$$

A critical limitation for this model for use in the design of a reservoir is the constant surface reservoir temperature assumption. In reality, the surface of the reservoir undergoes temperature changes in a cyclic manner between charging and discharging processes. For instance, during discharging periods, surface temperature of the reservoir decreases, leading to a reduced heat loss rate because of the smaller temperature gradient between reservoir and surrounding rock. Even a net flow of heat into the reservoir from the surrounding rock is possible if surrounding rock is sufficiently heated by previous cycles and the injected geo-fluid temperature during the discharging period is low. The developed model is not able to capture such phenomena, potentially leading to an overestimated result for heat loss. The results for heat losses of the model and the CFD simulation are compared in section 3-5, as part of the development of the point design model of the reservoir.

3.3.5 Reservoir Water Loss Modeling

It is important to note that the surrounding geometry of a reservoir is not absolutely devoid of all natural permeability. There will always be some small measure of permeability that causes finite water loss. Hence, the system is not completely closed and some make-up water would have to be supplied continuously. In terms of energy, leaking water carries thermal energy with it, causing additional energy loss on top of conductive loss. A water leakage model is developed in accordance with the following illustration:
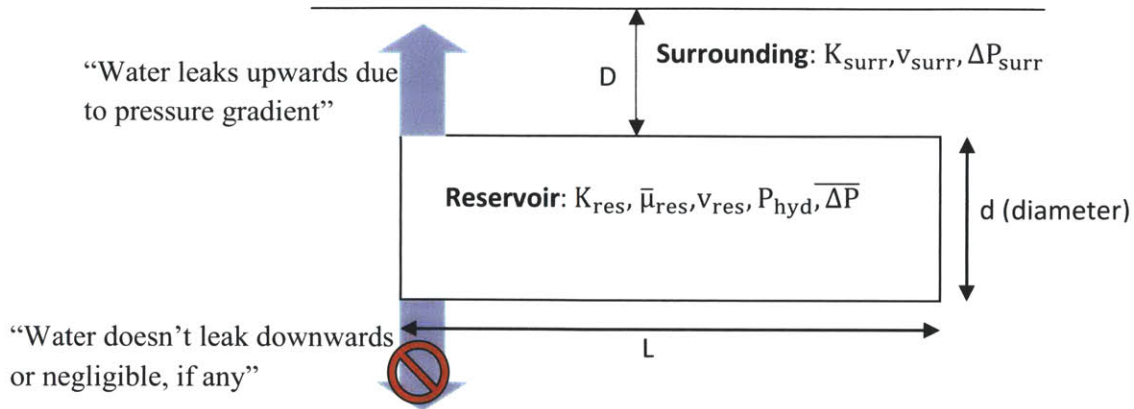
Fig.3-3 Reservoir Water Leakage Model

k_{surr}, v_{surr}, and ΔP_{surr} are natural permeability, water velocity, and pressure drop in the surrounding geology, respectively. $k_{res}, \bar{\mu}_{res}, v_{res}, P_{hyd}, \overline{\Delta P}$ are fractured permeability, average water viscosity, water velocity, hydraulic-static pressure, and average pressure drop in a reservoir. D, L, and d are burial depth, length, and diameter of a reservoir.

Some basic assumptions are made in the modeling.

A. The reservoir is assumed to be cylindrical in shape.

B. Water leaks effectively through the upper part of the cylindrical reservoir because the greater hydro static pressure at deeper depth prevents water from leaking through the bottom of the reservoir.

Rate of water leakage is expressed as follows:

$$\dot{m}_{leakage} = \rho_{avg} A v_{surr} = \rho_{avg} \frac{\pi d L}{2} v_{surr}$$

Eq.3-10

Where velocity of water in the surrounding rock can be expressed as follows according to Darcy's law:

$$v_{surr} = \frac{\overline{\Delta P} K_{surr}}{D \mu_{avg}}$$

Eq.3-11

It is assumed that when the pump stops, there is no water leakage. In other words, the average pressure rise ($\overline{\Delta P} = \frac{1}{2}\Delta P$) in the reservoir due to pumping is uniformly spread over burial depth D. This leads to the upward leakage.

Rearranging Eq.3-10 with Eq.3-11, the following expression results :

$$\dot{m}_{leakage} = \rho_{avg}\frac{\pi dL}{2}\frac{\overline{\Delta P}K_{surr}}{D\mu_{avg}}$$

Eq.3-12

The equation above states that water leakage is a function of several design parameters: diameter of reservoir (d), length of reservoir (L), burial depth of reservoir (D) and average pressure drop in the reservoir ($\overline{\Delta P}$). It is worth noting that the permeability of surrounding rock K_{surr} dominantly affects water leakage because the range of k_{surr} is orders of magnitude greater than that of the other design parameters that appear in the equation. Thus, it is a critical advantage for a reservoir to be in a geology with low natural permeability despite the increasing difficulty in hydraulic fracturing. From the design point of view, a reservoir with exceptionally low surrounding permeability practically eliminates concern over water loss in the design.

Actual sites will be more complex with low permeability zones, fractures, and possibly zones with high permeability. There are a variety of engineering methods to reduce water losses including (1) cement grouting of high fracture zones, (2) frozen ice walls, and (3) selected cold water injection to balance hydraulic forces. These engineering fixes will be site specific.

3.4 CFD Simulation of Reservoir Model

Development of an appropriate analytical design model is the key step in a preliminary design study. However, an analytical model, alone, has a limited ability to fully capture all important phenomena in a reservoir. Computational Fluid Dynamics (CFD) modeling may provide a more precise illustration of a reservoir, but relying on CFD only would leave the design study in the realm of computational empiricism. In the preliminary design stage, CFD modeling should be performed in the context of providing design directions by revealing complex relationships between design parameters and some phenomena that cannot be appropriately captured by an analytical model. Such a role of CFD simulation in the preliminary design stage can be realized through comparisons with analytical models and

modifying them by adding more reality in their terms. This section is dedicated to introduction of CFD model preparations. Results of simulations are discussed in chapter 4.

3.4.1 Governing Equations in the FLUENT Model [10]

A) Continuity

FLUENT uses the standard conservation of mass equation that is expressed as follows:

$$\frac{\partial \rho}{\partial t} + \nabla \cdot (\rho \vec{v}) = 0$$

Eq.3-13

Equation 3-10 is the general form of the mass conservation equation and is valid for incompressible as well as compressible flows. For 2D axisymmetric geometries, the continuity equation is given by

$$\frac{\partial \rho}{\partial t} + \frac{\partial}{\partial x}(\rho v_x) + \frac{\partial}{\partial r}(\rho v_r) + \frac{\rho v_r}{r} = 0$$

Eq.3-14

Where x is the axial coordinate, r is the radial coordinate, v_x is the axial velocity, and v_x is the radial velocity.

B) Momentum

Porous media are modeled by the addition of a momentum source term to the standard fluid flow equations. The source term is composed of two parts: a viscous loss term (Darcy, the first term on the right-hand side of Eq.3-15), and an inertial loss term (the second term on the right-hand side of Eq.3-15).

$$S_i = -\left(\sum_{j=1}^{3} D_{ij} \mu v_j + \sum_{j=1}^{3} C_{ij} \frac{1}{2} \rho v_{mag} v_j \right)$$

Eq.3-15

---

[10] This section of the chapter was referred from the FLUENT 6.3 Manual [19]

S_i is the source term for the i_{th} (x, y, or z) momentum equation, and D and C are matrices with relevant constants. This momentum sink contributes to the pressure gradient in the porous cell, creating a pressure drop that is proportional to the fluid velocity (or velocity squared) in the cell. A homogeneous porous media is characterized by the following equation:

$$S_i = -\left(\frac{\mu}{K}v_i + C_2\frac{1}{2}\rho v_{mag}v_i\right)$$

Eq.3-16

where K is the permeability and C_2 is the inertial resistance factor. Since fluid traveling velocity in a nuclear-geothermal reservoir is very small (10-4~10-5m/sec), the second term on the right-hand side of Eq.3-16 is negligible compared to the first term. Hence, the momentum sink in a nuclear-geothermal reservoir can be expressed as follows:

$$S_i = -\frac{\mu}{K}v_i$$

Eq.3-17

Therefore, in laminar flows through porous media, the pressure drop is typically proportional to velocity and the constant C_2 can be considered to be zero. The porous media model then reduces to Darcy's Law:

$\nabla p = -\frac{\mu}{K}\vec{v}$ The pressure drop that FLUENT computes in each of the three (x,y,z) coordinate directions within the homogeneous porous region, where permeability is isotropic, is then

$$\Delta p_x = \sum \frac{\mu}{K}v_x\Delta n_x$$

$$\Delta p_y = \sum \frac{\mu}{K}v_y\Delta n_y$$

$$\Delta p_x = \sum \frac{\mu}{K}v_z\Delta n_z$$

Eq.3-18

Where, v_x, v_y, v_z and Δn_x, Δn_y, Δn_z are velocities and thicknesses of the medium in the x, y and z directions. Note that Eq.3-17 and 3-18 are the same as Darcy's pressure drop point model, Eq.3-5. However, in FLUENT simulations, precise effects of temperature dependent viscosities and velocities are

simulated for each mesh point. Such CFD effects caused by temperature dependent properties will be used to understand the validity or limitations of the point model.

C) Energy

FLUENT solves the standard energy transport equation in porous media regions with modifications to the conduction flux and the transient terms only. In the porous medium, the conduction flux calculation uses an effective conductivity and the transient term includes the thermal inertia of the solid region on the medium as follows:

$$\frac{\partial}{\partial t}(\epsilon \rho_f E_f + (1-\epsilon)\rho_s E_s) + \nabla \cdot (\vec{v}(\rho_f E_f + P)) = \nabla \cdot \left[k_{eff} \nabla T - \left(\sum_i H_i J_i \right) + (\bar{\bar{\tau}} \cdot \vec{v}) \right] + S_f^H$$

Eq.3-19

Where

E_f = total fluid energy

E_s = total solid medium energy

ϵ = porosity of the medium

k_{eff} = effective thermal conductivity of the medium

S_f^H = fluid enthalpy source term

Total fluid energy E_f is defined as $E_f = H - \frac{P}{\rho} + \frac{v^2}{2}$ and sensible enthalpy H is defined for incompressible flow as

$$H = H_j + \frac{P}{\rho}$$

Eq.3-20

and P is the operating pressure and h_j is defined as follows:

$$h_j = \int_{T_{ref}}^{T} C_{p,j} dT$$

Eq.3-21

where T_{ref} is 298.15K.

In the porous medium, the conduction flux uses an effective conductivity and the transient term includes the thermal inertia of the solid region on the medium.

$$k_{eff} = \epsilon k_f + (1 - \epsilon)k_s$$

Eq.3-22

Where

k_f = fluid phase thermal conductivity

k_s = solid medium thermal conductivity

The first term on the left-hand side of Eq.3-19 shows that the porous body assumes instantaneous thermal equilibrium of fluid and solid upon contact. In other words, in terms of energy, the porous body does not make a distinction between fluid and solid. Rather it treats them as a thermally homogeneous mixture. Note that the same assumption is made in the development of the thermal front velocity point model in Eq.3-2 based on the fact that solid and fluid reach thermal equilibrium upon contact due to the large active conduction area in microscopic pores. The second term on the right-hand side of Eq.3-19 is the convective energy transport, which is taken into account in the point model development as the term $\dot{m}C_{p,f}\frac{\partial T}{\partial x}$ in Eq.3-3.

The first three terms on the right-hand side of Eq.3-19 represent energy transfer due to conduction, species diffusion, and viscous dissipation, respectively. The species diffusion effect is negligible compared to the bulk convection. Viscous heating is also negligible as fluid velocity in a nuclear-geothermal reservoir is small. The fluid enthalpy source term, S_f^H, representing volumetric heat sources is zero as no heat generation source exists in a nuclear-geothermal reservoir.

Taking these facts into account, Eq.3-19 reduces to Eq.3-2 except for the conduction term $\nabla \cdot k_{eff}\nabla T$ on the left-hand side of the equation. It is worth noting that the convective energy transport is the main driving force for thermal fronts to proceed in a nuclear-geothermal reservoir. However, the conduction effect may cause axial temperature profiles in a reservoir to deviate from the step-function behavior illustrated in Fig.3-1. The temperature tailing in a reservoir is expected to emerge from such the conduction effects. From the viewpoint of reservoir design, such a temperature tailing implies a dead-volume region in a reservoir, which reduces the actual energy storage volume.

57

Capturing the temperature tailing effect by means of an analytical approach is undeniably complicated because conduction between the reservoir and surrounding rock also significantly affects the temperature profiles in a reservoir near the interface.
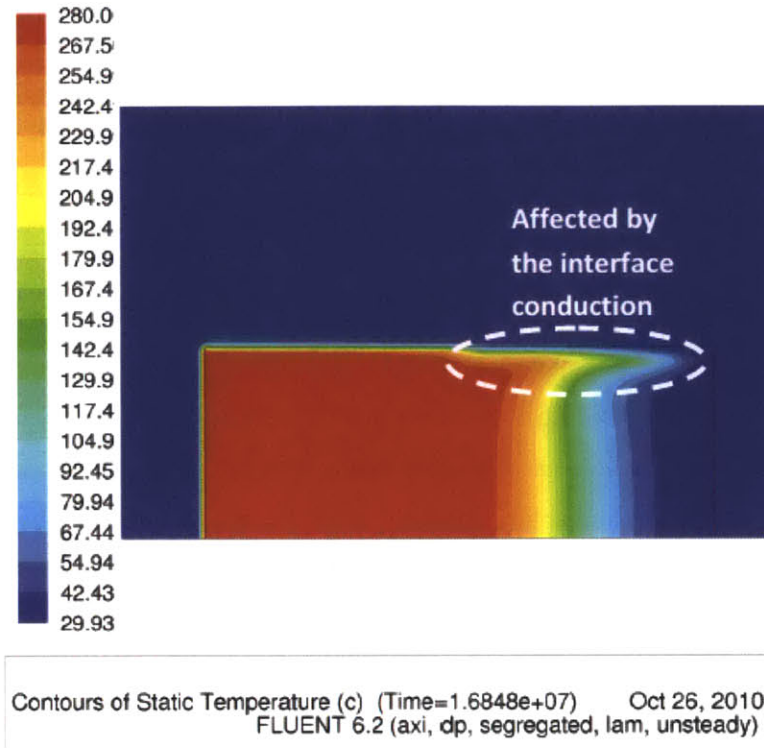
Fig.3-4 Temperature Profile of an Underground Storage Reservoir during a Charging Period

Figure.3-4 illustrates a typical temperature profile of a reservoir during a charging period as hot water flows left to right. An evident temperature tailing is witnessed. In addition, near the interface between the reservoir and surrounding geology, reservoir temperature profile is significantly affected by the temperature gradient across the interface.[11] Modeling of the witnessed multi-dimensional temperature tailing effects by means of an analytical approach is beyond the scope of this study.

Hence, in this study, CFD simulations are performed to capture temperature tailing effects, which are not modeled by the developed thermal-front velocity point model. Then, results for thermal front velocities of the point model are compared to independent predictions obtained using a CFD model over a wide range of conditions. Lessons from the comparisons are used to enhance – or at least understand- limitations of the point model in the preliminary design.

---

[11] Effects of the temperature tailing will be addressed in more detail in section 3.5

3.4.2 Geometry Description

As discussed at the beginning of the chapter, reservoir modeling requires, by its nature, a simplified model of a reservoir that can appropriately capture reality. In this study, the underground heat storage reservoir is modeled as a horizontal cylindrical porous body with a certain porosity, permeability and relevant properties of its geology. An illustration of a cylindrical reservoir is shown in Fig3-5.
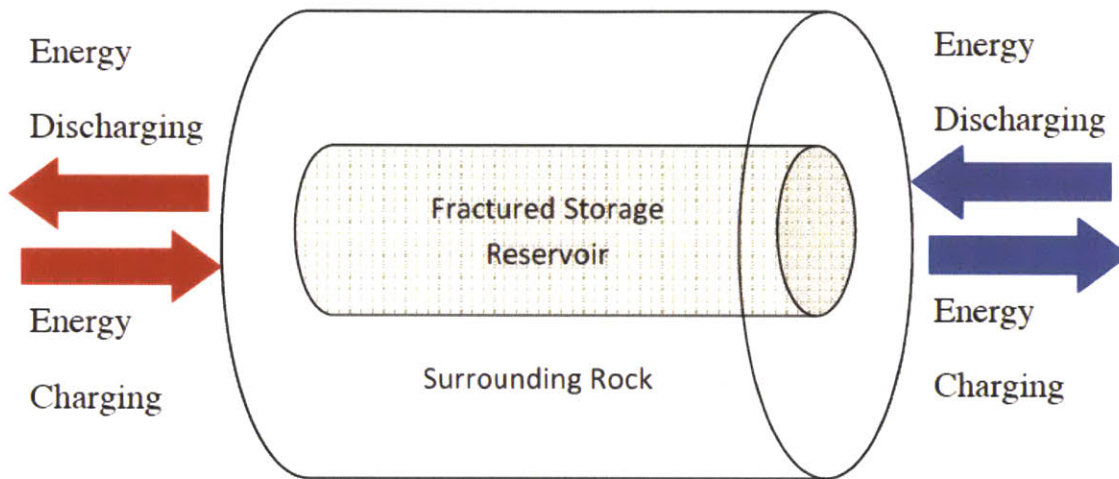
Fig.3-5 Geometry Illustration of CFD Reservoir Model

Two different geologies are modeled in the CFD simulations: the fractured storage reservoir and surrounding rock. These geologies differ essentially by their assigned permeability and porosity. In the CFD model, fluids flow only in the fractured reservoir region and surrounding rock effectively captures conductive heat losses through the sides of reservoir storage. The actual cylindrical reservoir model is simulated with the following geometry and boundary conditions.
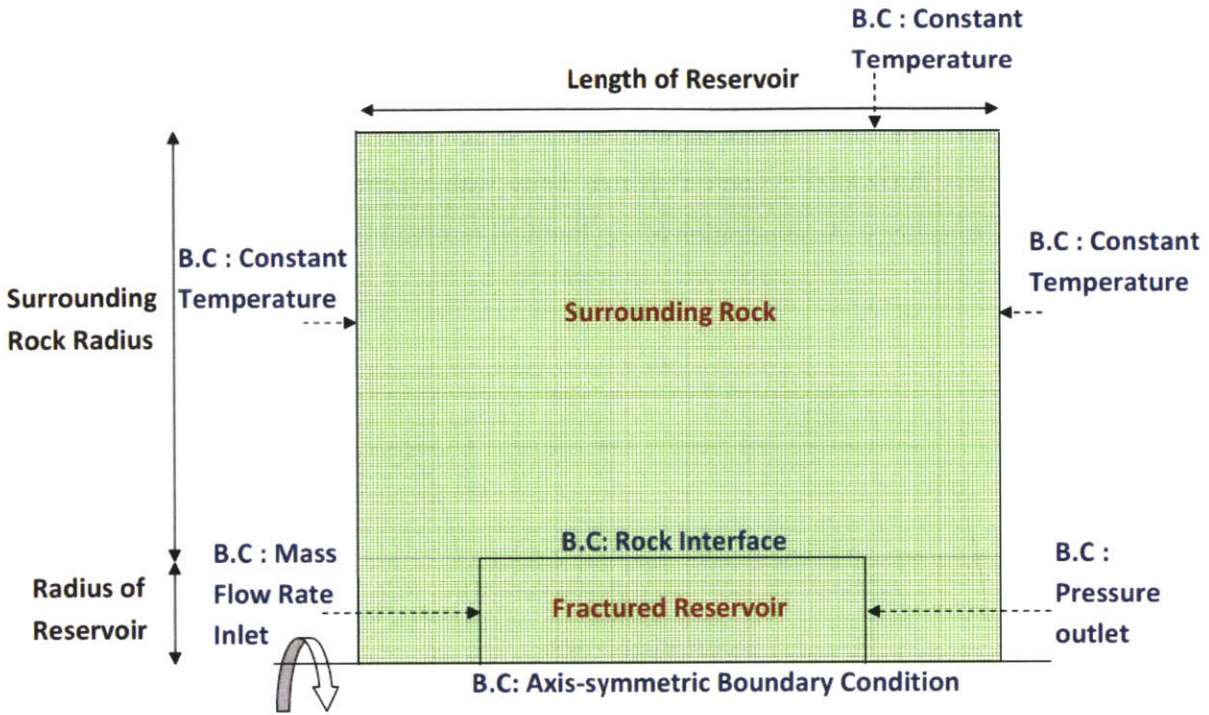
Fig.3-6 Geometry Illustration of CFD Reservoir Model with Boundary Conditions

It is worth noting that there is no essential difference between modeling a reservoir in the cylindrical coordinates or Cartesian coordinates. In this study, the cylindrical coordinate is picked to take advantage of the axis-symmetric boundary condition which effectively reduces computational costs. The 2-D axis symmetric boundary condition is used in the center of the fractured reservoir and the surrounding rock as illustrated in Fig.3-6. When rotated with respect to the center line that is assigned as the axis boundary, the 2-D planar reservoir model forms a 3-D cylindrical reservoir.

The 2-D axis boundary condition can appropriately model reservoir behavior appropriately if and only if there is no azimuthal dependency in flow behavior, such as velocity. Non-uniform fluid injection, gravitational head, locations of fluid inlet and outlet could possibly cause azimuthal dependency in flow behaviors in a cylindrical reservoir. The following assumptions with justifications are made in the CFD simulations for the point model development:

1) Fluid inlet and outlet are the end surfaces of a cylindrical reservoir with spatially uniform injection flow rate.

In reality, fairly spatially uniform fluid injection and recovery over the entire surface at both ends of a fractured region can be made by using a distributed piping system. Such a system is schematically illustrated in Fig.3-7.
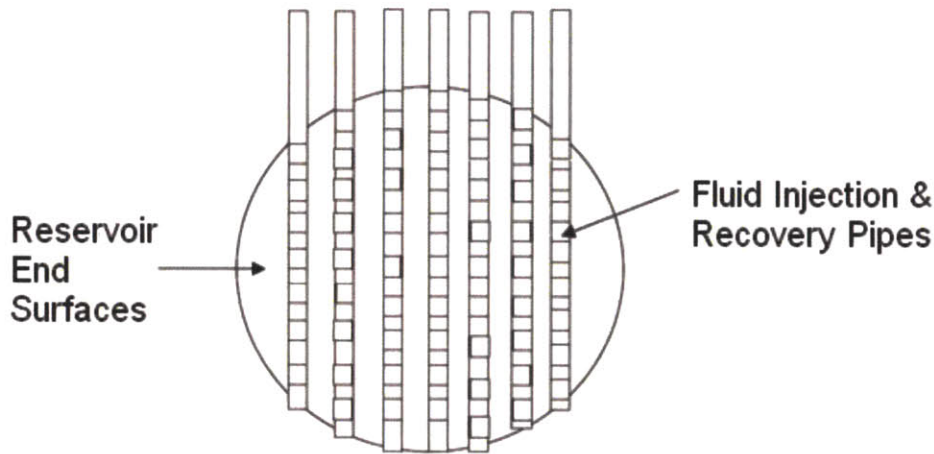
Fig. 3-7 Schematic of an End Surface Fluid Inlet and Outlet Piping Scheme

Use of the entire end surface of a reservoir for fluid inlet and outlet is desirable in terms of an efficient use of fractured volume. This is because the functionally dead-region of a reservoir can be minimized by uniform fluid distribution in a reservoir. On the other hand, the required enhanced piping could potentially increase the capital cost significantly, hence in reality such perfectly uniform fluid injection can be limited in terms of economic competitiveness. Nevertheless, for the purpose of developing a CFD-aided analytical model for conceptual design, the uniform flow injection & recovery assumption is justifiable, as the assumption still appropriately captures general reservoir behavior. In addition, the degree of accuracy in predicting reservoir behavior satisfies the required accuracy for preliminary design purposes. Therefore, in the CFD simulations, the two end surfaces of a fractured region have mass flow rate (injection) and pressure outlet boundary conditions imposed, respectively.

2) Gravity is not addressed in the CFD simulations. For ease of presentation, we show a horizontal reservoir. The actual reservoir geometry will depend upon the local geology. When practical, the reservoir

will be vertical with hot water on top of cold water to eliminate gravity driven flow due to density differences in the fluid.

3.4.3 Boundary Condition Description

A) Flow Injection- Mass Flow Boundary Condition

Flow injection is modeled in FLUENT by imposing the mass flow boundary condition. Mass flow boundary conditions are used in FLUENT to provide a prescribed mass flow rate or mass flux distribution at an inlet. Physically, specifying the mass flux permits the total pressure to vary in response to the interior solution. This is in contrast to the pressure inlet boundary condition, where the total pressure is fixed while the mass flux varies.

B) Flow Outlet- Pressure Outlet Boundary Condition

Pressure outlet boundary conditions require the specification of a static (gauge) pressure at the outlet boundary. In the simulations, the gauge pressure at outlet is set to be zero, hence fluid leaves the reservoir at the operating pressure which is mainly determined by hydraulic static pressure. The combination of the mass flow inlet boundary condition and pressure outlet boundary condition allows calculation of the inlet static pressure that is needed for the specified mass flow rate.

C) Reservoir-Surrounding Rock Interface – Coupled Conduction Interface

The coupled conduction interface boundary condition is imposed on surface interfaces between surrounding rock and the fractured reservoir. Conduction heat transfer between the fractured reservoir and surrounding geology is simulated. Hence, heat loss – or gain- rate are simulated in conjunction with transient reservoir and surrounding geology temperature.

D) Surrounding Rock Boundary– Adiabatic and Constant Temperature Boundary Condition

As illustrated in Fig. 3-5, surfaces of the surrounding geology are imposed with ambient constant temperatures (30°C). Since the outer boundaries of surrounding geology are substantially far from those of the reservoir, imposed boundary conditions on surrounding rock outer boundaries hardly affect reservoir behavior.

3.5 Results of Reservoir Models and Point Model Development

This section of the chapter is dedicated to establish reservoir models using both the discussed analytical methods and CFD modeling. Throughout the section, numbers of independent comparisons between the results of the analytical models and the FLUENT results are made. The following twenty different reservoirs simulated in FLUENT (see Table3-2) are used to assess the detailed behavior of nuclear-EGS reservoirs and to support analytical models.

Table 3-2 Reservoirs Tested in FLUENT Simulations

	Case No	Reservoir Length (m)	Reservoir Diameter (m)	Geology Density (kg/m^3)	Geology Specific Heat (J/kg-k)	Reservoir Permeability (Darcy)	Reservoir Porosity	Mass Flow Rate (kg/sec)	Fluid Temperature (°C)	Reservoir Initial Temperature (°C)
Charging Case	1	1000	500	2600	850	2	0.2	5000	280	30
	2	1000	500	2600	850	2	0.2	5000	280	130
	3	1000	250	2600	850	2	0.2	5000	280	30
	4	1000	250	2600	850	2	0.4	5000	280	30
	5	1000	750	2600	850	2	0.1	10000	280	30
	6	800	750	2400	850	1	0.1	10000	280	30
	7	800	300	2700	850	1	0.1	8000	290	30
	8	800	375	2700	750	1	0.1	3000	280	200
	9	500	375	2800	850	1	0.05	4000	270	50
	10	600	375	2900	900	1.5	0.15	6000	260	50
Discharging Case	11	600	375	2600	800	1.5	0.15	7000	30	250
	12	900	500	2600	850	1.5	0.15	12000	30	250
	13	900	500	2600	850	1.5	0.15	11000	50	250
	14	450	250	2600	850	1.5	0.2	2500	40	260
	15	450	1000	2600	850	1.5	0.2	20000	30	270
	16	300	250	2600	850	1.5	0.3	1000	50	250
	17	600	250	2600	850	1.5	0.1	1000	50	250
	18	600	250	2600	850	2	0.1	6000	70	230
	19	1200	250	2600	850	2	0.4	8000	60	230
	20	1200	250	2600	850	1	0.4	3000	60	230

3.5.1 Thermal Front Velocity

Prediction of thermal front velocity in a reservoir is of crucial importance in terms of both reservoir design and operation. Thermal front velocity determines charging and discharging rate in a reservoir. As discussed in the previous chapter, the analytical model does not capture heat conduction effects within the reservoir and between the reservoir and surrounding geology. In this section of the chapter, results of the analytical model and the FLUENT simulations are compared to quantitatively understand thermal front velocity in a nuclear-geothermal reservoir, which is further investigated for reservoir designs in the following chapter.

The following Table shows analytically obtained thermal front velocity for each of the different reservoir cases indicated in Table 3-2, as determined using Eq.3-4.

Table 3-3 Obtained Thermal Front Velocities Using Analytical Model

	Case No	Thermal Front Velocity (m/day)
Charging Case	1	3.90E+00
	2	3.97E+00
	3	1.56E+01
	4	1.39E+01
	5	3.69E+00
	6	3.95E+00
	7	1.81E+01
	8	4.93E+00
	9	5.67E+00
	10	7.43E+00
Discharging Case	11	1.02E+01
	12	9.42E+00
	13	8.64E+00
	14	7.68E+00
	15	3.86E+00
	16	2.87E+00
	17	3.26E+00
	18	1.94E+01
	19	2.13E+01
	20	8.01E+00

The thermal front velocities in Table 3-3 are step-function thermal front velocity. The following figures show time dependent development of the temperature contour of Case No.1, which shows temperature tailing effects of a reservoir.

Contours of Static Temperature (c) (Time=5.1840e+06)

Nov 14, 2010
FLUENT 6.3 (axi, dp, pbns, lam, unsteady)

Fig.3-7 Transient Temperature Contour During a Charging Process: Case No.1,
Length=1000m, Radius=250m: Time= 60 Days

Contours of Static Temperature (c) (Time=1.2096e+07)

Nov 14, 2010
FLUENT 6.3 (axi, dp, pbns, lam, unsteady)

Fig.3-8 Transient Temperature Contour During a Charging Process: Case No.1,
Length=1000m, Radius=250m: Time=140 Days

Contours of Static Temperature (c) (Time=1.9008e+07)

Nov 14, 2010
FLUENT 6.3 (axi, dp, pbns, lam, unsteady)

Fig.3-9 Transient Temperature Contour During a Charging Process: Case No.1,
Length=1000m, Radius=250m: Time=220Days

Fig.3-10 Transient Temperature Contour During a Charging Process: Case No.1:

Length=1000m, Radius=250m: Time=250Days

Fig.3-11 Transient Temperature Contour During a Charging Process: Case No.1:

Length=1000m, Radius=250m: Time=280Days

As illustrated in Figs. 3-7~3-11, the temperature distribution in a reservoir is not quite the simple binary step function – it indeed involves temperature tailing at its front. In a real reservoir, such a temperature tailing effect is more significant, as short circuits in a reservoir cause spatially inhomogeneous convection fronts. Temperature distribution in a reservoir is significantly distorted near the interface between the reservoir and its surrounding geology.

With respect to the temperature tailing effect in a reservoir, it is not straightforward how to define thermal front velocity from results obtained by FLUENT simulations. A strict definition of the term thermal front velocity would be the following:

$$\text{Thermal Front Velocity} = \frac{\text{Temperature Distance Traveled}}{\text{Unit Time}}$$

Eq.3-23

In CFD simulations, also in reality, it is not straightforward to evaluate the numerator of Eq.3-23. Figure.3-12 illustrates transient temperature development curves for the inlet, outlet and reservoir average of the reservoir case No.1.
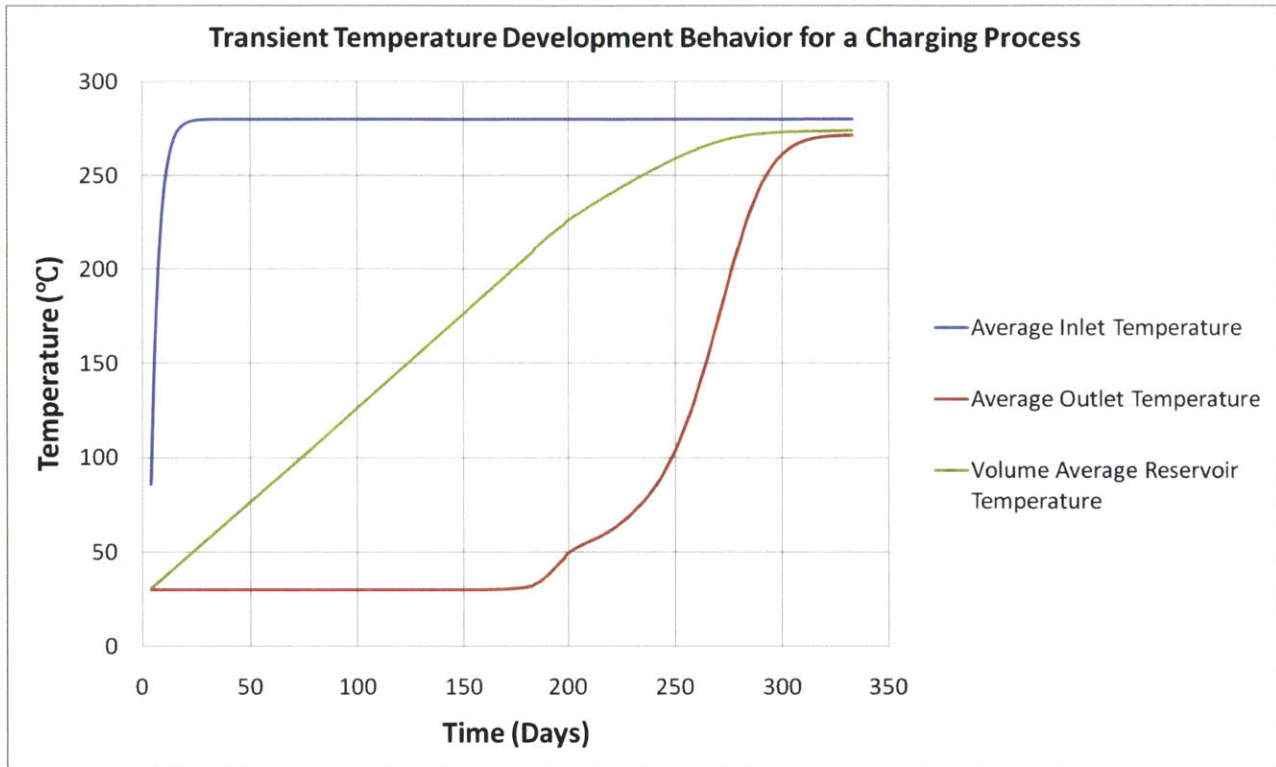
Fig.3-12 Transient Temperature Behavior for the Reservoir Case No.1

While charging, inlet temperature remains constant at the injecting temperature, in this case, 280°C. Outlet temperature remains constant before the thermal front reaches the outlet. In Fig.3-12, the gradient of the volume average reservoir temperature line with respect to time is the reservoir charging rate and is constant until the reservoir average outlet temperature starts to increase. As the thermal front reaches the outlet, the outlet temperature starts to increase, as can be seen around 180 days in Fig3-12. This is the time when the reservoir average temperature does not increase linearly; charging rate slows down. The constant reservoir charging rate starts to decrease upon the increase in reservoir outlet temperature. One can expect this because as reservoir outlet temperature starts to increase, the temperature difference between inlet fluids and outlet fluids decreases, leading to a decreasing charging rate. At this time,

69

everywhere in a reservoir is heated up from the initial temperature. As the charging process proceeds, the outlet temperature increases in a gradual manner because the reservoir has temperature tailing.

From the reservoir operation point of view, marginal charging after the beginning of outlet temperature increase does not charge the reservoir as effectively as the moment before. However, it seems unreasonable to stop charging the reservoir at the point the reservoir charging rate starts to decrease. This is because such an operation scheme would leave a considerable volume of a reservoir unused, eventually introducing "functionally dead volume". The illustration of a functionally dead volume region can be seen in Fig.3-9, at time = 220days. One can see that almost 1/3 of the reservoir volume remains not charged at 220days even though the outlet temperature has increased. An important observation is that the primary reason for increasing the reservoir outlet temperature at this point of operation is the distorted temperature region near the geology interface. Indeed, as can be seen in Fig.3-11, everywhere else in the outlet except the interface region remains quite 'unheated'. This means that there is still considerable room for storing energy even after the point charging rate starts to decrease. Hence, an operational scheme for the charging process should be determined based on the volume average temperature of a reservoir – the metric of energy charged, not on the local temperature condition.

Understanding the metric of charging performance, in this study, the following rationale is introduced to assess the thermal front velocity of CFD results. For the charging case, a reservoir is fully charged when the volume-average temperature of the reservoir reaches the injecting fluid temperature. However, reservoir volume-average temperature cannot reach exactly that of the injecting fluid temperature because of conduction losses. Here, 6% of fully stored energy is taken as a reasonable goal to take such conduction and temperature tailing into account.

$$u_{CFD} = \frac{\text{Length of Reservoir}}{\text{Time for reservoir to be charged to 94\% of maximum rock storage capacity}}$$

Eq.3-24

Stored energy of a solid matter upon a temperature change can be in general obtained in the following way:

$$E = M \int_{T_{initial}}^{T_{final}} C_p(T)dT = M\overline{C_p}(T_{final} - T_{initial})$$

Eq.3-25

70

Where, M, $Cp(T)$, $\overline{C_p}$, T_{final} and $T_{initial}$ are mass of the solid, temperature dependent specific heat at constant pressure, average specific heat at constant pressure, final temperature and initial temperature, respectively.

Following Eq.3-25, the amount of thermal energy charged into rock is as follows:

$$E_{Rock\_stored} = M_{rock}\overline{C_p}_{rock}(\overline{T}_{rock}(t) - T_{ref})$$

$$= V_{res}(1 - \varepsilon)\bar{\rho}_{rock}\overline{C_p}_{rock}(\overline{T}_{rock}(t) - T_{ref})$$

Eq.3-26

Where $M_{rock}, \overline{Cp}_{rock}, \overline{T}_{rock}, T_{ref}, V_{res}, \varepsilon, \bar{\rho}_{rock}$ are mass of rock, average specific heat of rock, spatially averaged rock temperature, reference temperature, porosity and average rock density, respectively. Reference temperature, T_{ref} represents the lowest temperature – the cold fluid temperature of the discharging process. The reference temperature is the initial temperature of a reservoir during the charging process. One can reason that a reservoir is fully charged when $\overline{T}_{rock}$ reaches maximum, which is the injecting temperature during the charging process.

$$E_{Stored\_Max} = V_{res}(1 - \varepsilon)\bar{\rho}_{rock}\overline{C_p}_{rock}(T_{injecting} - T_{ref})$$

Eq.3-27

Hence, achieving 94% of maximum energy storage capacity of rock can be expressed as follows:

$$0.94 = \frac{E_{stored}}{E_{Stored_{Max}}} = \frac{\overline{T}_{rock}(\tau) - T_{ref}}{T_{injecting} - T_{ref}}$$

Eq.3-28

Equation.3-28 can be arranged to obtain the thermal front velocity as follows:

$$\overline{T}_{rock}(\tau) = 0.94(T_{injecting} - T_{ref}) + T_{ref}$$

$$= 0.94T_{injecting} + 0.06T_{ref}$$

Eq.3-29

71

$T_{injecting}$ and T_{ref} are design parameters. Time for a reservoir to reach the volume average temperature that gives 94% of maximum rock energy storage capacity - τ - is found from the FLUENT results. Then, according to Eq.3-24, the length of a reservoir is divided by τ to give thermal front velocity.

A similar approach holds for the discharging process. The following figures illustrate time dependent temperature history during a discharging process for case No.16 of Table 3-2.
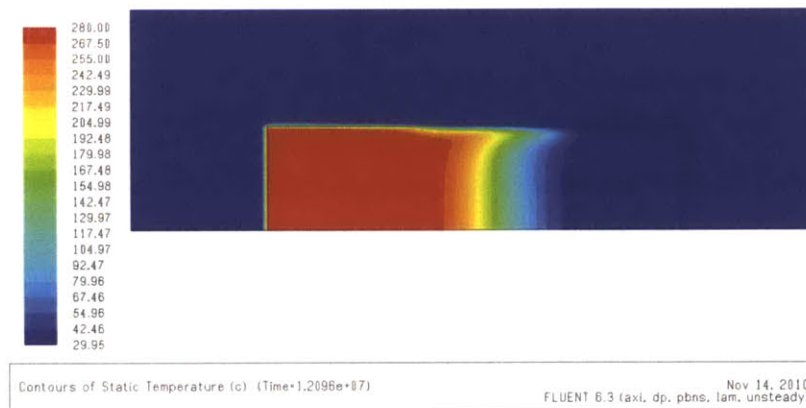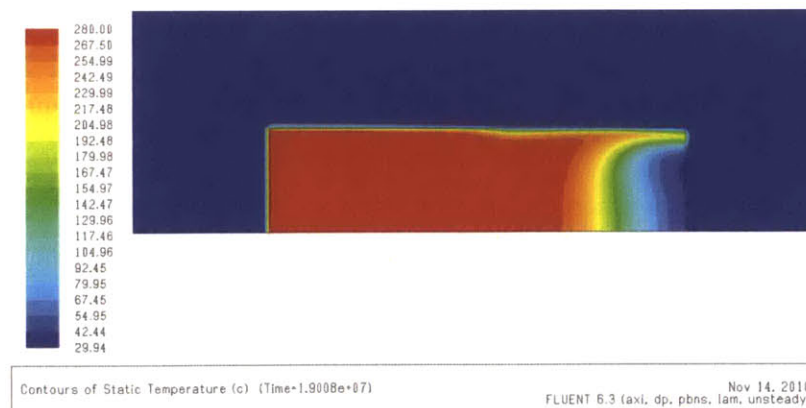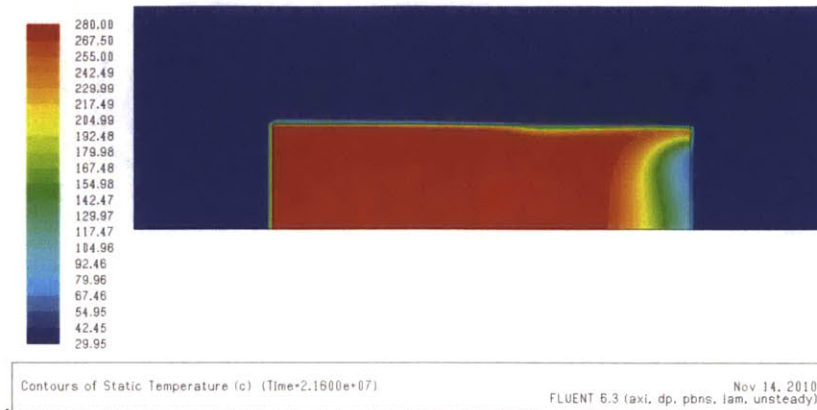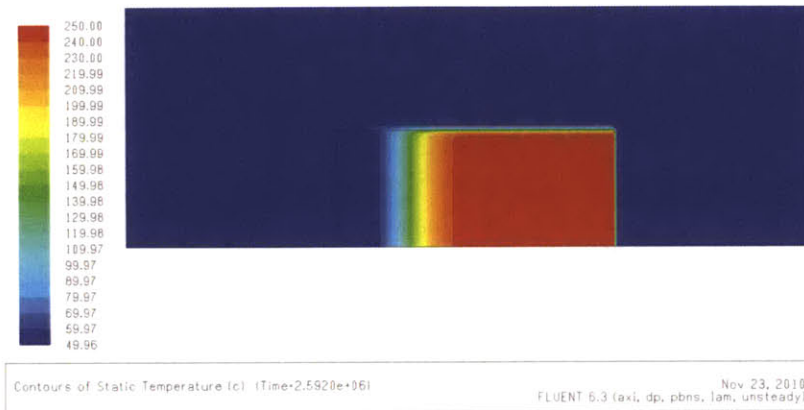

Fig.3-13 Transient Temperature Contour During a Charging Process: Case No.1:
Length=300m, Radius=125m: Time=30Days
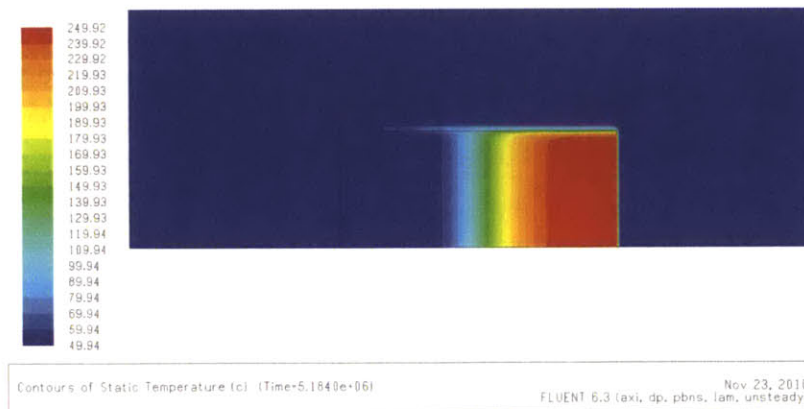
Fig.3-14 Transient Temperature Contour During a Charging Process: Case No.1:
Length=300m, Radius=125m: Time=60Days

226.11
217.30
208.49
199.68
190.87
182.06
173.25
164.44
155.63
146.82
138.01
129.20
120.40
111.59
102.78
93.97
85.16
76.35
67.54
58.73
49.92

Contours of Static Temperature (c) (Time=7.7760e+06)   Nov 23, 2010
                                                    FLUENT 6.3 (axi, dp, pbns, lam, unsteady)
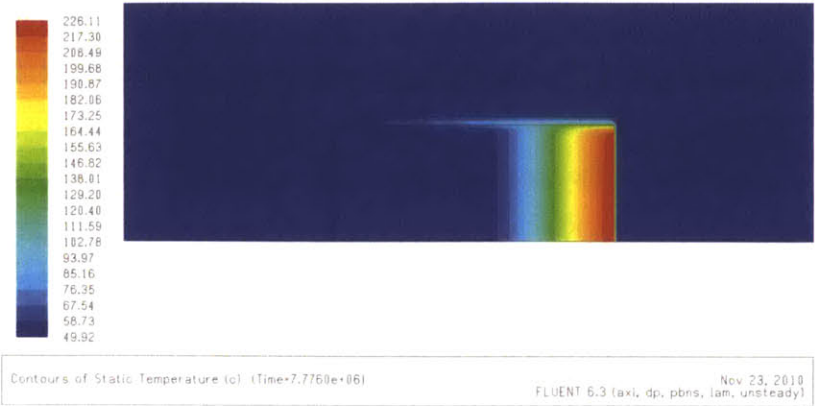
Fig.3-15 Transient Temperature Contour During a Charging Process: Case No.1:

Length=300m, Radius=125m: Time=90Days

109.23
106.26
103.29
100.33
97.36
94.39
91.43
88.46
85.49
82.53
79.56
76.59
73.62
70.66
67.69
64.72
61.76
58.79
55.82
52.86
49.89

Contours of Static Temperature (c) (Time=1.0368e+07)   Nov 23, 2010
                                                    FLUENT 6.3 (axi, dp, pbns, lam, unsteady)

Fig.3-16 Transient Temperature Contour During a Charging Process: Case No.1:

Length=300m, Radius=125m: Time=120Days

89.30
87.33
85.36
83.38
81.41
79.44
77.47
75.49
73.52
71.55
69.58
67.60
65.63
63.66
61.69
59.71
57.74
55.77
53.80
51.82
49.85

Contours of Static Temperature (c) (Time=1.2960e+07)   Nov 23, 2010
                                                    FLUENT 6.3 (axi, dp, pbns, lam, unsteady)
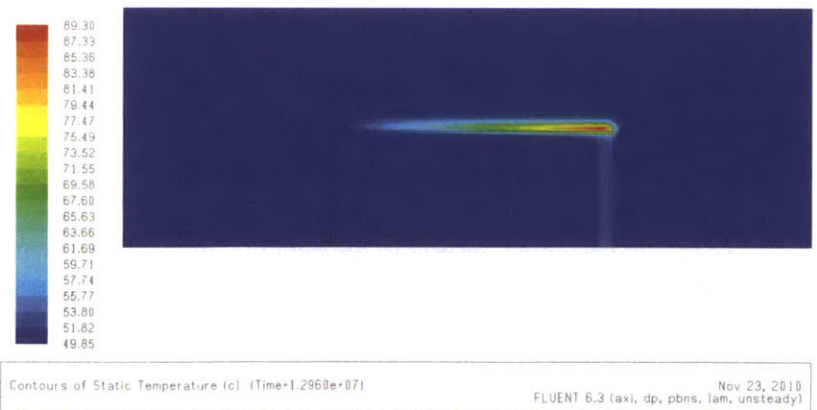
Fig.3-17 Transient Temperature Contour During a Charging Process: Case No.1:

Length=300m, Radius=125m: Time=150Days

As illustrated in Fig.3-13~3-17, cold water injected at the inlet of a reservoir pushes hot water inside the reservoir to the outlet. The hot water is fed into geothermal power plants to produce electricity. Unlike the charging process, outlet temperature of a reservoir has significant design importance. This is because as mentioned, the outlet temperature is the temperature that is used to produce electricity, meaning that the efficiency of the coupled geothermal power plants, hence overall cycle efficiency, is determined by the outlet temperature. Hence, from the operational point of view, the duration of the discharging process should be determined based on monitoring of the outlet temperature, so that the discharging process is stopped when temperature at the outlet drops below the limit for economic production of electricity.
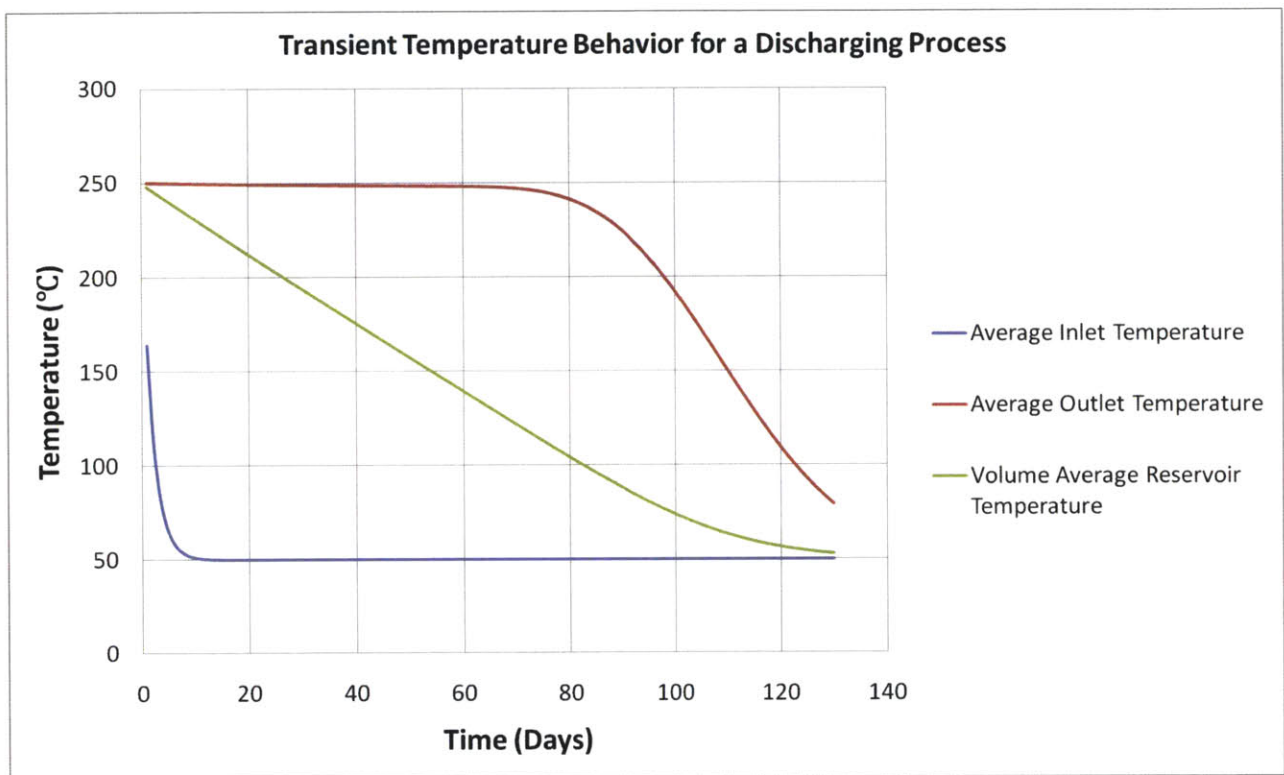
Fig.3-18 Transient Temperature Behavior for the Reservoir Case No.16

As illustrated in Fig.3-18, volume average reservoir temperature drops linearly until average outlet temperature starts to drop. The time the reservoir outlet temperature starts to drop (around 60 days in Fig.3-18) is when everywhere in a reservoir is cooled down from the initial temperature. From the reservoir operation point of view, marginal discharging after the beginning of outlet temperature decrease does not discharge the reservoir as effectively as the moment before. This can be simply read from the decreasing absolute gradient of volume average reservoir temperature with respect to temperature. Also,

74

efficiency of geothermal power plants starts to decrease with decreasing outlet temperature. Like the charging process, early stopping of the discharging process upon the outlet temperature decrease will unfavorably introduce a functionally dead volume fraction in the reservoir. Hence, in the actual reservoir operation, a careful judgment between dead volume reduction and power production in geothermal power plants should be made to determine the optimal discharging period for a reservoir in a grid. Determining such an ideal discharging process period is not within the scope of this study, as it requires analyses beyond preliminary design. In this study, consistent with the charging process reference period, the time for a reservoir to discharge 94% of its stored energy in rock is selected as the reference discharging process period for the purpose of preliminary design studies. u_{CFD} is the thermal front velocity calculated by the CFD simulation.

$$u_{CFD} = \frac{\text{Length of Reservoir}}{\text{Time for reservoir to be discharged to 94\% of maximum rock storage capacity}}$$

Eq.3-30

Hence, achieving 94% of maximum energy storage capacity of rock can be expressed as follows:

$$0.94 = \frac{E_{Discharged}}{E_{Stored_{Max}}} = \frac{T_{ref} - \bar{T}_{rock}(\tau)}{T_{ref} - T_{injecting}}$$

Eq.3-31

Equation.3-31 can be arranged to obtain the thermal front velocity as follows:

$$\bar{T}_{rock}(\tau) = T_{ref} - 0.94(T_{ref} - T_{injecting})$$
$$= 0.94T_{injecting} + 0.06T_{ref}$$

Eq.3-32

Eq.3-32 can be used to tell us the required average temperature of reservoir when the reservoir is fully charged, thus the corresponding time, τ.

$T_{injecting}$ and T_{ref} are design parameters. Time for a reservoir to reach the volume average temperature that gives 6% of minimum rock energy storage capacity - τ - is found from the FLUENT results. Then, according to Eq.3-30, length of a reservoir is divided by τ to give thermal front velocity. Table 3-4 summarizes analytical & CFD obtained thermal front velocities.

Table 3-4 Analytical & CFD Obtained Thermal Front Velocities

	Case No	Analytical Model		CFD Model	
		Thermal Front Velocity (cm/sec)	Thermal Front Velocity (m/day)	Thermal Front Velocity (cm/sec)	Thermal Front Velocity (m/day)
Charging Case	1	4.51E-05	3.90E+00	4.47E-05	3.86E+00
	2	4.59E-05	3.97E+00	4.63E-05	4.00E+00
	3	1.80E-04	1.56E+01	1.75E-04	1.15E+01
	4	1.61E-04	1.39E+01	1.63E-04	1.41E+01
	5	4.27E-05	3.69E+00	4.27E-05	3.69E+00
	6	4.57E-05	3.95E+00	4.61E-05	3.98E+00
	7	2.09E-04	1.81E+01	2.01E-04	1.74E+01
	8	5.71E-05	4.93E+00	4.98E-05	4.30E+00
	9	6.56E-05	5.67E+00	6.43E-05	5.56E+00
	10	8.60E-05	7.43E+00	8.57E-05	7.41E+00
Discharging Case	11	1.18E-04	1.02E+01	1.10E-04	9.52E+01
	12	1.09E-04	9.42E+00	1.04E-04	9.00E+00
	13	1.00E-04	8.64E+00	9.65E-05	8.33E+00
	14	8.89E-04	7.68E+00	8.27E-05	7.14E+00
	15	4.47E-05	3.86E+00	4.20E-05	3.63E+00
	16	3.32E-05	2.87E+00	3.13E-05	2.70E+00
	17	3.77E-05	3.26E+00	3.65E-05	3.16E+00
	18	2.24E-04	1.94E+01	2.04E-05	1.76E+01
	19	2.47E-04	2.13E+01	2.28E-04	1.97E+01
	20	9.27E-05	8.01E+00	8.85E-05	7.64E+00

The following graphs compare analytically obtained thermal front velocities, Table 3-2 with CFD thermal front velocities, Table 3-4.
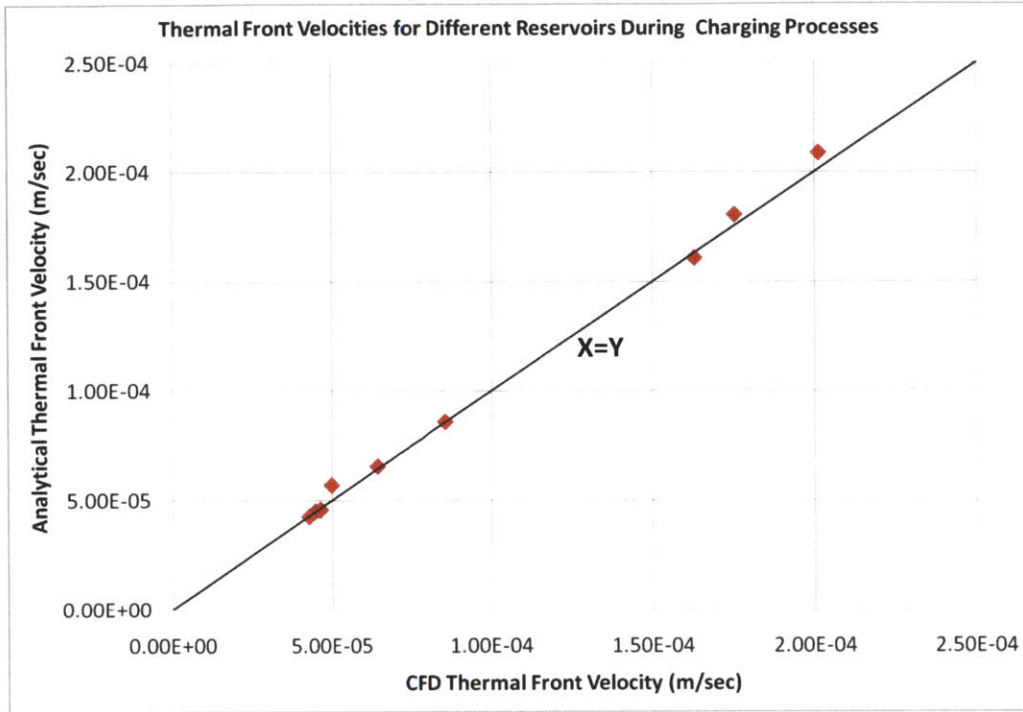
Fig.3-19 Thermal Front Velocity Comparisons for Ten Different Reservoirs: Charging Processes
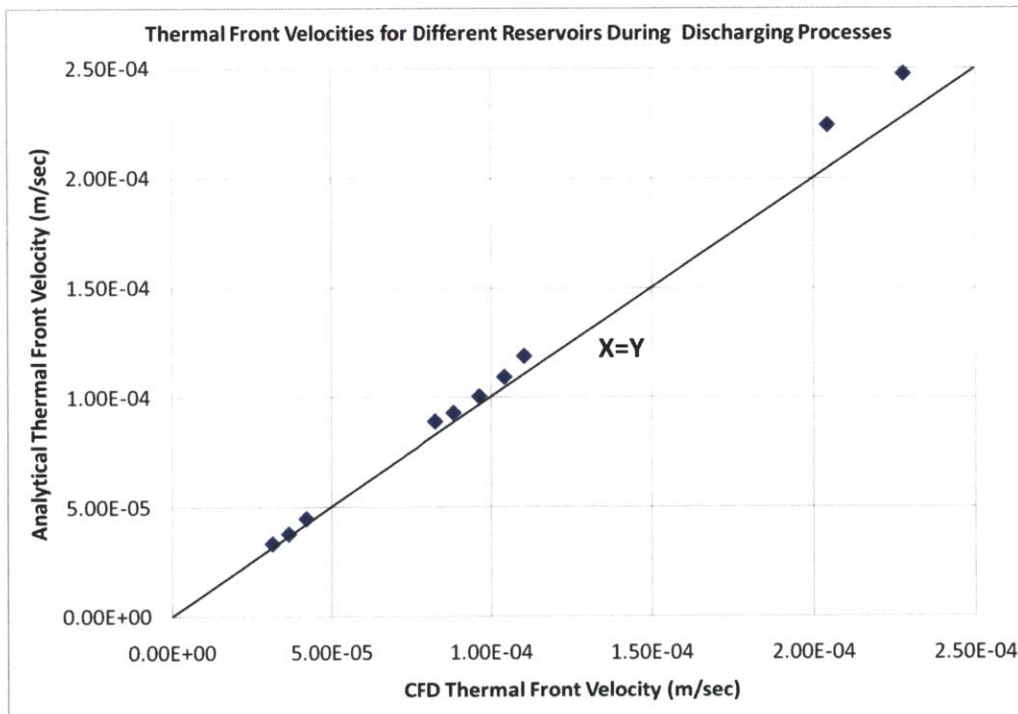
Fig.3-20 Thermal Front Velocity Comparisons for Ten Different Reservoirs: Discharging Processes

Analytically obtained thermal front velocities are in good agreement with CFD obtained thermal velocities within the tested design parameters, which are realistic for the actual system. This finding greatly facilitates designing the nuclear geothermal system as thermal front velocities obtained from the point model can be readily used for the preliminary design process with the analytical understanding of relationships between design parameters. Use of thermal front velocity of a reservoir for preliminary design is addressed in section 3.8.

3.5.2 Storage Size

Thermal energy in a reservoir is stored either in rock or water. Hence, the overall thermal storage of a reservoir is the sum of the thermal energy stored in both rock and water.

$$E_{stored} = E_{Rock} + E_{Water}$$

Eq.3-33

Thermal energy stored in rock and water can be expressed as follows:

$$E_{stored} = V_{reservoir}(1 - \varepsilon)\bar{\rho}_{rock}\overline{C_{p_{rock}}}(T_{hot} - T_{cold}) + V_{reservoir}\varepsilon\bar{\rho}_{water}\overline{C_{p_{water}}}(T_{hot} - T_{cold})$$

Eq.3-34

Eq. 3-34 can be rearranged as the following equation

$$E_{stored} = V_{reservoir}(T_{hot} - T_{cold})\left((1 - \varepsilon)\bar{\rho}_{rock}\overline{C_{p_{rock}}} + \varepsilon\bar{\rho}_{water}\overline{C_{p_{water}}}\right)$$

Eq.3-35

where V, T, ε, ρ and Cp are volume, temperature, porosity and specific heat at constant pressure of the corresponding subscript. It is assumed that rock and geo fluids reach the same temperature upon contact, hence they both experience the same temperature variation. It can be seen from Eq.3-34 and 3-35 that thermal energy stored is evaluated with respect to the reference temperature, T_{cold}. The reference temperature, T_{cold} is the lowest temperature of a reservoir, which is equivalent to the cold piston temperature of a reservoir. The cold piston temperature is determined by the condensing temperature of a geothermal power plant.

It is evident that the temperature difference of a reservoir, $(T_{hot} - T_{cold})$ determines the amount of thermal energy storage for a given reservoir. Increasing the temperature difference, hence the hotter the injecting water temperature from the nuclear power plant, and the colder the condensing temperature of a geothermal power plant, increases thermal energy storage content of a reservoir.

It can be seen in Eq.3-34 that porosity is the parameter that determines the relative amount of thermal energy stored in water and rock. Porosity of a geology gives the fraction of fluids with respect to the total volume. Although the volumetric fraction of fluids in a hydro-fractured geology is small, the large thermal capacity of water makes it necessary to take into account energy storage in water along with that of the rock. The following equation and figure show the ratio of energy storage in water and rock.

$$\frac{E_{water}}{E_{Rock}} = \frac{V_{reservoir}\varepsilon\bar{\rho}_{water}\overline{C_p}_{water}(T_{hot} - T_{cold})}{V_{reservoir}(1 - \varepsilon)\bar{\rho}_{rock}\overline{C_p}_{rock}(T_{hot} - T_{cold})} = \frac{\varepsilon\bar{\rho}_{water}\overline{C_p}_{water}}{(1 - \varepsilon)\bar{\rho}_{rock}\overline{C_p}_{rock}}$$

<div align="center">Eq.3-36</div>
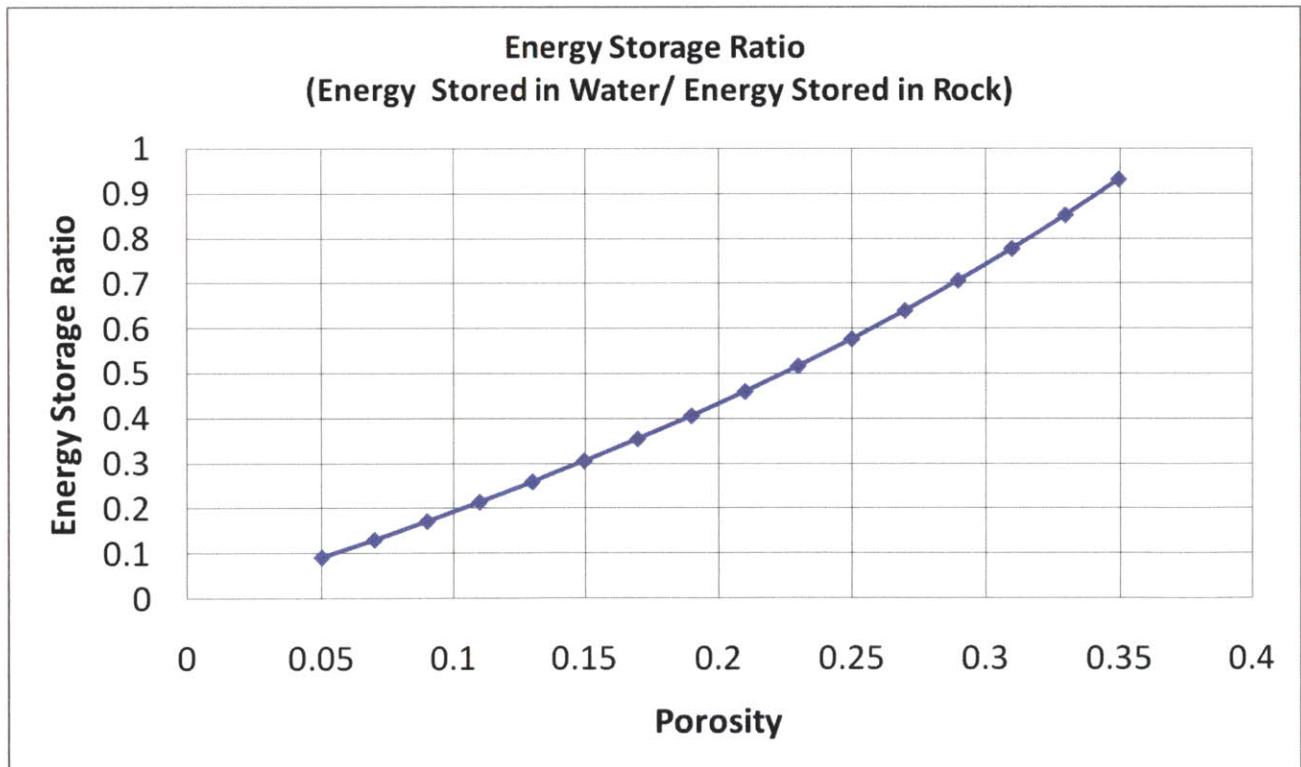
<div align="center">Fig.3-21 Ratio of Energy Storage in a Reservoir</div>

Table 3-5 Parameters Used to Calculate Ratio of Energy Storage in a Reservoir

Fixed Parameters	Values
Density of Water ($\bar{\rho}_{water}$) (at 250°C)	850 kg/m^3
Specific Heat of Water ($\bar{C}_{p_{water}}$)	4500 J/kg-K
[Density * Specific Heat]$_{Water}$ ($\bar{\rho}_{water} * \bar{C}_{p_{water}}$)	3825E3 J/K-m^3
Density of Rock ($\bar{\rho}_{rock}$)	2600 kg/m^3
Specific Heat of Rock ($\bar{C}_{p_{rock}}$)	850 J/kg-L
[Density * Specific Heat]$_{Rock}$ ($\bar{\rho}_{rock}\bar{C}_{p_{rock}}$)	2252.5E3 J/K-m^3

A typical range of porosity associated with the target permeability of a nuclear-geothermal reservoir (greater than 1 Darcy), is between 0.1 ~ 0.25 [12]. In that range of porosity, energy stored in water is not negligible to that of rock, as it amounts 20~65% of energy stored in rock. In the case of a block-caved reservoir, whose porosity is around 0.35[12], the amount of energy stored in water is fairly equivalent to that of rock. Hence, conceptually speaking, nuclear-geothermal energy storage system becomes more or less hydrothermal storage as porosity increases. A block caved reservoir is an extreme example that significantly relies on water for energy storage.

Understanding the parameters that determine energy storage size, Eq.3-35 is used to evaluate energy storage size in Chapter 4 for the design studies.

3.5.3 Cycle Periods

Charging and discharging periods of the nuclear geothermal system are essentially determined by the requirements of the electrical grid. The status of a grid, in the context of cycle periods – specifically, the availability of charging energy during the off peak season and the demand for seasonally peak power electricity[13]. From the view point of the design, meeting such a desired cycle period requires understanding of the reservoir behavior. Cycle length can be mathematically expressed as follows:

$$\text{Cycle length } (\tau) = \frac{\text{Length of Reservoir}}{\text{Thermal Front Velocity}} = \frac{V_{reservoir}\left[\epsilon\bar{\rho}_{water}\bar{C}_{p_{water}} + (1 - \epsilon)\bar{\rho}_{rock}\bar{C}_{p_{rock}}\right]}{\dot{m}\bar{C}_{p_{water}}}$$

Eq.3-37

---

[12] Porosity of block caved reservoir is assumed to be that of a randomly packed bed with spheres [20]
[13] Our analysis is based on seasonal electricity storage; however, actual operations will be highly variable. Most of the heat input would be during the seasons of low electrical demand with more heat inputted at night when electrical demand is lowest. Similarly, output is likely to be variable on a daily basis.

Thermal front velocity, which is found to yield the time for a reservoir to charge or discharge 94% of reservoir capacity is used in Eq. 3-37. One can see that Eq.3-37 is basically the same expression as Eq.3-24 and Eq-30. It implies that the cycle length represents the time for a reservoir to charge to 94% of the full reservoir capacity (during a charging process) or to discharge to 94% of the stored energy (during a discharging process). Although real cycle lengths of nuclear geothermal systems could be different from the cycle length defined in this study, depending on the operation scheme of a reservoir, the cycle length defined here is sufficiently representative of general reservoir operation and design.

Equation.3-37 can be rearranged to give the required mass flow rate to meet a cycle length for a given reservoir as follows:

$$\dot{m} = \frac{V_{reservoir}\left[\epsilon\bar{\rho}_{water}\overline{C_{p_{water}}} + (1 - \epsilon)\bar{\rho}_{rock}\overline{C_{p_{rock}}}\right]}{\overline{C_{p_{water}}}\,\tau}$$

Eq.3-38

By introducing the stored energy term expressed in Eq3-35, Eq.3-48 can be further rearranged to a form that is useful for the preliminary design purpose as follows:

$$\dot{m} = \frac{E_{stored}\left[\epsilon\bar{\rho}_{water}\overline{C_{p_{water}}} + (1 - \epsilon)\bar{\rho}_{rock}\overline{C_{p_{rock}}}\right]}{\overline{C_{p_{water}}}\,\tau(T_{hot} - T_{cold})\left((1 - \epsilon)\bar{\rho}_{rock}\overline{C_{p_{rock}}} + \epsilon\bar{\rho}_{water}\overline{C_{p_{water}}}\right)}$$

Eq.3-39

It is worth noting that the temperature averaged properties in Eq.3-39 are a sole function of reservoir temperature, T_{hot} and T_{cold}. Hence, Eq.3-39 essentially describes the following relation for a given geology of a reservoir:

$$\dot{m} = f(E_{stored}, T_{hot}, T_{cold}, \tau)$$

Eq.3-40

Required mass flow rate to meet target energy storage, hot and cold piston temperatures and cycle length can be obtained using Eq.3-39. Such a relationship between the design parameters of a nuclear geothermal system is exploited for the preliminary design studies addressed Chapter 4.

3.5.4 Conductive Heat Losses

Heat Loss is an important metric that could potentially determine feasibility of the nuclear-geothermal system. Heat losses can be divided into conductive heat losses and convective heat losses. Conductive heat loss occurs due to the temperature gradient between storage volume and surrounding rock while convective heat loss occurs due to energy carried out by leaking fluids. In this section, conductive heat losses are addressed.

As discussed previously, Eq.3-9 models time dependent conductive heat losses for a semi-infinite solid when the boundary surface temperature is fixed constant. This analytical model is compared with the cylindrical CFD reservoir model described in section 3.4.2, Fig.3-5, while the surface temperature of the reservoir is fixed constant. The reservoir case 11 is tested with the constant temperature of 250°C imposed on the interface surface between the reservoir and surrounding rock. Initial temperature of surrounding rock is set to be 50°C.
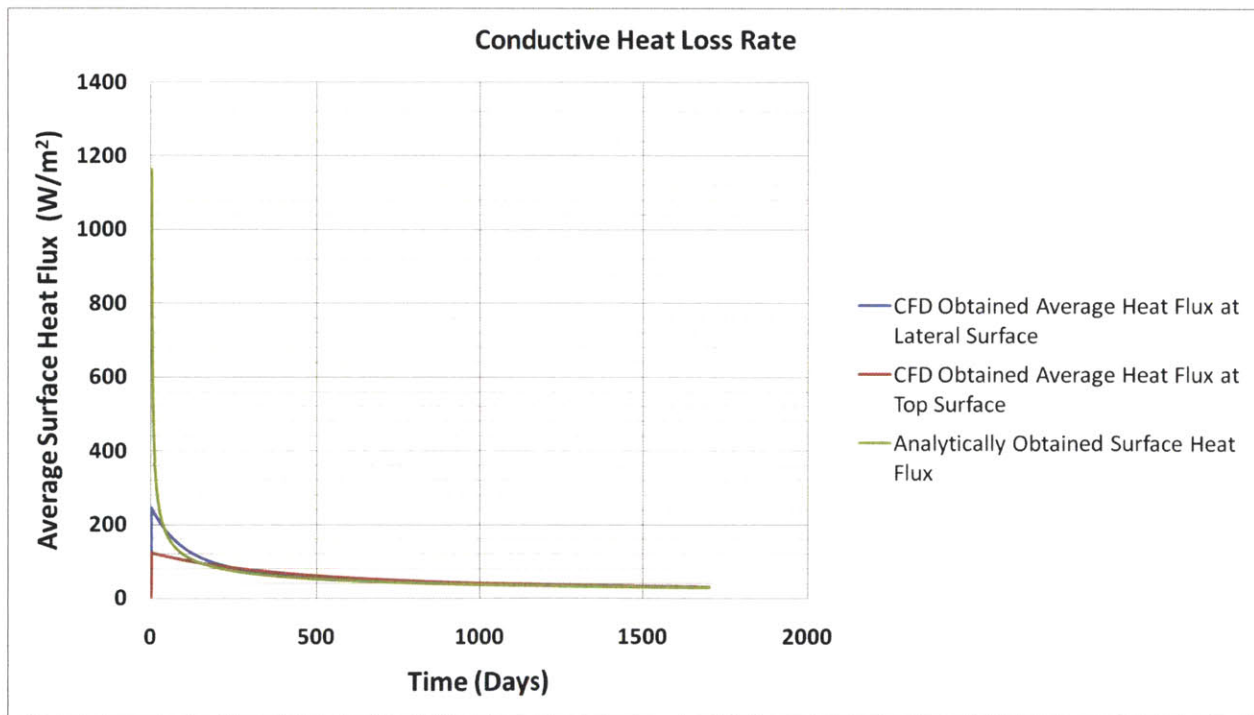
Fig.3-22 Comparison for Conductive Heat Loss Rates Obtained from CFD Simulation and Analytical Modeling

It is clear that CFD results and analytical results are in good agreement except for the early time of the transient. The analytical model excessively over-estimates heat loss rates at the early time of the transient. This can be directly read from the model expressed as Eq.3-9. As square root of time is in the denominator of the equation, heat loss rate starts at infinity when time is 0. This implies the inherent limitation of the analytical model for the use of early transient analyses. There exists a disagreement between average heat flux at the lateral surface of the reservoir and at the cap surfaces of the reservoir early in a transient, according to the CFD result. This may occur because of the different distance from the corresponding surface of the reservoir to the boundary of the surrounding rock. In the CFD model, as illustrated in Fig.3-5, the lateral surface of the reservoir sees the surrounding rock as more like an infinite medium than the cap surfaces do. Nevertheless, such a difference is not worth further modification of the CFD model or detailed analyses, as the two surfaces soon reach coincidence in terms of average heat flux rate and the difference is negligible over long periods of reservoir operation.

In reality, quantitatively assessing conductive heat losses requires more complex analyses. This is mainly due to the cyclic operation of the reservoir for charging and discharging processes. The surface temperature of the reservoir is heated up along the travel direction of hot injecting fluids during a charging process while it is cooled down along the travel direction of cold injecting fluids during a discharging process. Hence, the surface temperature of the reservoir varies at all times. During a discharging process, heat may even flow into the reservoir if surrounding rock is hotter than cold piston temperature. In addition, as illustrated in Fig.3-4, the water inlet for the charging process is opposite to the water inlet of the discharging process. This implies that the region near the inlet of the charging process remains always heated: hot fluids are injected at the inlet during the charging process and the cold fluids get heated when they reach the inlet of the charging process from the opposite side of the reservoir during the discharging process. Conversely, the region near the inlet of the discharging process remains always cooled: cold fluids are injected at the inlet during the discharging process and the hot fluids get cooled when they reach the inlet of the discharging process from the opposite side of the reservoir during a charging process.

Such complexities in the heat loss mechanism of nuclear-geothermal energy storage reservoirs were further investigated by CFD simulation of a reservoir with FLUENT 6.3. The reservoir case 11 in Table 3-2 is tested for ten full cyclic operations (Each full cycle consists of a charging and discharging process). The following table summarizes relevant operational parameters that characterize the reservoir simulation of reservoir case 11.

Table 3-5 Operational Parameters Tested for Reservoir Simulation: Case 11

Operational Parameters	Values
Hot Injecting Fluid Temperature (Hot Piston Temperature)	250°C
Cold Injecting Fluid Temperature (Cold Piston Temperature)	30°C
Initial Surrounding Rock Temperature	50°C
Charging Period	63 Days
Discharging Period	63 Days
Length of a full Cycle	126 Days

Figure.3-23 shows cyclic temperature variation at the inlet and the outlet of the reservoir during ten full cyclic operations.
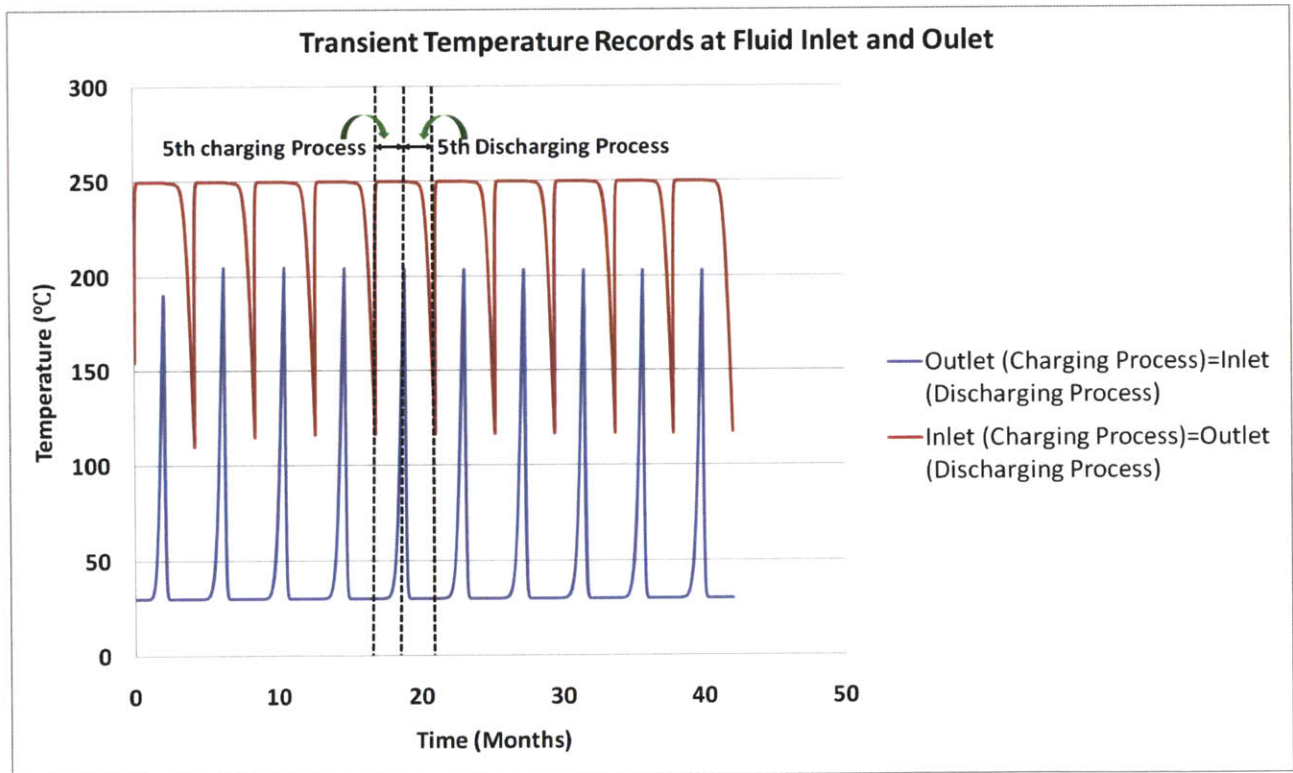
Fig.3-23 Transient Temperature Records at Fluid Inlet and Outlet: Case 11

Inlet and outlet temperature remain constantly hot or cold except for the time that the thermal front reach one end of the reservoir from the opposite end of the reservoir. Soon after the perturbation of temperature at either inlet or outlet, the process changes from charging to discharging or from discharging to charging.

The dominant fraction of conductive heat losses occurs on the lateral surface of a cylindrical reservoir model. CFD-obtained heat fluxes during 10 cycles on the lateral surface of reservoir case 11 are shown in Fig.3-24.
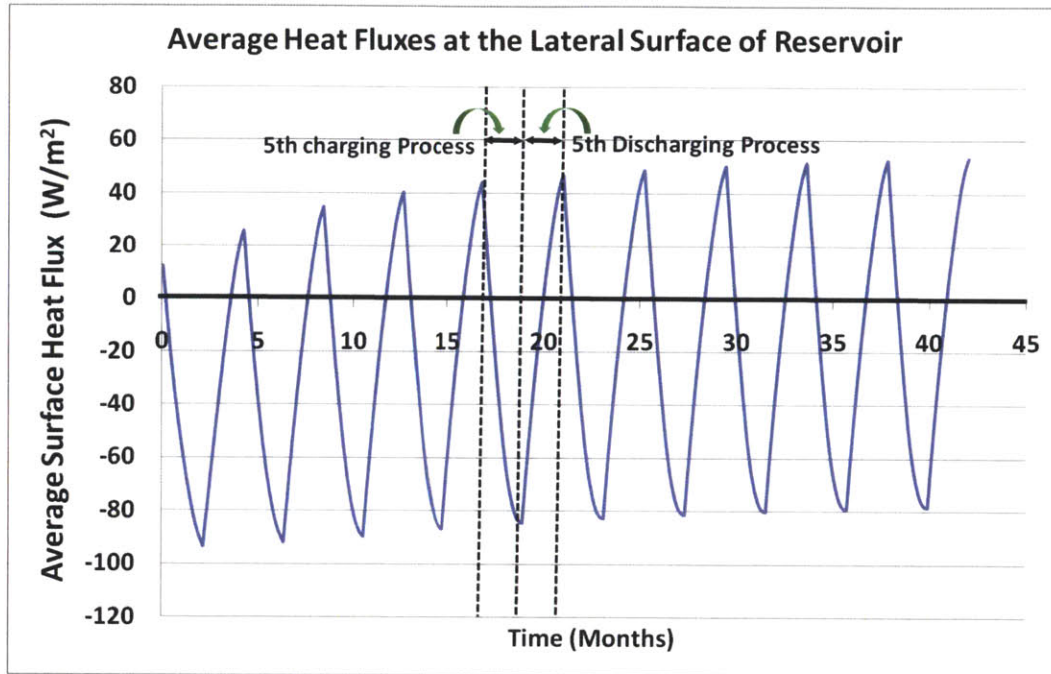
Fig.3-24 Transient Average Heat Fluxes at the Lateral Surface of Reservoir: Case 11

In Fig.3-24, negative surface heat flux represents a flow of energy from the reservoir to the surrounding rock, hence heat loss, while positive heat flux means a flow of energy from the surrounding rock to the reservoir. From the figure, a few important observations for heat loss of nuclear-geothermal energy storage systems can be made as follows:

A. Heat loss rate increases as the charging process proceeds.

During a charging process, reservoir average temperature increases, leading to an increasing temperature difference between the reservoir and surrounding rock.

B. Heat loss rate decreases during a discharging process even to a point where overall heat gain occurs.

During a discharging process, reservoir average temperature decreases, leading to a decreasing temperature difference between reservoir and surrounding rock. Overall net gain of heat usually happens during the late phase of the discharging process due to: (1)Temperature of heated surrounding rock near the interface of the reservoir is higher than the average reservoir temperature determined by the cold piston temperature, (2) Temperature of the cold piston is lower than that of the original surrounding rock.

Surrounding rock is heated during a discharging process and heated surrounding rock acts as a thermal shield for a reservoir as Fig.3-25 illustrates.
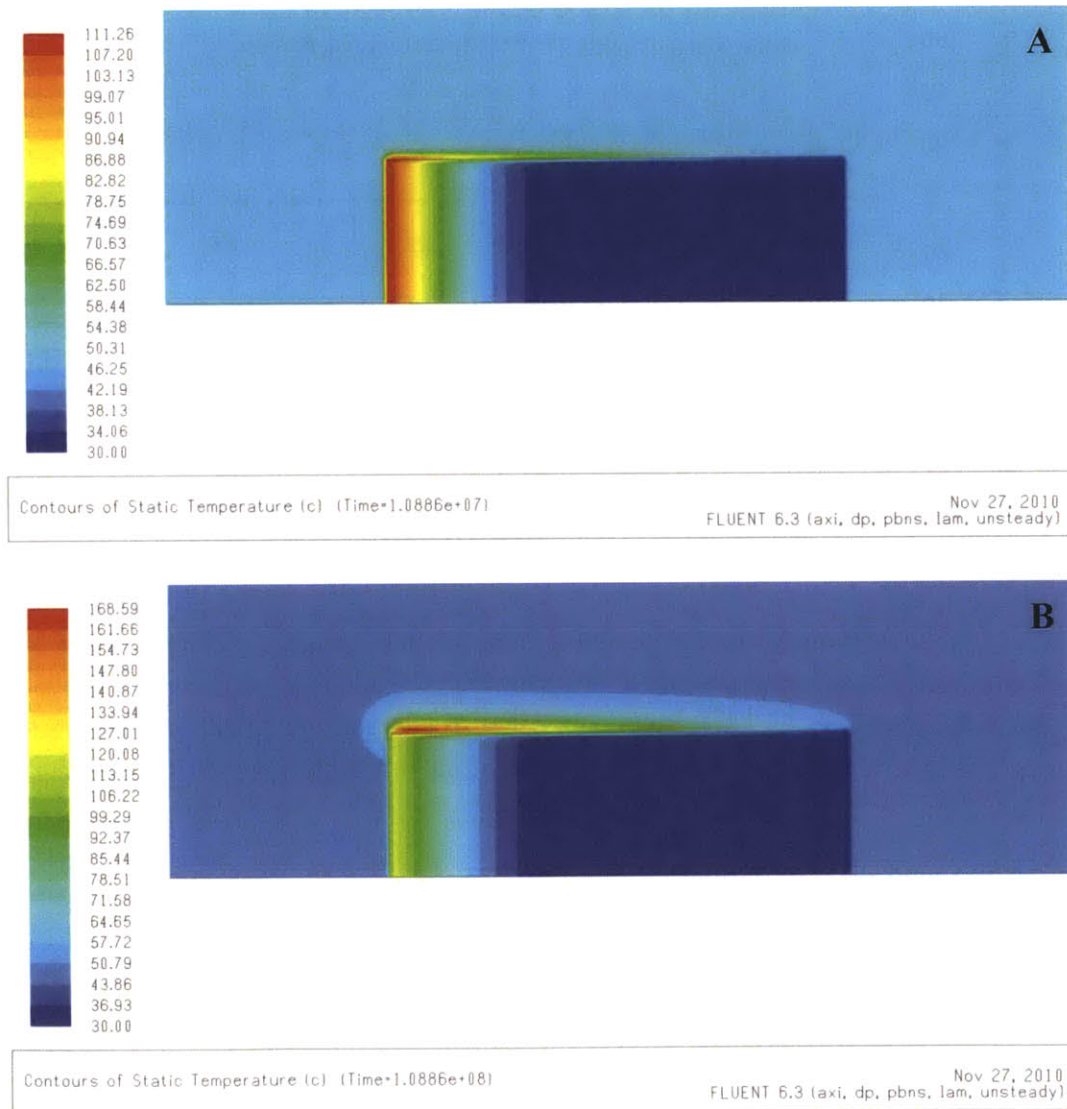
Fig.3-25 Temperature Contour of Reservoir Case 11- A: End of 1st Cycle B: End of 10th Cycle

It can be seen that the periphery of surrounding rock is heated as a result of the charging process. The heated rock makes the reservoir gain (net) thermal energy during the late period of a charging process. Such thermal shielding effects become more significant as the reservoir operating lifetime increases. As graphically illustrated in Fig.3-25, the degree of thermal shielding is more enhanced for the end of the 10th cycle compared to the end of the 1st cycle. This is because surrounding rock, whose initial temperature is initially closer to cold piston temperature than hot piston temperature, gains more heat during a charging process than it loses during a discharging process. Therefore, thermal shielding effects become more significant with the lifetime of the system. Thermal shielding effect is a local phenomenon. As can be seen from Fig.3-25, the region near the inlet of the charging process (outlet of discharging process), remains heated at all times, hence leading to a surrounding rock temperature increase. The locally enhanced thermal shielding effect near the inlet of the charging process causes a locally concentrated thermal energy gain in a reservoir during a discharging process.

The relative temperature difference between initial surrounding rock and cold piston also affects the rate of heat flux at the surface of a reservoir. For instance, if surrounding rock temperature at the reservoir burial depth is greater than cold piston temperature, heat gain into the reservoir occurs without the aid of a thermal shielding effect during a discharging process. It is worth noting however, that, such an effect due to the temperature difference between the initial reservoir and cold piston temperature is of second order importance compared to the thermal shielding, in terms of heat loss rate. This is because the thermal shielding effect dominantly takes place after a few cyclic operations. Hence the difference in surface heat fluxes between the reservoir whose cold piston temperature is colder than initial surrounding rock temperature and the reservoir whose cold piston temperature is hotter than the initial surrounding rock temperature dies out after a few cyclic operations. Therefore, hot piston temperature, which dominantly determines the degree of thermal shielding of a nuclear-geothermal reservoir, is the main design parameter that controls heat loss rate of a reservoir with given dimensions.

C. A startup energy cost of a nuclear geothermal system exists due to the comparatively high heat loss rate for the early phase of reservoir operation. Asymptotical heat loss rate sets in soon after the early phase of reservoir operation. Amount of heat gain is comparable to amount of heat loss after the asymptotic heat loss rate sets in.

Rate of heat loss is comparatively higher for the early phase of reservoir operation because the thermal shielding effects enhance with reservoir operation time. Such a fact can be translated as a startup cost of the system. Soon after the early phase of reservoir operation, heat fluxes reach the

asymptotic region. Such a trend can be seen by tracking the values of the peak heat loss and peak heat gain rate at each cycle of Fig.3-24. Results are shown in Fig.3-26.
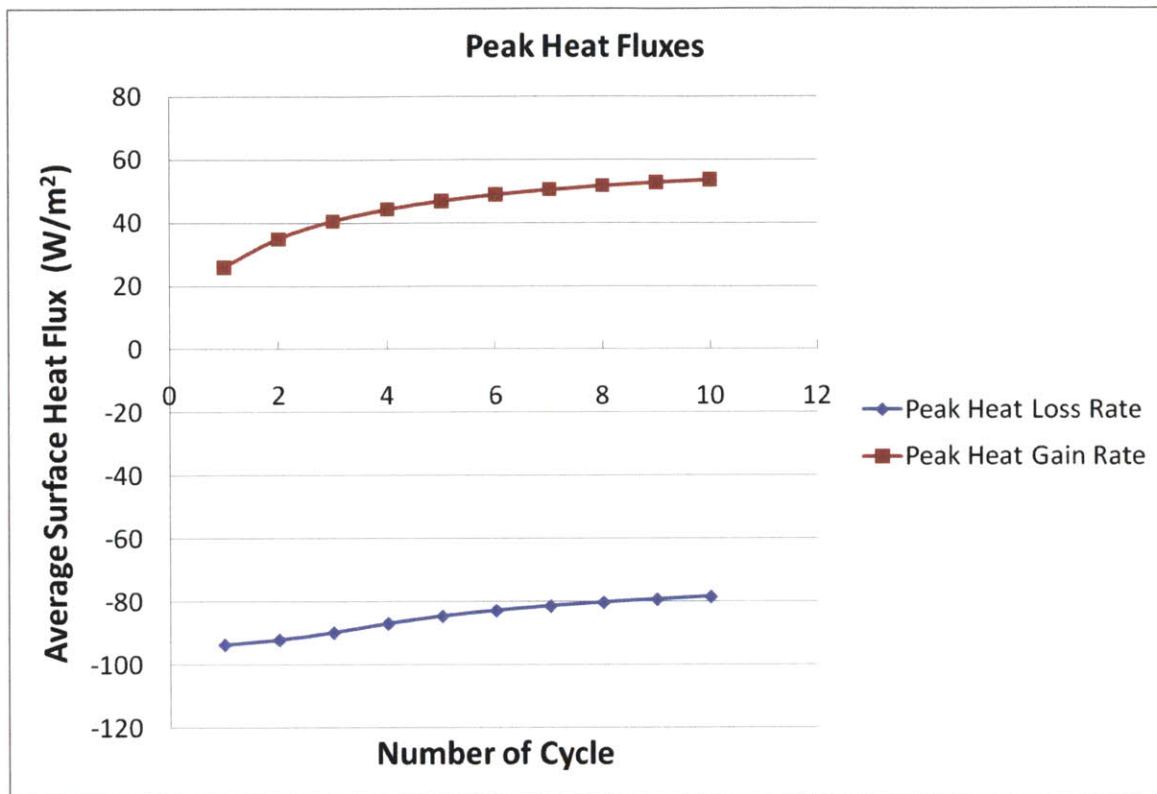
Fig.3-26 Peak Average Surface Heat Fluxes for Loss and Gain

As can be seen in Fig.3-26, heat fluxes for both gain and loss behave asymptotically with the increasing number of cycles. An important observation is that after the first few cycles of operation, the amount of heat gain is comparable to the amount of heat loss for a cycle. This can be evidenced by the relative size of the area of the curve above zero and the area of the curve below zero after a few initial operations. This implies that, if heat loss matters, it is likely to be a problem of the initial phase of reservoir operation.

Given an understanding of the general behavior of the nuclear geothermal reservoir in terms of heat loss, exploring the amount of heat loss with respect to the reservoir storage size determines the importance of heat loss in the design of a nuclear-geothermal reservoir. Figure.3-27 illustrates the average surface heat rate that is obtained by multiplying the lateral surface area with the identified heat flux shown Fig.3-24.
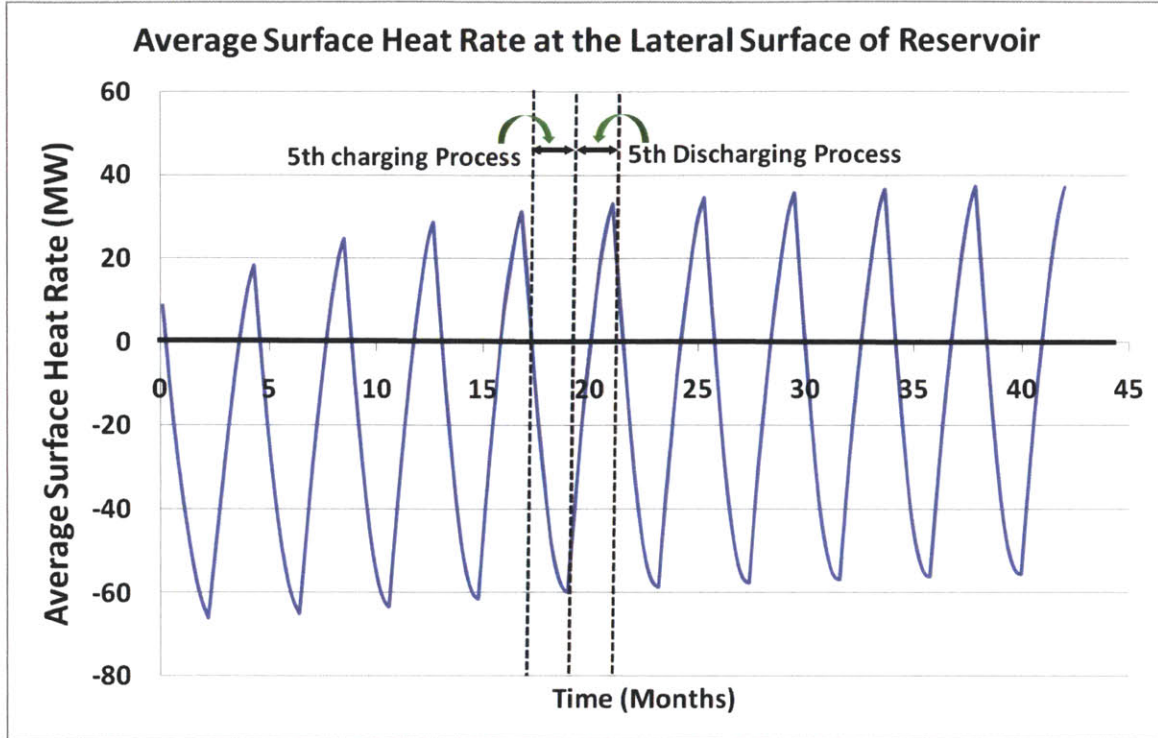
Fig.3-27 Average Surface Heat Rate at the Lateral Surface of the Reservoir: Cycles of No.11
Reservoir Length: 600m, Diameter: 187.5m

The range of a typical geothermal power plant's thermal power rating is 10MW~100MW [6]. According to Fig.3-27, heat loss rate is comparable to that of a typical geothermal power plant. This implies that during the operation of a nuclear geothermal system, an amount of power that is equivalent to the size of a typical geothermal power plant can be dumped to the environment through conductive heat loss. The following figure shows the amount of net thermal energy loss of reservoir case 11 for each cycle, which is basically obtained by summing up the average surface heat rate of each cycle with respect to time as the following expression shows:

$$Q_{cycle,j} \cong \sum_{i=1}^{I} q_i \Delta t$$

Eq.3-41

Where q_i is average surface heat rate at the i th time in the CFD simulation (see Fig.3-27), Δt is the time step for the transient simulation[14], and I is the total number of time steps for each cycle.

---

[14] A day (24 hours) was used for the CFD simulations of this study
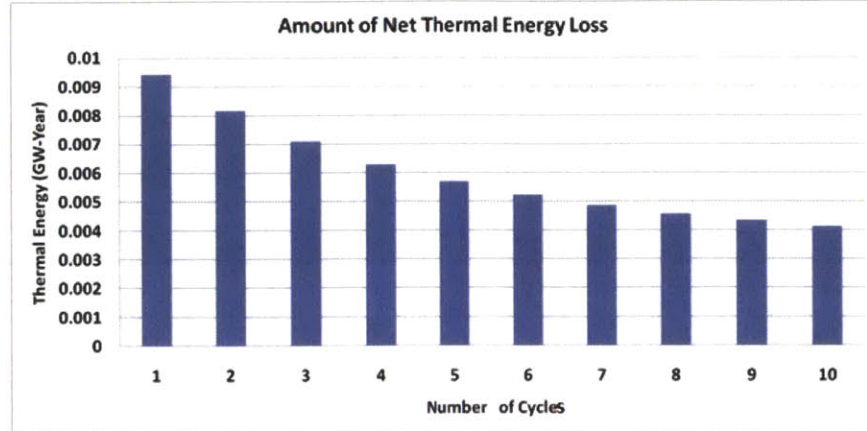
Fig.3-28 Amount of Net Conductive Thermal Energy Loss for Reservoir Case 11
with Heat Storage Capacity of 1.1 GW(th)-year

Each bar in Fig.3-28 takes into account every heat loss and heat gain phase for a corresponding cycle. Hence, despite thermal shielding effects, thermal energy is still lost, but with decreasing amount, with respect to increasing operation time as shown.

The amount of thermal energy stored in reservoir case 11, according to Eq.3-35, is found to be 1.07GW-Year. The absolute amount of the net thermal energy losses shown in Fig.3-28 is divided by the total thermal storage size to give the fraction of thermal energy loss as follows:

$$\alpha_J = \frac{\sum_1^J Q_{cycle,j}}{J \times E_{stored}}$$

Eq.3-42

Equation.3-42 shows that cumulative net thermal energy loss is a fraction of cumulative thermal storage amount at cycle number J, and results are shown in Fig.3-29.

Fractional Thermal Energy Loss
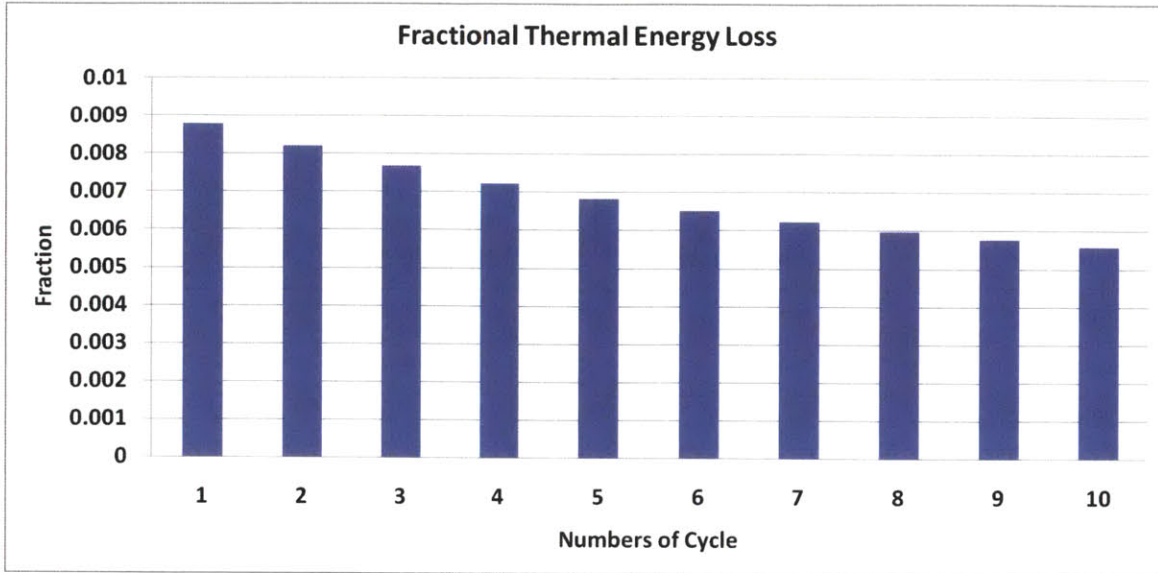
Fig.3-29 Amount of Net Conductive Thermal Energy Loss for Reservoir Case 11

Figure.3-29 indicates that the fraction of thermal energy loss by conduction is less than 1% of the total amount of heat storage. Such a low fraction of conductive energy is due to the large charging power rate compared to heat loss rate. In a typical nuclear geothermal energy storage system, a few tens of megawatt of heat loss rate is negligible compared to a few thousands of megawatts of charging power rate.

Fractional thermal energy loss, however, becomes increasingly important with decreasing storage size. In order to explore the storage sized dependent fractional heat loss, the following three reservoirs which differ only by storage size are tested.

Table 3-6 Design Features of Tested Reservoirs for Fractional Thermal Energy Loss

Reservoir Number	1	2	3
Storage Size (GW(th)-year)	0.90	0.13	0.013
Volume of Reservoir	54,862,841 m³	7,837,543 m³	783,750 m³
Diameter	285m	149m	69m
Length	861m	450m	209m
Hot Piston Temperature	250°C		
Cold Piston Temperature	50°C		
Porosity	0.2		
Diameter to Length Ratio	0.331		
Cycle Length	6months (3months charging, 3months discharging)		
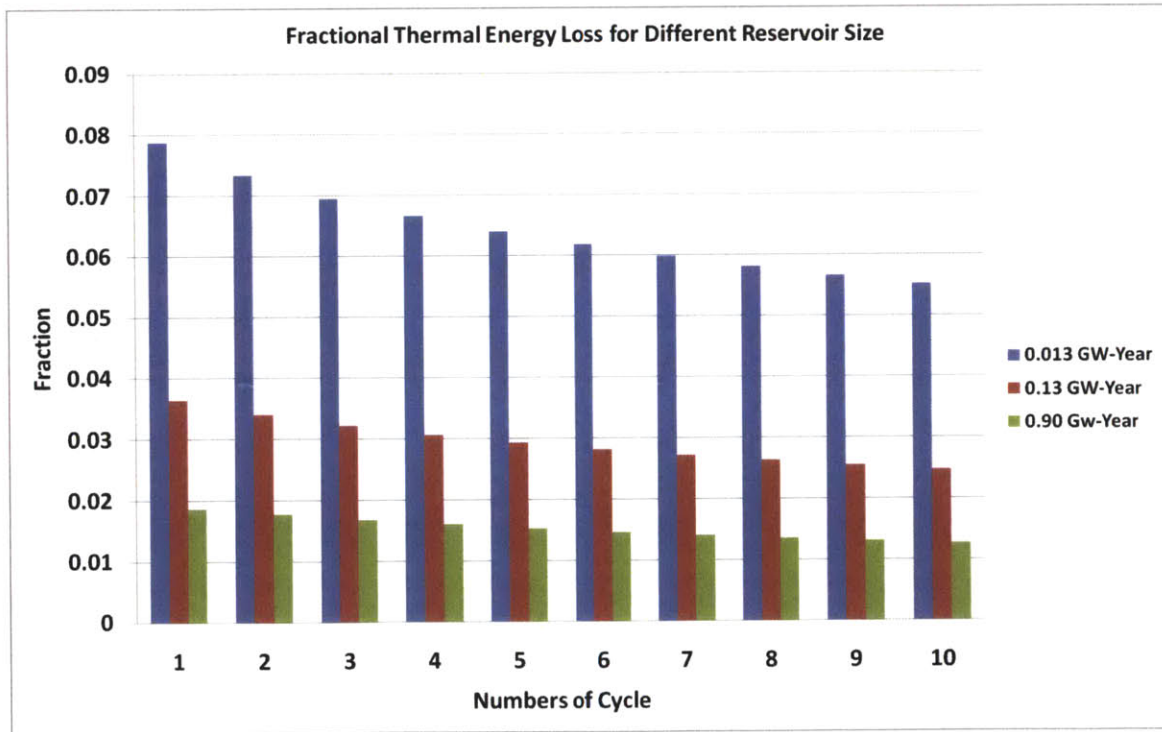
Fig.3-30 Fractional Thermal Energy Loss for Three Different Reservoir Sizes

General trends and design implications of the nuclear geothermal heat storage system can be studied using the results shown in Fig.3-30. Heat loss affects the performance of a nuclear geothermal heat storage system only for a small scale of heat storage. This justifies that underground heat storage intrinsically works only on seasonal storage scale. A small amount of energy storage is not compatible with the concept of underground heat storage unless the reservoir is sealed with an insulator or buried at a deep depth so that the temperature of surrounding rock matches that of the hot reservoir. Both of these options, however, are not practical from the viewpoint of economics[15].

As clearly illustrated, fractional thermal energy loss takes up only a small percent (~1%) of total thermal storage size for storage scales that are compatible with seasonal storage (order of a few GW-year)[16]. Even for the smallest tested storage size in Fig.3-30, 0.013Gw-Year, which is much smaller than typical seasonal energy storage requirements, the heat loss fraction is around 5%. Hence, as far as energy storage scales comparable to seasonal storage requirements are concerned, fractional energy loss through conduction bears negligible importance in the overall system performance.

Hence, developing an analytical heat loss model that appropriately captures the conductive heat loss mechanism is not required for a preliminary design study of a nuclear-geothermal heat storage system. In this study whose primary focus is seasonal heat storage, fractional heat loss rate is assumed to be negligible.

---

[15] The significant cost associated with drilling is addressed in chapter 4.
[16] Detailed studies of seasonal heat Storage size are addressed in chapter 4.

3.5.5 Pressure Drop

The strong dependency of water viscosity on temperature has implications on pressure drop across the reservoir. Figure.3-31 illustrates water viscosity as a function of temperature, and a fitted line to the points.
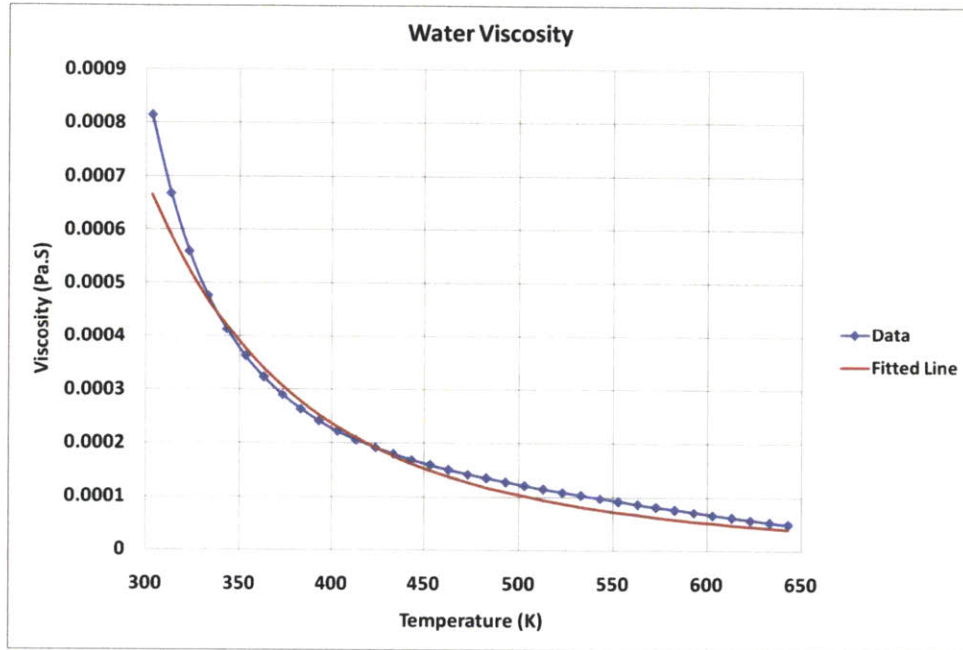
Fig.3-31 Temperature Dependent Water Viscosity

As can be seen in Fig.3-31, viscosity of water differs by more than eight-fold between 300K (26.85°C) and 600K (326.85°C). The viscosity can be fitted by the following power law equation:

$$\mu = \frac{1205000}{T^{3.73045}}$$

Eq.3-43

Where μ is viscosity in Pa.S and T is temperature in Kelvin.

This implies that the pressure drop, hence required pumping power, differs by roughly a factor of eight between the charging and discharging processes. The following figure illustrates time dependent pressure drop during a cycle of reservoir operation.
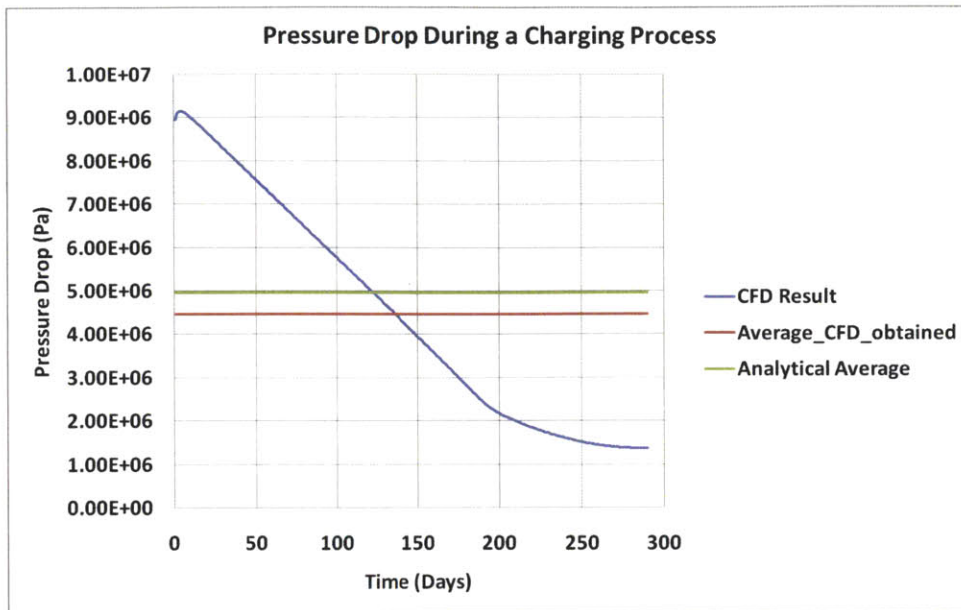
Fig.3-32 Time Dependent Pressure Drop during a Charging Process: Reservoir Case#1

In the beginning of a charging process, pressure drop is the maximum. This is because the reservoir is filled with cold water, which is almost eight times "thicker" than hot water. As hot water injection proceeds, pressure drop decreases accordingly because it replaces cold water in the reservoir.

From the design point of view, the maximum pressure drop, hence the maximum pumping power, determines the size of the pump for the system. The average pressure drop, hence the average pumping power is an important measure of average parasitic energy required to run the system.

As can be seen in Fig.3-32, pressure drop decreases linearly before time reaches a certain point (around 200 days in this case). This time - the pressure drop deviates from the linear behavior with respect to time - is when the everywhere in the reservoir has experienced temperature change. Hence, as discussed in section 3.5.1, the constant heat injection rate at the inlet no longer leads to a linear average reservoir temperature change, hence, the pressure drop deviates from the linearly decreasing behavior. Nevertheless, understanding that the time for the pressure tailing is comparatively short and does not significantly deviate from the linearly decreasing trend, the average pressure drop can be approximated assuming that the pressure decreases linearly during a process (for both charging and discharging).

$$\overline{\Delta P} \cong \frac{P_{max} + P_{min}}{2}$$

Eq.3-44

The analytical pressure drop tends to overestimate the real pressure drop by roughly 10% as it does not take into account the tailing effect. The difference is not significant for the purpose of preliminary design studies.

3.5.6 Water Loss

It is expected that a certain fraction of water in the nuclear-geothermal reservoir leaks to the surrounding rock. The water leakage bears importance in the system design mainly for the following two reasons:

A. Water leakage makes the nuclear-geothermal reservoir deviate from a perfectly closed system in terms of mass. Hence, a water make-up system is needed.
B. When water leaks, it carries out energy with it. Hence, it is another energy loss mechanism in addition to besides conductive heat loss.
C. Leaked water could potentially cause environmental effects in the surrounding geology.

In this section, water leakage, hence associated energy loss, is quantitatively evaluated based on the analytical model introduced in section 3.3.5. Degree of reservoir pressurization due to pumping affects leakage rate while surrounding rock permeability plays the major role in determining water leakage rate. The following graph shows water leakage rate as a function of average pressure built up in a reservoir due to pumping and surrounding rock permeability.
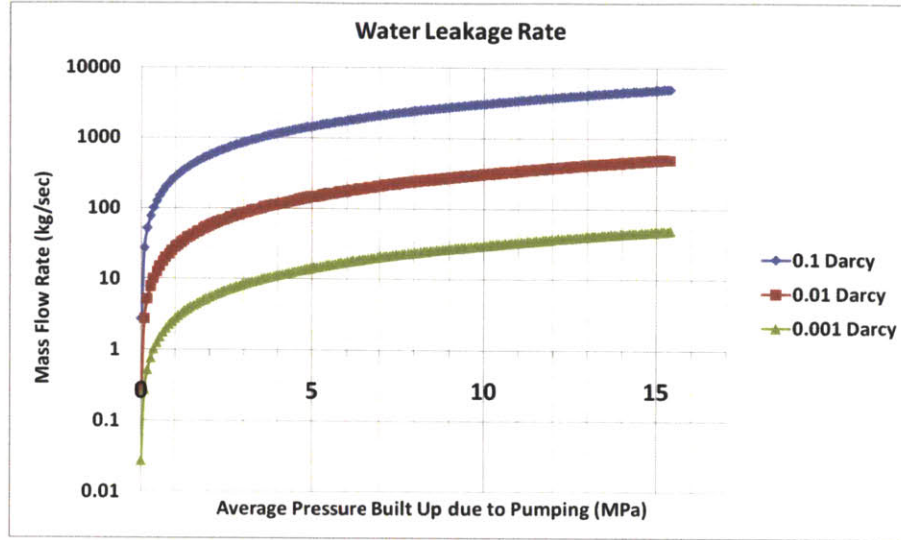
Fig.3-33 Water Leakage Rate of a Nuclear-Geothermal Reservoir

Table 3-7 Fixed Parameters Used for Fig.3-33

Average Water Temperature of Reservoir	842.3 kg/m^3
Average Viscosity of Reservoir	2.38E-4 Pa.s
Length of Reservoir	1000m
Diameter of Reservoir	500m
Burial Depth	1000m

Inserting Eq.3-5 into Eq.3-12, the following equation describes the water leakage rate as a function of reservoir mass flow rate and some other design parameters

$$\dot{m}_{leak} = \frac{\rho_{avg} \pi d L^2}{2} \frac{K_{surr}}{D \mu_{avg}} \frac{\dot{m}_{res}}{A_{superficial} K_{res}} \left(\frac{\mu_{max}}{\rho_{max}} + \frac{\mu_{min}}{\rho_{min}} \right)$$

$$= \frac{\dot{m}_{res} \rho_{avg} L}{2 D \mu_{avg}} \left(\frac{A_{lateral}}{A_{superficial}} \right) \left(\frac{K_{surr}}{K_{res}} \right) \left(\frac{\mu_{max}}{\rho_{max}} + \frac{\mu_{min}}{\rho_{min}} \right)$$

Eq.3-45

Where $\pi d L$ is the lateral surface of a cylindrical reservoir, hence denoted as $A_{lateral}$. $\dot{m}_{leak}$ is the time average leakage rate (kg/sec). ρ_{avg}, K_{surr}, K_{res}, $\dot{m}_{res}$, D, μ_{avg}, μ_{max}, μ_{min}, ρ_{max} and ρ_{min}, are the time

average reservoir water density, surrounding rock permeability, reservoir permeability, reservoir mass flow rate, burial depth, time average water viscosity, maximum viscosity of water, minimum viscosity of water, maximum water density and minimum water density, respectively[17].

It is worth noting that Eq.3-45 can be rearranged to give the following expression that determines the fractional water leakage with respect to the reservoir geofluid mass flow rate.

$$\frac{\dot{m}_{leak}}{\dot{m}_{res}} = \frac{\rho_{avg}L}{2D\mu_{avg}}\left(\frac{A_{lateral}}{A_{superficial}}\right)\left(\frac{K_{surr}}{K_{res}}\right)\left(\frac{\mu_{max}}{\rho_{max}} + \frac{\mu_{min}}{\rho_{min}}\right)$$

Eq.3-46

The terms on the right hand side of Eq.3-46 are reservoir design parameters except for the surrounding rock permeability, K_{surr}, which is primarily determined by the location of the reservoir. It is worth noting that the deeper the reservoir is buried, the lesser the fractional leakage. Hence, a deeper reservoir can be a solution to reducing the water leakage rate. However, as discussed in chapter 4, drilling cost is one of the most limiting factors for the economics of a typical EGS reservoir. Hence, a deeper reservoir is regarded as a least preferred option from the view point of economics. A more reasonable option is to choose a site where the surrounding rock is characterized with sufficiently low permeability compared to the reservoir. The presence of a cap rock above the reservoir is an example. In general, the range of permeability of geology is much greater (10^{-4} ~10^{0} Darcy) than any other parameter in Eq.3-53. This means that the permeability ratio term, $\frac{K_{surr}}{K_{res}}$, basically controls water leakage rate. Thus, a reasonable design strategy of a nuclear-geothermal reservoir for reducing water leakage is to build the reservoir under cap rock, as is common practice for typical EGS systems.

The major constraint found from Eq.3-46 is that leakage rate should not be greater than the reservoir mass geofluid rate ($\frac{\dot{m}_{leak}}{\dot{m}_{res}} < 1$). Hence, with the given design parameters, Eq.3-53 finds the maximum allowable surrounding rock permeability for a reservoir to operate. In reality, however, a more strict limitation is imposed on the water leakage rate for economic operation of reservoir. A typical hydrothermal reservoir is penalized with up to 10% of water loss [8]. The fractional loss of mass flow rate is equal to the fractional heat loss rate with respect to charging rate (or discharging rate). Hence, 10% of water leakage will reduce charging or discharging rate by 10%.

An important implication of Eq.3-46 is that a mined reservoir is essentially free of water leakage concern as pressure built up inside a block-caved reservoir due to pumping is much smaller than that of a

---

[17] Maximum, minimum and average in terms of reservoir operating time.

hydraulic fractured reservoir. This can be inferred from Eq.3-53 by inserting a large value for K_{res}, for the block-caved reservoir.

There are also a variety of site specific technologies to reduce water losses [16]. These include injected grout into high leakage fractures, frozen walls some distance away, and injection of cold water in appropriate locations to create appropriate hydraulic gradients underground.

The water leakage models are taken into account in the reservoir design study in Chapter 4.

3.5.7 Geothermal Power Plant Performance

In order to assess the overall performance of the nuclear-geothermal system, it is necessary to acquire information on relevant performance metrics of the geothermal power plant of interest. Since the basic approach of this study is to borrow the existing geothermal power plant technology, the performance metrics of geothermal power plants are adopted from the current technology of geothermal power plants. This section of the chapter is dedicated to the establishment of geothermal power plant performance metrics to be used in the preliminary design study.

There are two metrics of performance that are used by geothermal power plant designers

A. A utilization efficiency which gives the net power relative to the max power (exergy or availability) possible for specific geothermal fluid conditions

B. Specific power output (Kw(e)/kg/sec) of geofluid.

For the purpose of the performance assessment for nuclear geothermal heat storage systems, the later-specific power output of geo fluid- is of prime interest as it can be readily used to evaluate the amount of peak power electricity production for a given reservoir design. As stated in Chapter 2, a double-flash power cycle is the common power cycle that is used for geothermal power plants with a geo fluid temperature of 250°C.

A previous study was conducted to analyze the thermodynamic optimum conditions, ie. the highest specific power output for a representative geofluid temperature, for a fixed condensing temperature of 50°C [9]. The parasitic power requirements have been assumed to be 5% of the gross turbine power. That is, in arriving at the mass flow rates needed for a specified MW power output, the specific turbine power was first multiplied by 0.95 [6]. The following table shows the results of the thermodynamically optimized double flash geothermal power plant operating at 250°C (geo fluid) ~ 50°C (condensing).

Table 3-8 Reference Geothermal Power Plant

Geo-fluid temperature °C	Energy conversion system	Flash Temperature 1 °C	Flash Temperature 2 °C	Specific turbine power kW/kg/sec
250	Double-flash	185	122	123.5

The geothermal power plant shown in Table 3-17 is the reference geothermal power plant used in this study. Geo-fluid temperature is determined by nuclear temperature output. Condensing temperature, however, can vary depending on the local conditions and power cycle design. Although the condensing temperature is not likely to significantly deviate from the reference condensing temperature, 50°C, condensing temperature can vary slightly without significantly altering the current design. It is important to note that condensing temperature is the same as the cold piston temperature of the reservoir for a direct power cycle such as the flash cycle because condensed water is reinjected into the reservoir. As we explored in the previous sections, cold piston temperature of a reservoir affects every aspect of nuclear-geothermal heat storage system design. To investigate the performance of nuclear geothermal heat storage system design for the possible range of cold piston temperatures, hence condensing temperatures, specific turbine power output of the reference geothermal power plant should be expressed as a function of condensing temperature.

It is worth noting that condensing temperature, being the lowest temperature of a power cycle, affects efficiency of energy conversion. Such an efficiency change associated with the cold piston temperature should be captured in order to properly interpolate the specific turbine power output from the reference point. The following equation gives the efficiency of an internally reversible, ideal heat engine operating at maximum power output [21].

$$\eta_{th} = 1 - \left(\frac{T_c}{T_H}\right)^{1/2}$$

Eq.3-47

The lower the condensing temperature, the higher the efficiency of the power cycle becomes, basically following the Carnot efficiency trend. Although Eq.3-54 does not specifically model the efficiency of the double flash power cycle, the general trend it demonstrates is applicable to the double flash power cycle.

100

Eq.3-54 is used to make an interpolation for the specific turbine power output centered at the reference design.

$$\dot{Q}_{turbine}(kW/kg/sec) = 123.5 \left[\frac{1 - \left(\frac{T_c}{T_H}\right)^{1/2}}{0.214} \right] \left[\frac{T_H - T_c}{200} \right]$$

Eq.3-48

Where T_H is the hot piston temperature, which is fixed as 250°C. T_c is the cold piston temperature and we allowed the varying range to be ±25°C from the reference case, 50°C. 0.214 is the efficiency of the reference design and 200 is the reference temperature difference between the hot and cold piston temperatures. It is assumed that the enthalpy change of water in the turbine increases linearly with the temperature difference. Equation.3-55 basically interpolates the turbine specific output by taking into account changes in efficiency and fluid enthalpy change associated with the cold piston temperature[18].
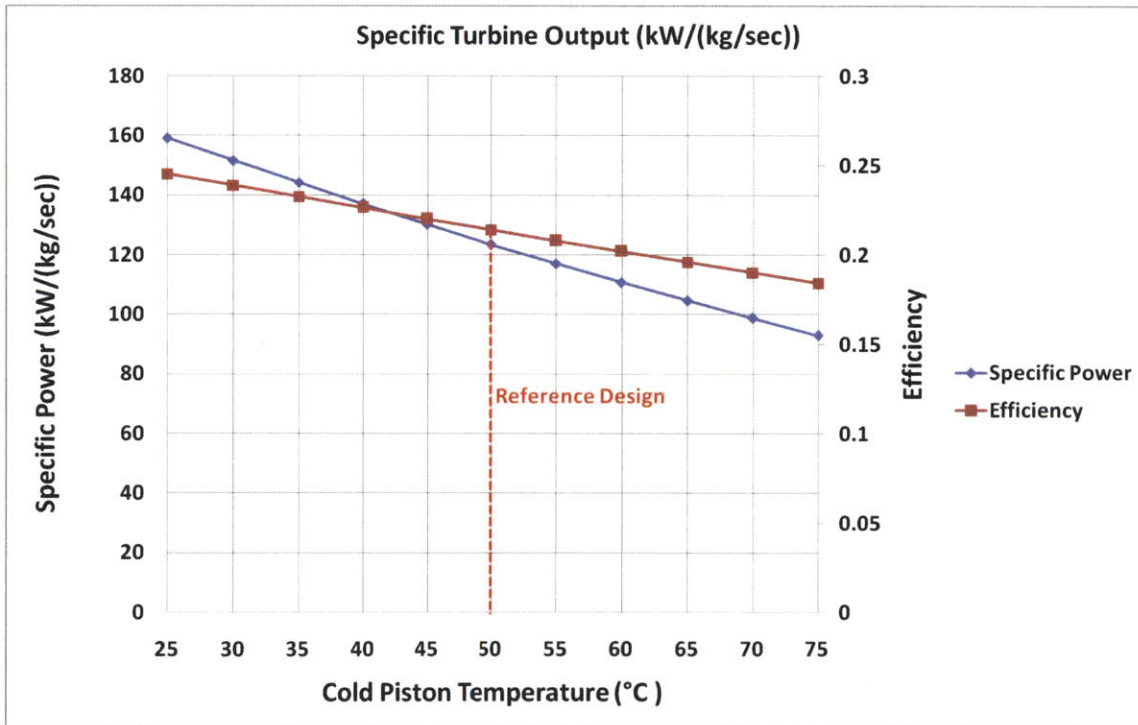
Fig.3-34 EGS Electricity Conversion Performance as a Function of the Minimum Temperature

---

[18] Specific heat of water is assumed to be the same for the range of cold piston temperatures of interest (25°C ~75°C) in this study.

Figure.3-34 illustrates the result of specific power interpolation from the reference design using the discussed methodology. Specific power decreases with increasing cold piston temperature. Also, as noted in the previous discussion, thermal storage size becomes smaller with increasing cold piston temperature for a given reservoir. Hence, it is evident that as far as the geothermal power plant with flash cycle – direct geo-fluid cycle- is concerned, the performance of the nuclear geothermal system is penalized by higher cold piston temperature, except for pumping.

If an indirect cycle is used, analysis will be different. For a nuclear geothermal heat storage system that uses an indirect geothermal power cycle, cold piston temperature of the reservoir is determined independently from the condensing temperature of the geothermal power plant. For the indirect power cycle, the smaller the temperature drop of geo-fluid across the heat exchanger that provides heat for electricity generation, the higher the efficiency of the cycle becomes. This is because the heat transfer with a smaller temperature change in a heat exchanger facilitates an enhanced reheating process. This means that the hotter the cold piston temperature, the better the power cycle efficiency becomes. On the other hand, a larger reservoir volume is needed for the same amount of thermal storage for the hotter cold piston temperature. Therefore, cost-benefit analyses are needed to assess the economic gain (enhanced geothermal power plant performance) and the loss (larger reservoir volume).

Table 3-9 Comparisons of Direct and Indirect Geothermal Power Plants

	Direct Cycle	Indirect Cycle
Cold Piston Temperature	Condensing Temperature	Independent of Condensing Temperature
Power Cycle Performance	Decreases with Increasing Cold Piston Temperature	Increase with Increasing Cold Piston Temperature
Reservoir Size	Determined by Condensing Temperature, hence, the local condition	Determined by the cold piston temperature
Cost Benefit Analysis with Reservoir Size	System performs best at the lowest cold piston temperature	Higher Cold Piston Temperature VS Larger Reservoir Volume

The geo-fluid temperature of a nuclear geothermal heat storage system is around 250°C[19]. Hence, in this study, performance metrics of the double-flash cycle geothermal power plant are used to evaluate the system performance.

It is worth noting that the geothermal power plant performance metrics discussed here are adopted from existing technologies, whose size is typically between 10MW~100MW. Considering the relative power output of a nuclear power plant (Few thousands of MW) and geothermal power plants, a few tens of individual geothermal power plants may be needed for a single nuclear geothermal heat storage system. The other approach is to scale up the current geothermal power plant to be comparable to a nuclear power plant in terms of power output. Scaling up the current geothermal power plant is beyond the scope of this study. However, it is expected that the efficiency of the power plant, performance metrics, and economics will be enhanced with increasing power plant scale. Hence, performance metrics used for the geothermal power plant can be regarded as conservative as they do not take into account the potential improvements in the future.

3.5.8 Reservoir Temperatures

It is worth noting that the choice of the reservoir temperature range is related to the power cycles. The temperature range for the reference reservoir is between 50°C~250°C with EGS flash cycles. There, however, can be another reservoir temperature range option - a smaller temperature difference (200°C~250°C) with binary cycles. When heat storage in a reservoir is practiced with a smaller temperature difference, the efficiency of associated power cycles increase due to the smaller entropy generation. However, a larger volume of the reservoir is required, in proportion with the ratio for the temperature difference. Also, higher heat losses by conduction are expected due to a larger temperature gradient between the reservoir and surrounding. Investigating such engineering trade-offs is out of scope of this study, but is recommended for future work in the context of exploring the best power cycle options with reservoir performance.

---

[19] Geofluid temperature of the system cannot exceed that of the PWR primary side, 328.9°C~293.3°C. Depending on the heat exchanger design and parasitic loss of thermal energy in the heat injection facility, geo fluid temperature can vary. In this study, a geofluid temperature of 250°C is used as the reference value.

3.5.9 Operating Conditions

The nuclear geothermal system consists of three individual sub systems: nuclear power plant, underground reservoir, and geothermal power plant. How well these systems are interfaced is an important measure for the realization of the system. System compatibility can be assessed by evaluating operating conditions of the system.

The interface between the reservoir and geothermal power plant is not a concern. This is because the study assumes borrowing an existing double flash geothermal power plant, and the conditions of the nuclear geothermal reservoir fit the operating conditions of typical double flash geothermal power plants except that a larger pressure drop may be experienced compared to the current geothermal power plants.

A more important concern in terms of the system interface is the interface between the nuclear power plant and the reservoir. This section is dedicated to exploring the operating conditions of the system interface between the nuclear power plant and the reservoir. Figures.3-35 and 3-36 show an example reservoir and identified operating condition at every representative point in the system. As discussed in chapter 2, an indirect hot water injection system with primary water bypass of a PWR is used. A pump is placed in the cold leg of the reservoir system in order to avoid cavitation. The reservoir system can be equipped with a pressurizer (the need for a pressurizer is addressed in the following discussion). The two different systems shown in Table 3-9 are examined.

Table 3-10 Two Different Charging Systems Illustrated in Fig.3-36

Case	Pressure Drop in a Reservoir	Presence of Pressurizer	Depth of Reservoir
A	5MPa	No	1.5km
B	2MPa	Yes	1.5km
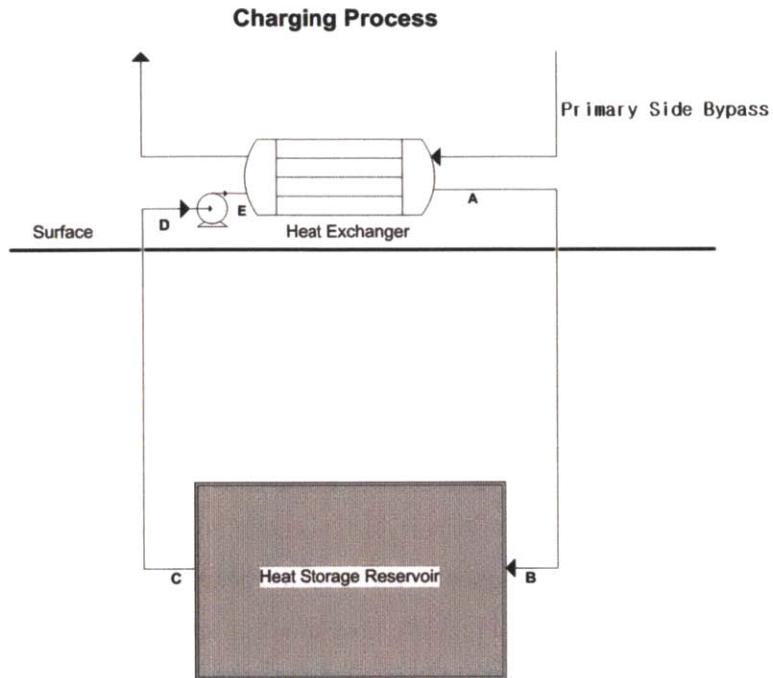
Charging Process

Fig.3-35 Schematic Diagram of a Charging Process
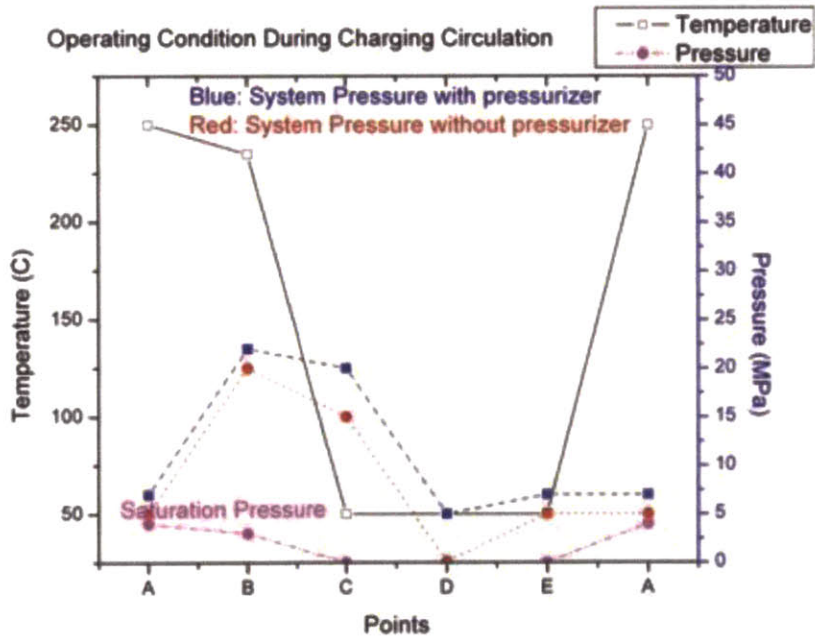
Fig.3-36 Operating Conditions at Different Points in the System

The black line with empty square marker represents temperature at each identified point. 250°C of geo fluid is injected and undergoes a few Celsius of fluid temperature drop while the water travels down to the reservoir from the surface (A-B). Water transfers its heat to the reservoir rock as it travels through the reservoir (B-C). It was assumed that after water leaves the reservoir, there is no significant water temperature change before it enters the heat exchanger (C-E). The cooled water is heated back to the original temperature 250°C.

The purple line represents saturation pressure at the identified water temperatures and it plays as the minimum operating pressure of the system during a charging process. In order to suppress boiling of water, system pressure has to be above the saturation pressure at every point in the system.

Note that the pressure drop that occurs in the reservoir (B-C) is equal to the increase in pressure across the pump (D-E). This is because the pump is designed to make up the head loss in reservoir. For the reservoir case A, which is illustrated as the red line in Fig.3-36, pressure drop in the reservoir is sufficient enough for the pump to pressurize water just above the saturation level at the outlet of the heat exchanger (A), which is the point where boiling margin is smallest in the system[20]. Assuming that the system pressure right before the pump (D) is atmospheric if there is no pressurizer in the system, the pump needs to pressurize water at least to 5MPa (Saturation pressure at 250°C) to avoid boiling. Because the degree of pressurization across a pump is essentially determined by the total pressure drop inside a reservoir, we can say that the system can suppress boiling with no extra equipment, but with a pump if pressure drop in the reservoir is greater than 5MPa.

If pressure drop in the reservoir is not sufficient for pumps to pressurize water above 5MPa, a pressurizer can be used to raise the system pressure to assure that no boiling occurs. An example of the reservoir with a pressurizer is illustrated with the blue line in Fig.3-36. In this case, the reservoir pressure drop is 2MPa, hence boiling is expected to occur at the outlet of the heat exchanger if the pressure before the pump (D) is atmospheric. As can be seen in Fig.3-36, system pressure is raised to 5MPa at point D, using a pressurizer. The pump adds 2MPa on top of this operating pressure and gives 7MPa at the outlet, leading to a suppression of boiling with a larger margin. However, the use of a pressurizer introduces additional system complexity in the reservoir water circulation system.

An alternative way to circumvent boiling concerns without the use of a pressurizer for a system with insufficient pump pressurization is to introduce additional form losses in the system. By doing this, we can artificially increase pressurization across the pump to sufficiently suppress boiling. However, this

---

[20] The outlet of the heat exchanger (A) is the most vulnerable point in the system.

method increases parasitic pumping power. Hence, a careful cost-benefit analysis is needed, if one wants to get rid of a pressurizer by increasing the pumping power.

3.6 Conclusion

As an essential prerequisite for the preliminary design study of nuclear-geothermal energy storage systems, models for the following list of pivotal design parameters and system performance metrics are established. Implications of the listed metrics on the feasibility and performance of the nuclear-geothermal system are discussed.

- Thermal front velocity
- Storage size
- Cycle periods
- Conductive heat loss
- Pressure drop
- Water loss
- Geothermal power plant performance
- Operating conditions

Listed individual models are combined to identify a viable design space and to understand the nuclear-geothermal energy storage system in perspective through the comprehensive assessment of design trade-offs and sensitivity of performance metrics in Chapter 4.

CHAPTER 4

Design of Nuclear EGS System

4.1 Introduction

This chapter is dedicated to the conceptual design study of a Nuclear EGS System using the individual models discussed in Chapter 3. A reasonable range design parameters, performance metrics and constraints were investigated with an aid of a design map to identify representative nuclear-EGS system performance metrics. Sensitivity studies of some important performance metrics and design parameters were conducted. Design directions and effectiveness of each design parameter were explored. Results of this chapter are used for the economic study of the system in Chapter 5.

4.2 Seasonal Variation in Electricity Demand & Design Implications

Before studying nuclear-EGS system design, it is necessary to understand the demand characteristics of the grid which is utilized by the system. As discussed in Chapter 1, electricity demand is never constant. The time variation for the charging and discharging rate of a nuclear EGS system introduces a number of design and operational implications. If averaged over minutes, hours and days, one can fit the real electricity demand with a sinusoidal curve that shows seasonal (monthly) electricity demand as illustrated by Fig.4-1.
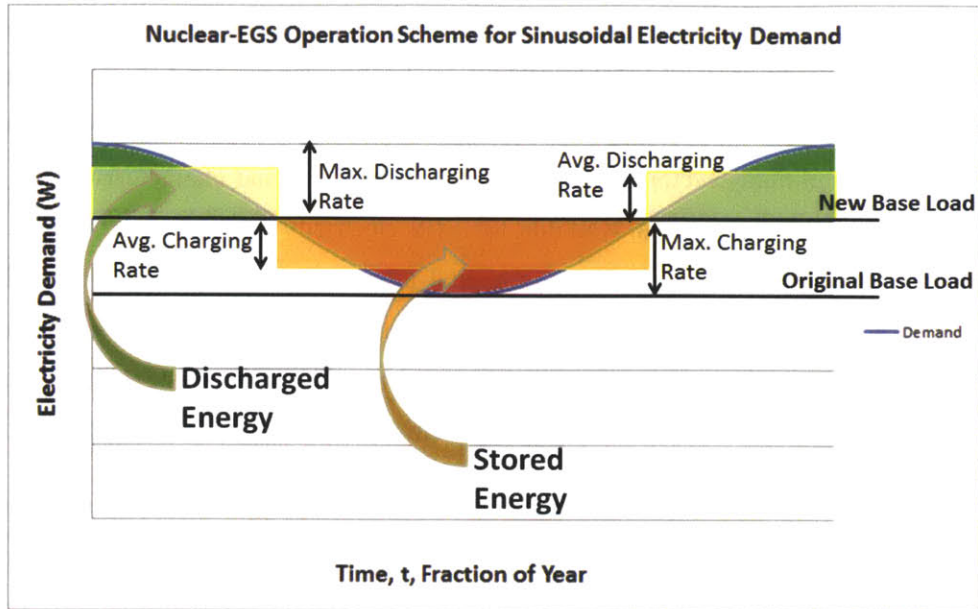
Fig.4-1 Operating Conditions at Different Points in the System[21]

The period and amplitude of the sinusoidal demand curve vary with different electricity grids. More details about the sinusoidal characteristics of seasonal electricity demand are discussed in the economics section of the chapter.

As shown in Fig.4-1, deployment of a nuclear-EGS system raises the original base load to a higher level. As a result of the increase in base load, there exist time periods when base load is above the demand curve. During this time period, base load alone is enough to supply electricity demand of a grid and there is a surplus of energy. The nuclear-EGS system stores surplus of energy in the form of heat underground. The difference between the electricity production rate and electricity demand (in terms of rate) in Fig.4-1, when production is greater than demand illustrates the charging rate. The area enclosed by the straight new base load line and the sinusoidal demand curve represents the amount of energy that is stored. It can be seen that the required charging rate varies with time as electricity demand changes while the base load nuclear power plants produce constant energy output (in terms of thermal energy). The average charging rate can be defined as a constant charging rate that gives the same amount of heat storage for the same period of time. The semi-transparent rectangular box in Fig.4-1 fictitiously represents the amount of energy that would be stored if constantly charged. By definition, this area is the same as the shaded area - the actual stored energy - enclosed by the new base load line and the demand curve.

---

[21] Fig.4-1 merely illustrates concepts. In this study, the original base load is defined at the lowest point of seasonal electricity demand. The new base load level drawn in the figure is for illustrative purposes. The actual level for new base load can vary depending on a number of factors discussed in the following chapters.

Similarly, required discharging rate is also subject to changes. When the grid faces a period of time (season) during which electricity demand is higher than base load production, it uses the stored heat to produce electricity using geothermal power plants. The amount of electricity production using geothermal power plants is contingent on many factors including design parameters and characteristics of the grid. Depending on the amount of energy that is available for EGS electricity production, EGS could play a role of providing intermediate load while other less capital intensive power technologies such as gas turbines provide peak power. For cases where EGS provides intermediate load, the discharging rate is likely to be rather constant as most demand fluctuations are accommodated by the peak power providers. More details about the energy provider portfolio for peak electricity are discussed in Chapter 5.

It is important to note that Fig.4-1 does not show hourly demand variation whose amplitudes exhibit a greater oscillation, as illustrated in Fig.1-1. The actual charging and discharging take place on an hourly basis during the most economically advantageous hours in a day. The hourly charging and discharging rates depend on many economic factors, including the strategy of utilities, which may change continuously. The hourly fluctuations by nature are far more erratic than the seasonal fluctuation, leading to inherent difficulties for general predictions for different regions. Understanding these complexities and the empirical nature of the actual practice for charging and discharging, it is difficult to analytically evaluate the maximum charging or discharging rate of a nuclear-EGS system. The maximum charging & discharging rate, however, is important in the design of a nuclear-EGS system. This is because the maximum pressure drop and pumping power occur during the times of maximum charging & discharging periods which are associated with the peak mass flow rates. Excessively high pressure drop not only hurts the economics of the system, but it causes excessive leakage and possibly "unintentional" hydraulic fracture of the reservoir. Hence, it is important to know the tolerable level of maximum charging & discharging rates. At this point of discussion, it is worth noting that the charging & discharging power, mass flow rate and fluid velocity discussed in Chapter 3 for the nuclear-EGS model are the time average values, as they are evaluated as constants that meet desirable energy storage for a given period of time. Nevertheless, the models are still applicable for the maximum charging and discharging rate if appropriate properties and conditions are used. Hence in this study, the tolerable maximum charging and discharging rate are evaluated so that economic strategies for hourly charging and discharging can be made within engineering tolerance. Throughout this chapter, the distinction between average and peak charging & discharging has been made where appropriate. The time average parameters are used to size and to evaluate the system performance metrics within the design limits imposed during times of peak charging or discharging.

110

4.3 Design Study

4.3.1 Engineering Map

Using models developed in chapter 3, performance metrics of a nuclear-EGS system have been mapped with respect to dominant design parameters. To assess performance metrics of the representative system design, the following constants were used.

Table 4-1 Constants Used for Mapping Performance Metrics

Length/Radius ratio of reservoir	4
Inlet hot water temperature (Hot piston Temperature)	250°C
Porosity	0.15
Density of Geology	2600 kg/m^3
Specific Heat of Geology	850 J/kg°C
Permeability of Reservoir	2 Darcy (1.9738E-12 m^2)
Reservoir Period	6 months (3 months charging, 3 months discharging)
Geothermal Power Plant Type	Double Flash
Burial Depth	1500 m
Surrounding Rock Permeability	0.02 Darcy (1.9738E-14 m^2)
Nuclear Power Plant Efficiency	0.3333

Fig.4-2 illustrates thermal storage size, electricity storage size, mass flow rate, and charging heat rate as a function of minimum reservoir temperature (cold piston temperature) and reservoir volume. The calculations were made for the specified cycle period indicated in Table 4-1. As shown in Fig.4-2, thermal storage capacity monotonically increases with the physical size of the reservoir. As the cold piston temperature increases, thermal storage size is decreased for a given reservoir volume. This is because the density of water increases faster than its specific heat with temperature, leading to a smaller amount of stored energy in water in the pores of the reservoir. Such a cold piston temperature effect on storage size becomes more evident for electricity storage, as cold piston temperature exerts additional effects through EGS efficiency. Electricity storage is defined as the amount of electricity that would be produced by converting stored heat into electricity using EGS.

111

$$\text{Electricity Storage} = \text{Thermal Storage} \times \text{EGS Efficiency}$$

Eq.4-1

EGS performance, expressed in terms of either specific turbine output (electric power/geo fluid mass flow rate) or efficiency, is improved as the cold piston temperature decreases. Hence, it is beneficial to maintain the cold piston temperature as low as possible to maximize energy storage for the same size of reservoir. The black dotted line in Fig.4-2 represents the reference geothermal power plant design which operates at a 50°C cold piston temperature.

An important limiting design factor is charging heat rate. There is a limit on the average charging heat rate that a grid can afford. As discussed in section 4.2, maximum hourly charging is limited by engineering limitations such as maximum tolerable pressure drop. Average charging and discharging rates, however, are likely to be limited by grid constraints, which are related to the number of nuclear power plants and associated economics. Hence, it is difficult to determine the exact maximum average charging rate unless information on a real grid situation is provided, which is beyond the scope of the conceptual design. Nevertheless, it is reasonable to assume in a grid, that no more than two nuclear power plants are solely prepared for charging, where the number of nuclear power plants at a single site does not usually exceed six, at most. Imposing such a limiting factor in the system design, the following figure shows the possible design range.
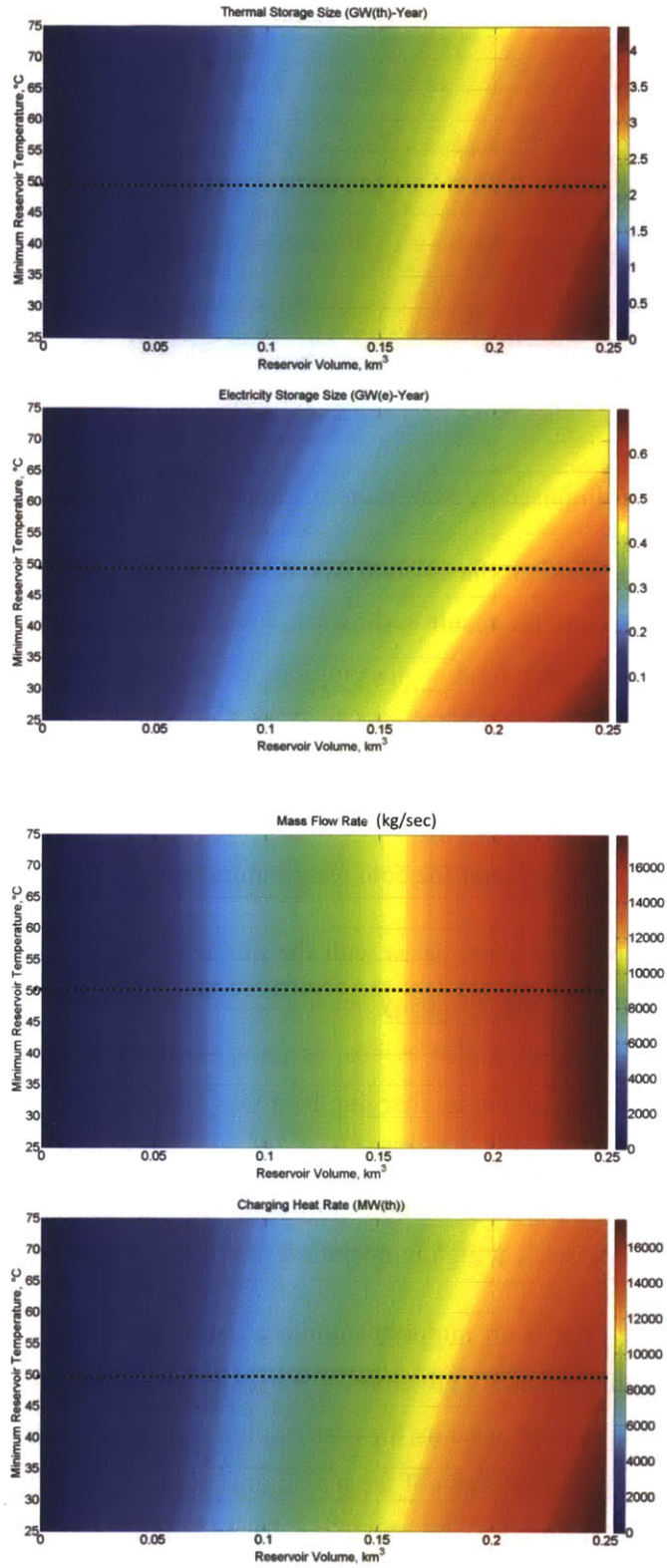
Fig.4-2 Energy Storage Performance Metrics of Nuclear-EGS System: Thermal Storage size, Electricity Storage Size, Mass Flow Rate, and Charging Heat Rate (average)
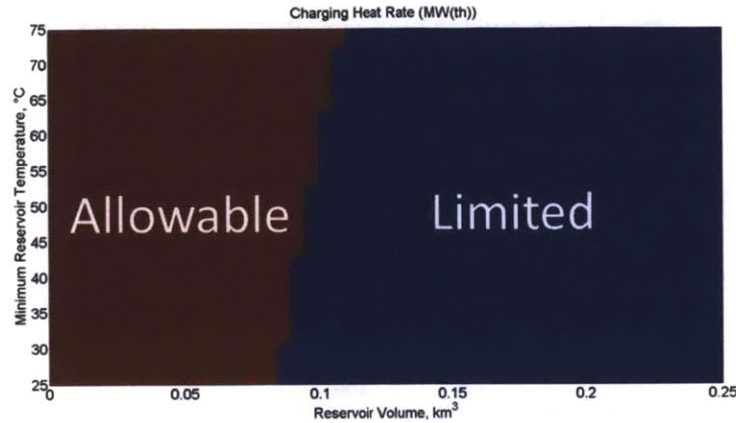
Fig.4-3 Design Limit Imposed by Maximum Average Charging Heat Rate at 6000 MWth

Assuming one nuclear power plant produces 3000 MWth, two nuclear power plant worths, 6000 MWth, is set to be the limiting value, and the result is shown in Fig.4-3. Any design belonging to the allowable area in Fig.4-3 is possible as far as tolerable charging rate is concerned. It is worth noting that reservoir designs on the far left side of the allowable region in Fig.4-3 are neither of interest nor feasible because small reservoir size leads to excessive conductive heat loss rate. Fig.4-3 can be put on top of Fig.4-2 to find the range of storage performance metrics. It is shown that required mass flow rate to meet the target cycle periods is more or less constant over the cold temperature range.

Average pressure drop monotonically increases with the physical size of reservoir. The higher the cold piston temperature, the lower the water viscosity becomes, leading to a lower average pressure drop for a fixed size of reservoir. Such a trend is also evident in pumping power. From the view point of system performance, fraction of pumping power to charging heat rate is an important measure of reasonableness of the required pumping power. As shown in Fig.4-4, fraction of pumping power is at most around 2% of charging rate. The low required pumping power is primarily due to (1) charging over a large volume of storage medium (2) system operation at high temperature (low water viscosity).

The mass flow rate leakage ratio is an important limiting factor for the reservoir design. As discussed previously, leakage rate is predominantly governed by surrounding permeability. $1/100^{th}$ of the stimulated reservoir permeability (2 Darcy) was used as the surrounding rock permeability (0.02 Darcy) and it was found that at most 5% of the geo-fluid leaks. If the maximum charging rate of 6000 MWth is imposed, the maximum leakage rate would decrease to 4% due to the decrease in reservoir volume. Such a leakage rate is compatible with typical hydrothermal reservoirs whose typical mass flow leakage ratio is around 5% [8]. If surrounding rock permeability increases 10 times, then leakage rate would increase 10 time

proportionally, leading to an unreasonable leakage rate. Hence, a strict limitation on the surrounding rock permeability should be met when choosing a site.

It is important to note that the results shown in Fig.4-4 are subject to changes with different values for the fixed constants shown in Table 4-1. Reservoir porosity, permeability of reservoir, length/radius ratio and burial depth are site-specific.
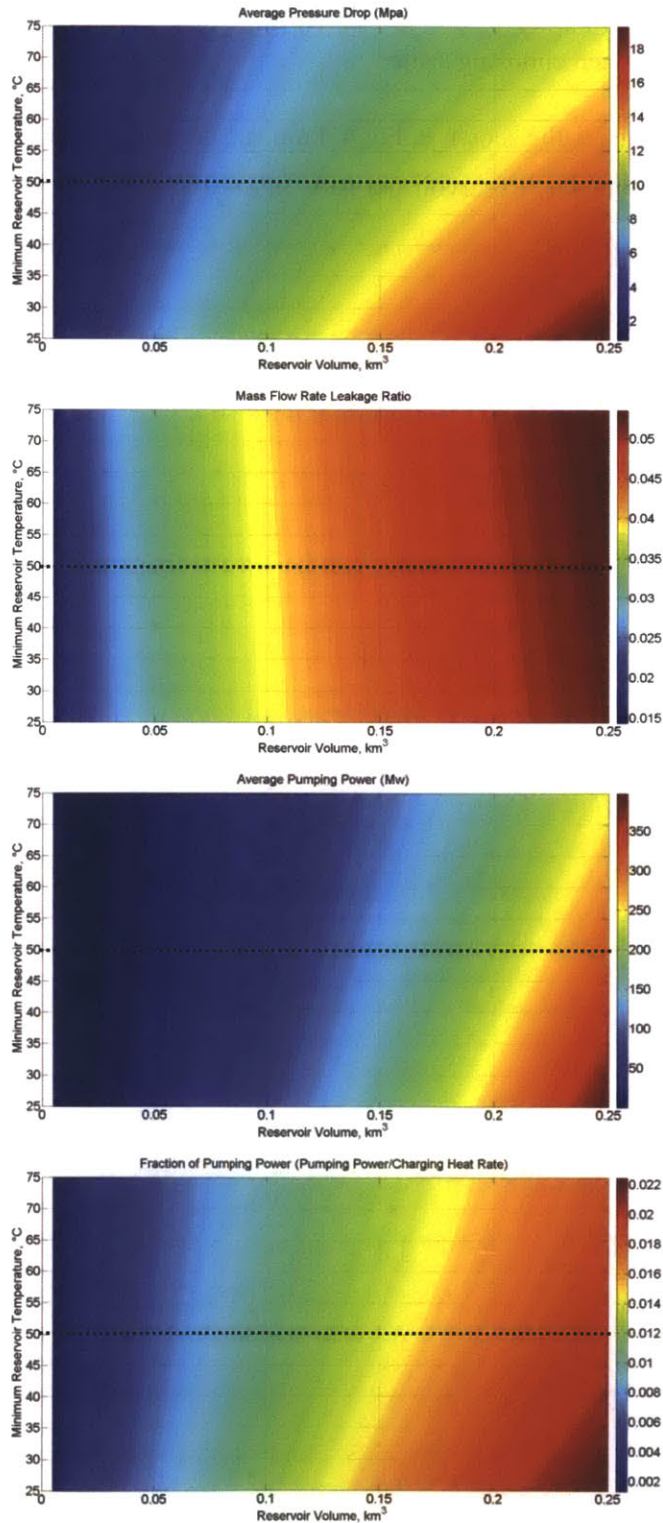
Fig.4-4 Charging Effort Performance Metrics of Nuclear-EGS system: Average Pressure Drop, Mass Flow Leakage Ratio, Average Pumping Power, Fraction of Pumping Power[22]

---

[22] Pump efficiency was assumed to be 100%. Hence, the result shows the minimum pumping power.

System storage efficiency is one of the most important system performance metrics beside size. Nuclear-EGS energy system efficiency is defined as the amount of electricity that is recovered through geothermal power plants per amount of forgone electricity that is charged using nuclear power plants. For clarity, the amount of electricity that is charged using nuclear power plants is the amount of electricity that could have been produced using nuclear power plants plus additional energy spent for charging that would have not been present if not stored in the form of heat underground. Equation.4-2 shows the nuclear-EGS storage round trip equation.

$$\eta_{Storage} = \frac{Electricity\ Recovered}{Electricity\ Charged} \times Energy\ Loss\ Fraction$$

$$= \frac{Electricity\ Recovered}{Electricity\ Stored + Pumping\ Energy} \times Energy\ Loss\ Fraction$$

Eq.4-2

Eq.4-2 can be expressed in terms of thermal storage size, and the efficiencies of nuclear & geothermal power plants as follows

$$\eta_{Storage} = \frac{\dot{m}\dot{Q}_{turbine}\Delta t_{discharging}}{E_{stored}\eta_{nuclear} + Q_{pump,charging}}(1 - \psi)$$

Eq.4-3

Where $\dot{m}, \dot{Q}_{turbine}, \Delta t_{discharging}, E_{stored}, \eta_{EGS}, Q_{pump,charging}$ and ψ represent geo fluid flow rate, specific turbine output of EGS, nuclear efficiency, energy for pumping during the charging process and fractional energy loss, respectively. The term $\dot{m}\dot{Q}_{turbine}\Delta t_{discharging}$ represents the total amount of electricity that is produced in the EGS during a discharging period where mass flow rate, $\dot{m}$ and turbine specific output, $\dot{Q}_{turbine}$ are assumed to be average values that are constant during a discharging process. $\dot{m}$ is as obtained in Fig.4-2 and $\dot{Q}_{turbine}$ is as discussed in Section 3.5.7, which takes into account efficiency as a function of the operating temperature ratio and total rate of thermal energy conversion expressed as a function of temperature difference. The $E_{stored}\eta_{nuclear}$ term represents electricity that would have been produced using nuclear power plants if not stored in the underground. E_{stored} is the thermal energy storage size of a reservoir, as expressed in Eq.3-42 . Thermal efficiency of the nuclear power plant, $\eta_{nuclear}$ is assumed to be the typical value of current PWRs (0.333). $Q_{pump,charging}$ is

117

pumping power integrated over charging period. The result for average pumping power shown in Fig.4-4 is multiplied with the charging period of 3months. Fractional energy loss (ψ) consists of conductive heat loss and energy carried out by water leakage. As discussed in Section 3.5.4, the fractional energy loss due to conduction is around 1% for the reference reservoir size. Energy loss due to water leakage, however, is more substantial than the conductive energy loss as shown in Fig.4-4. Hence, for the storage efficiency evaluation, the fractional energy loss ψ is assumed to be related to the energy carried away by water leakage only.

As can be inferred from Eq.4-3, the discrepancy between EGS electricity production capability and nuclear electricity production capability is the main cause for a nuclear-EGS storage system to deviate from being an 'ideal storage system', which has a round trip efficiency of unity. This is a characteristic that is unique to nuclear-EGS energy storage systems. Fractional heat loss is a negligible factor $(1 - \psi \approx 1)$ for determining the round trip efficiency compared to the efficiency differences between EGS and nuclear power plants. $Q_{pump,charging}$ is negligible compared to $E_{stored}\eta_{nuclear}$ as pumping power is only 1~2% of charging heat rate. As discussed in 3.5.7, the geothermal electricity production efficiency of current systems expressed as specific turbine power output is less than that of current nuclear power plants at the nearly the same operation temperature (~250°C). This is because the smaller size of the current geothermal power plants introduces comparative disadvantages in terms of the law of scale which limits power plants from fully leveraging the theoretical maximum electricity production capability[23]. Conventional geothermal power plant size (few tens of MW) is limited by the size of the natural thermal resources relative to nuclear or fossil power plants. As a result of the difference in the power plant electricity production capabilities, electricity production is unavoidably decreased for the same amount of thermal energy if a geothermal power plant is used instead of a nuclear power plant, and it eventually results in a decrease in round-trip efficiency.

Since geothermal power plants to be used in a nuclear-EGS system will exploit artificially charged thermal resources whose sizes are big enough to let discharging rate be equivalent to that of nuclear power plants, such a size limiting condition for the geothermal power plant is no longer applicable for a nuclear-EGS system. Hence, geothermal power plant size can be increased from the current level to the level equivalent to typical nuclear power plants (~3000MWth). If such geothermal size augmentation specific to nuclear-EGS systems is realized, the round trip efficiency will move closer to unity as fractional heat loss is then the dominant factor that makes the system deviate from ideal energy storage. In addition to that, such a size augmentation is expected to cut the capital cost of the system dramatically by

---

[23] Impurities in the water interfere with heat transfer- another factor that prevents EGSs from theoretical optimum efficiencies. EGS power plant efficiency is about 2/3~3/4 of nuclear system.

leveraging economics of scale and saving the required land space that otherwise would have been needed for tens of required geothermal power plants. Therefore, it is strongly suggested to augment the size of the current geothermal power plants if used in nuclear-EGS systems.

On the other hand, the lower bound of the system performance for storage round-trip efficiency is found when assuming the current turbine specific power output of geothermal power plants. The results are shown in Fig.4-5.
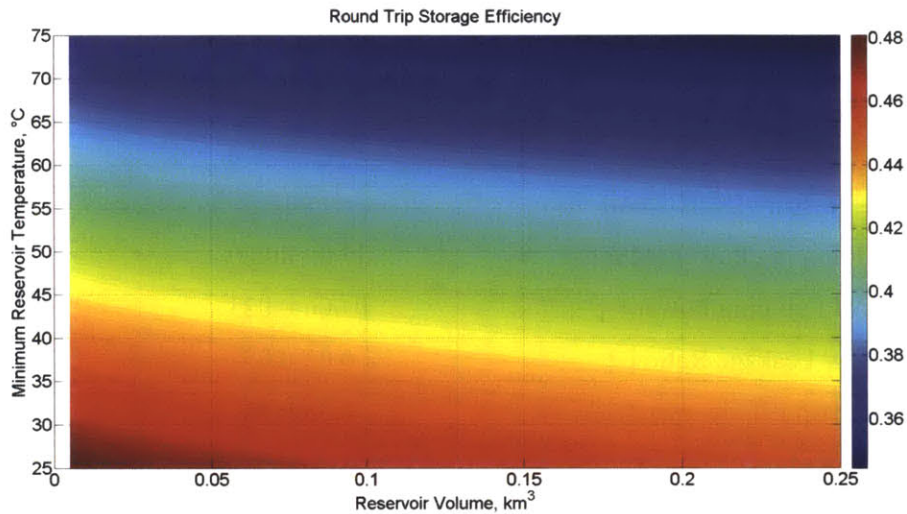
Fig.4-5 Round Trip Storage Efficiency of Nuclear-EGS System

Round trip storage efficiency increases with decreasing minimum reservoir temperature (cold piston temperature) because the turbine specific power output of the EGS increases. The larger the reservoir becomes, the lower the round trip storage efficiency because of increasing pumping power and mass flow leakage ratio. Round trip storage efficiency ranges from 0.33 to 0.46, meaning that a fraction 0.33~0.46 of charged electricity is recovered.

The following Table 4-2 summarizes the range of performance metrics and design parameters of the nuclear-EGS energy storage system under the prescribed conditions indicated in Table 4-1.

Table 4-2 Performance Metrics of the Reference Nuclear-EGS Energy Storage Systems

Representative Performance Metrics and design Parameters	Values	
	Unlimited charging rate	Limited charging rate 6000MWth
Reservoir Volume [km^3][24]	0.05 – 0.25	0.05 – 0.25
Minimum Reservoir Temperature [°C]	25-75°C	25-75°C
Thermal Storage Size [GW(th)-Year]	0.7 – 4.4	0.7 – 1.5
Electricity Storage Size [GW(e)-Year]	0.08-0.7	0.08- 0.2
Mass Flow Rate [kg/sec]	3.6E3 – 1.8E4	3.6E3-7.7E3
Charging Heat Rate [MW]	2.8E3-1.8E4	2.8E3-6.0E3
Average Pressure Drop [MPa]	4.1 - 19.5	4.1-9.3
Average Pumping Power [MW]	17.0 - 402.0	17.0-64.4
Fraction of Pumping Power [-]	0.006-0.023	0.006-0.01
Mass Flow Leakage Ratio [-]	0.03-0.05	0.03-0.04
Round Trip Efficiency [-]	0.33-0.46	0.34-0.46

As indicated in the Table 4-2, when limited by the charging rate, the range of reservoir design and performance metrics become narrowed down. Especially, the maximum storage size, both in thermal and electricity decrease nearly 1/3 of the unlimited case while the range for the overall round trip efficiency remains more or less the same.

It is necessary to note that the results discussed so far are based on the fixed parameters shown in Table 1. Nevertheless the reference fixed parameters are chosen carefully to be representative values based on the discussions in chapter 2 and 3. Hence, the discussions regarding the reservoir design direction are yet incomplete – there is room for investigating the sensitivity of reservoir performance metrics upon changes of the fixed parameters in order to attain a comprehensive understanding of the reservoir design direction. In the following sections, the sensitivity studies of reservoir performance upon changes of the L/D ratio, hot piston temperature, porosity, thermal properties of geology, permeability, period, and permeability, are investigated.

---

[24] Reservoir volume smaller than 0.05 km^3 is not regarded as a design candidate because of the small size of the storage volume and excessive conductive heat loss fraction.

4.3.2 Sensitivity Studies for Engineering Performance of the Nuclear-EGS Energy Storage System

In Section 4.3.2, performance of nuclear-EGS energy storage systems were explored as a function of the minimum reservoir temperature and reservoir volume – two important independent design parameters, while using a fixed set of other representative design parameters and constraints as shown in Table 4-3. The same analysis can be reproduced with a different set of the fixed parameters & constraints if the system is to be deployed under off-representative design conditions.

In this Section, sensitivities of engineering performance metrics of the nuclear-EGS system upon reasonable perturbations for the representative design parameters and constraints are investigated. Having discussed the effects of minimum reservoir temperature on performance of the nuclear-EGS system in Section 4.3.1 in the context of the design map, the sensitivity studies were conducted with the minimum reservoir temperature fixed at 50°C. Therefore, sensitivities of the system were explored along the representative cold piston temperature trace marked with black dotted lines in Figs.4-2 and 4-4. Table 4-3 shows the test matrix that was used to conduct the sensitivity studies.

Table 4-3 Test Matrix of Sensitivity Studies

Variable	Tested Values				
	Low bound	Low-mid	Reference[25]	High-mid	High bound
L/R ratio	1	2.5	4	5.5	7
Inlet temperature	220°C	235°C	250°C	265°C	280°C
Porosity	0.05	0.1	0.15	0.2	0.25
Permeability	0.5 Darcy	0.1 Darcy	0.15 Darcy	0.2 Darcy	0.25 Darcy
Reservoir period	2 months	4 months	6 months	8 months	10 months
Volumetric thermal capacity of rock, $(\rho C_p)_{rock}$	1.12 MJ/m^3°C	1.66 MJ/m^3°C	2.21 MJ/m^3°C	2.76 MJ/m^3°C	3.32 MJ/m^3°C

---

[25] The reference designs are plotted with solid black lines in this section

4.3.2.1 L/R Ratio Effect

Energy storage capability related performance metrics, such as thermal & electricity storage size, mass flow rate, and charging heat rate are not functions of the shape of the reservoir. This is because energy storage capability of a reservoir is solely determined by the volume and thermal capacity of the corresponding geology. Hence, as long as the volume and underground composition (type of rock and porosity – a measure of relative thermal capacity of rock and water) do not change, energy storage capability of a reservoir is essentially insensitive to the L/R ratio, which represents the shape of a reservoir. This is illustrated in Fig.4-6 where electricity storage is merged into a single line for various L/R ratios.

The shape of a reservoir, however, does affect effort for geo-fluid circulation significantly. Pressure drop, associated pumping power and fractional pumping power to charging heat rate ratio decrease by pancaking a reservoir. This is because pancaking a reservoir while maintaining the volume constant, fluid travel area increases with decreasing reservoir length. This results in a reduction in both fluid travel velocities for the same mass flow rate and shorter fluid travel length; giving rise to smaller pressure drop per unit distance for a shorter total distance. Such pancaking effects become more evident in terms of absolute magnitude with increasing reservoir volume as shown in Figs.4-6 and 4-7.

The pancaking effect is transferred to mass flow leakage ratio through reducing the pressure gradient built up in a reservoir. As shown in Fig.4-7, making L/R small could practically keep almost all water flow inside a reservoir. On the other hand, the stretched reservoir with L/R =7 demonstrates a leakage ratio greater than 0.1 even for relatively small reservoir volume. The combination of increasing leakage ratio and parasitic pumping results in a significant reduction in the system round trip efficiency, as shown in Fig.4-7. Such a reduction in the system round trip efficiency harms the economics of the system, while storing the same amount of energy, as more parasitic work is expended.

Theoretically, the more the pancaking, the better the system performs for the same storage size. In reality, however, the benefit of pancaking is fully leveraged only when the geo-fluid injection and recovery piping system in a reservoir can make the flow uniformly distributed over the lateral surface of a reservoir, as illustrated in Fig.3-6. Hence, after a certain degree of pancaking, the reservoir performance is likely to be limited not because of the degree of pancaking but because of the piping that serves the pancaked reservoir in terms of both technical and economic issues. Also, the reservoir needs to be drilled deeper if L/R decreases. Therefore, the cost associated with pancaking a reservoir at some point can outweigh the benefits.

122
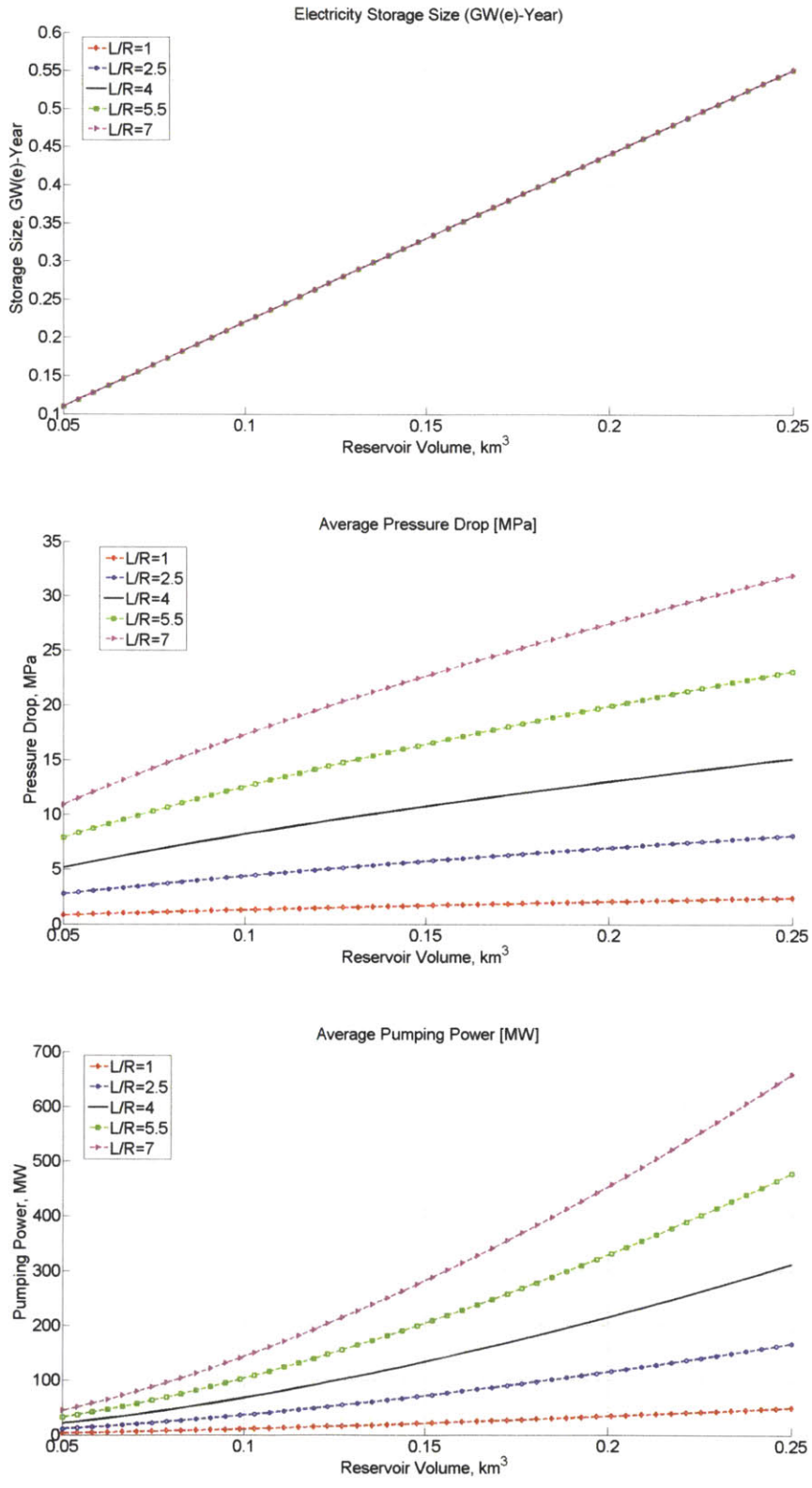
Fig.4-6 System Storage and Geo-Fluid Circulation Effort Performance Metrics with Varying L/R Ratio

(1) : Electricity Storage size, Average Pressure Drop, and Average Pumping Power

123
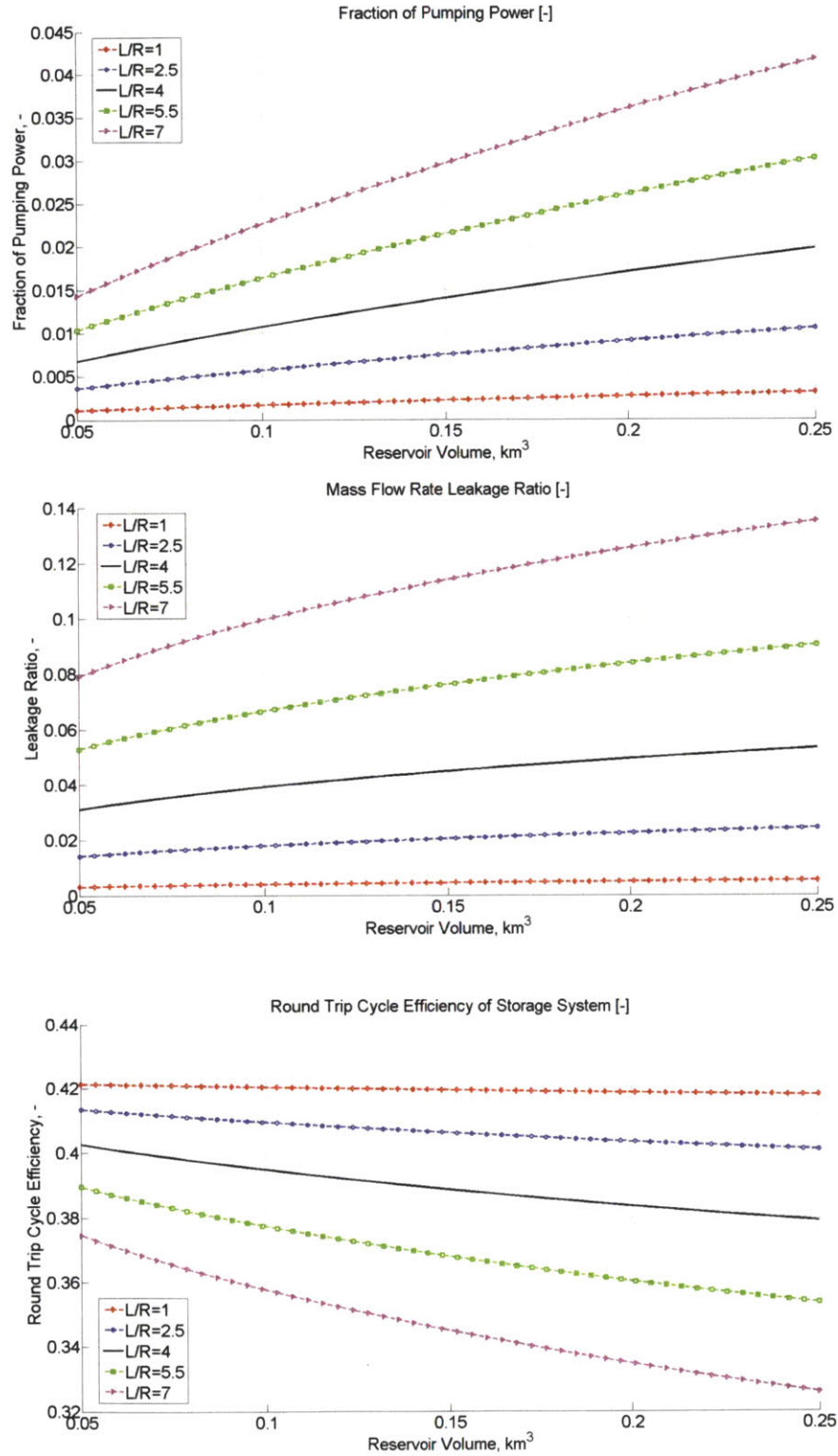
Fig.4-7 System Efficiency Performance Metrics with Varying L/R Ratio (2): Fraction of Pumping Power, Mass Flow Rate Leakage ratio, and Round Trip Cycle Efficiency of Storage System

4.3.2.2 Maximum Reservoir Temperature Effect

Maximum reservoir temperature is determined by the hot piston temperature, which is the hottest geo-fluid temperature injected from the nuclear power plant. Because of the temperature drop across a heat exchanger, the actual injection temperature is inevitably lower than the reactor temperature. With 250°C being the representative injection temperature, the upper bound is set to be 280°C: the typical PWR operating temperature. The lower bound is set to be the equal distance between the representative value and the maximum value, hence 220°C – representing a poor performance of PWR heat injection systems.

With increasing reservoir maximum temperature, average reservoir temperature increases while the minimum reservoir temperature is fixed to be 50°C. Upon the increase of the temperature difference between the two extreme states of the storage, thermal storage size increases in proportion with the temperature difference (temperature dependent thermal properties of geology and water are comparatively negligible). Electricity storage size also increases in accordance with thermal storage size and the degree of increase is further enhanced by increasing EGS power plant efficiency. The non-linear behavior of the power plant efficiency with respect to the maximum geo-fluid temperature shown in Eqs.3-54 and 3-55 is not clearly visible in the electricity storage size plot in Fig.4-8 because of the dominant linear behavior of the storage size increase with a finite temperature difference. As the storage size increases, charging heat rate should increase proportionally to meet the fixed cycle period. Hence, in Fig.4-8, it can be seen that the relative magnitude of changes in thermal storage size with respect to maximum reservoir temperature is roughly the same as those of charging heat rate.

Regarding performance metrics related to effort expended for geo-fluid circulation shown in Fig.4-9, the performance metrics are almost insensitive to the tested range of the maximum temperatures. This is because the changes come only through changes in average thermal properties of water, whose magnitudes of changes within the range of the tested maximum temperatures are not significant. Interestingly, pumping power remains essentially constant with respect to different inlet temperatures because the slight decreases in pressure drop and mass flow rate with increasing maximum reservoir temperature is compensated by decreasing water density.

Overall, the system becomes more efficient upon the increase of maximum reservoir temperature as shown in Fig.4-10. While the efforts for charging remain essentially the same, the increase in storage capacity leads to a smaller fraction of parasitic pumping power. In addition, mass flow rate leakage decreases slightly with increasing maximum reservoir temperature due to the smaller pressure gradient built into a reservoir with a lower water viscosity. With these effects combined, the round trip efficiency increases with quite noticeable gains upon the increase of the reservoir maximum temperature.

Fig.4-8 System Storage Performance Metrics with Varying Maximum Reservoir Temperature (1) :
Thermal Storage Size, Electricity Storage Size, Charging Heat Rate

126
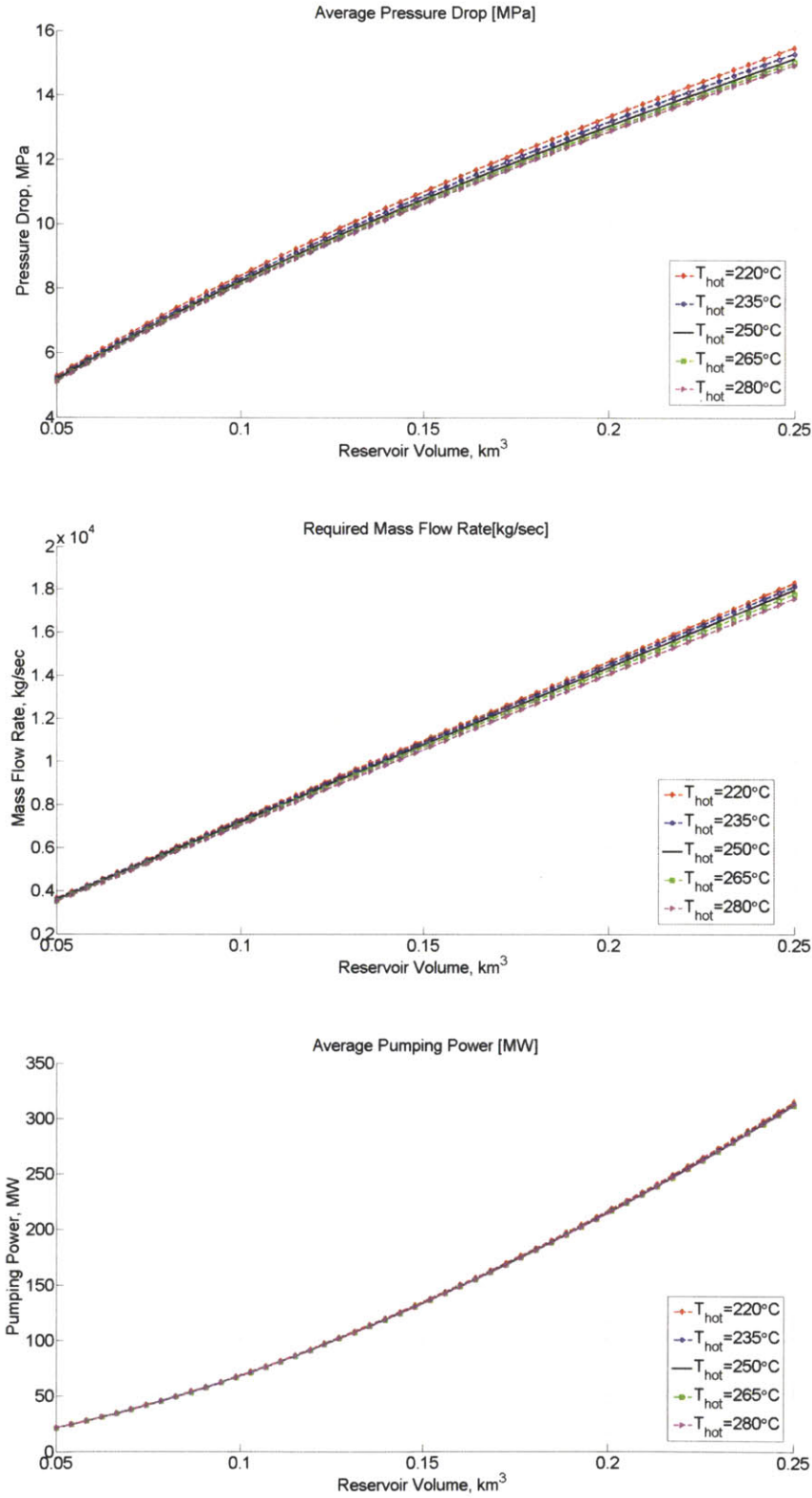
Fig.4-9 System Geo-Fluid Circulation Effort Performance Metrics with Varying Maximum Reservoir Temperature (2) : Average Pressure Drop, Required Mass Flow Rate, Average Pumping Power

Fig.4-10 System Efficiency Performance Metrics with Varying Maximum Reservoir Temperature (3) :
Fraction of Pumping Power, Mass Flow Leakage Ratio, Round Trip Cycle Efficiency of Storage System

4.3.2.3 Porosity Effect

Porosity of a reservoir is not an independent parameter that designers can control. Porosity is related to permeability, and vice versa. There have been continuing studies to find analytical relationships between permeability and porosity [23]. Yet, such relationships abide in the realm of empiricism as they are heavily site dependent; studies related to underground geology, by nature, are empirically site dependent. In this study, porosity and permeability are regarded independent. The range of reasonable porosity and permeability to be used in the model of nuclear-EGS reservoirs was investigated in Chapter 2.

Unconnected with permeability, parametric changes in porosity cannot capture corresponding charging effort and hence, system efficiency performance metrics properly in this study. In other words, in this study, porosity merely provides information only about the volumetric fraction of water to rock – not linked to hydraulic resistivity. Therefore, in this sensitivity design study with varying porosity, charging effort and system efficiency performance metrics were not explored. Theses parameters are investigated in 4.3.2.3, where sensitivities to permeability are analyzed.

Yet, porosity, by definition, can capture System storage performance metrics as shown in Fig.4-11. The lower the porosity, the lower the storage size becomes for both thermal and electric energy. This is because volumetric thermal capacity of water is greater than that of rock by roughly by a factor of 1.7. Hence, no matter in what the geology of the system, the trend shown in Fig.4-11 is not likely to be changed as variations in volumetric thermal capacity of water to most rock types is near 1.7. Thermal storage size, electricity storage size and charging heat rate vary the same in terms of the relative magnitudes with respect to different porosities, as porosity affects through changing the overall thermal capacity of a reservoir – no complicated non-linearity involved. The relative magnitudes of system storage performance metric changes with the porosity are dependent on the comparative value of rock volumetric thermal capacity to that of water. In general, as shown in Fig.4-11, system storage performance metrics are not overly sensitive to porosity. As far as the storage size is concerned, it is better to have a higher porosity, because water is a superior thermal energy storage medium.
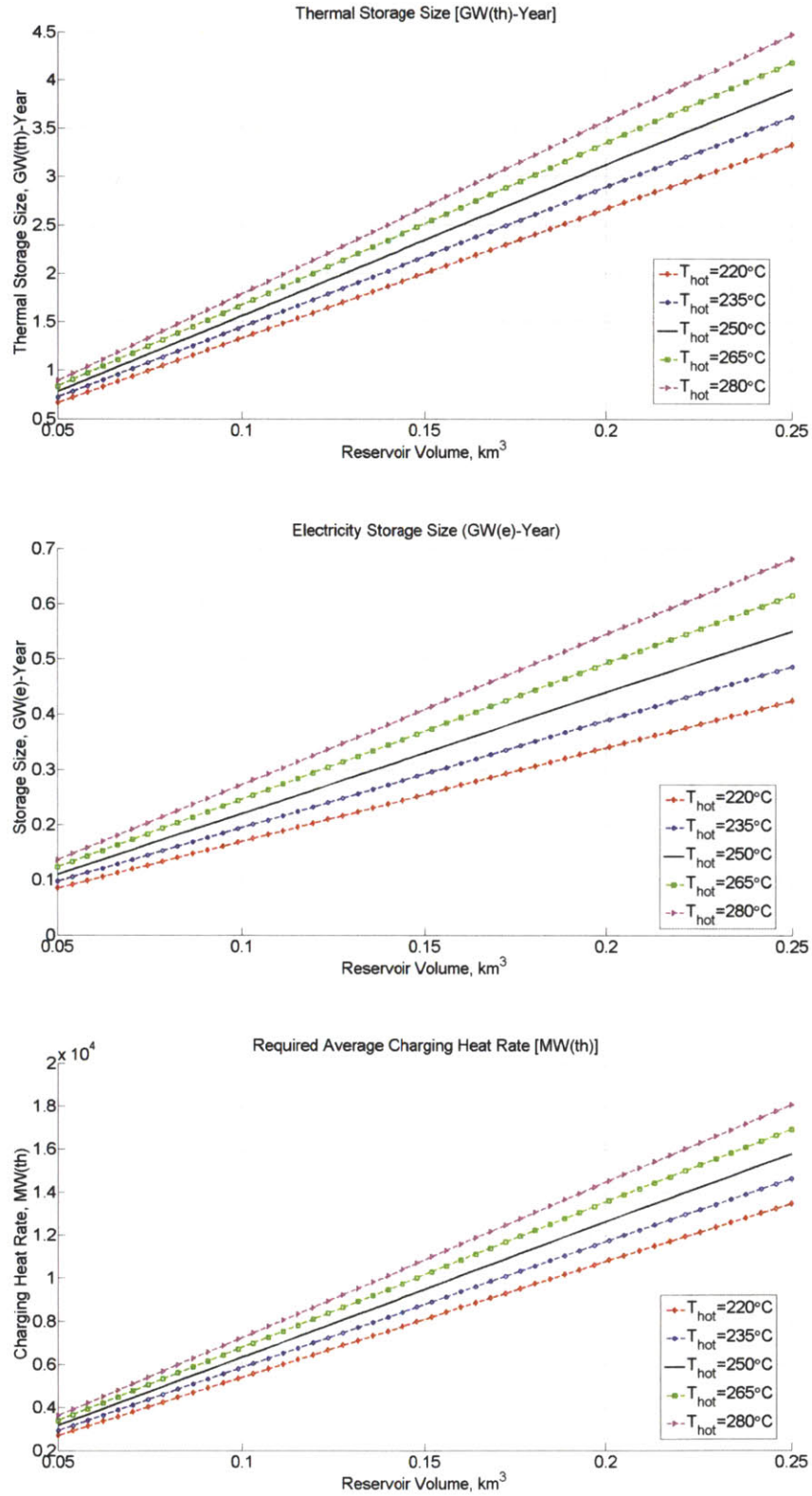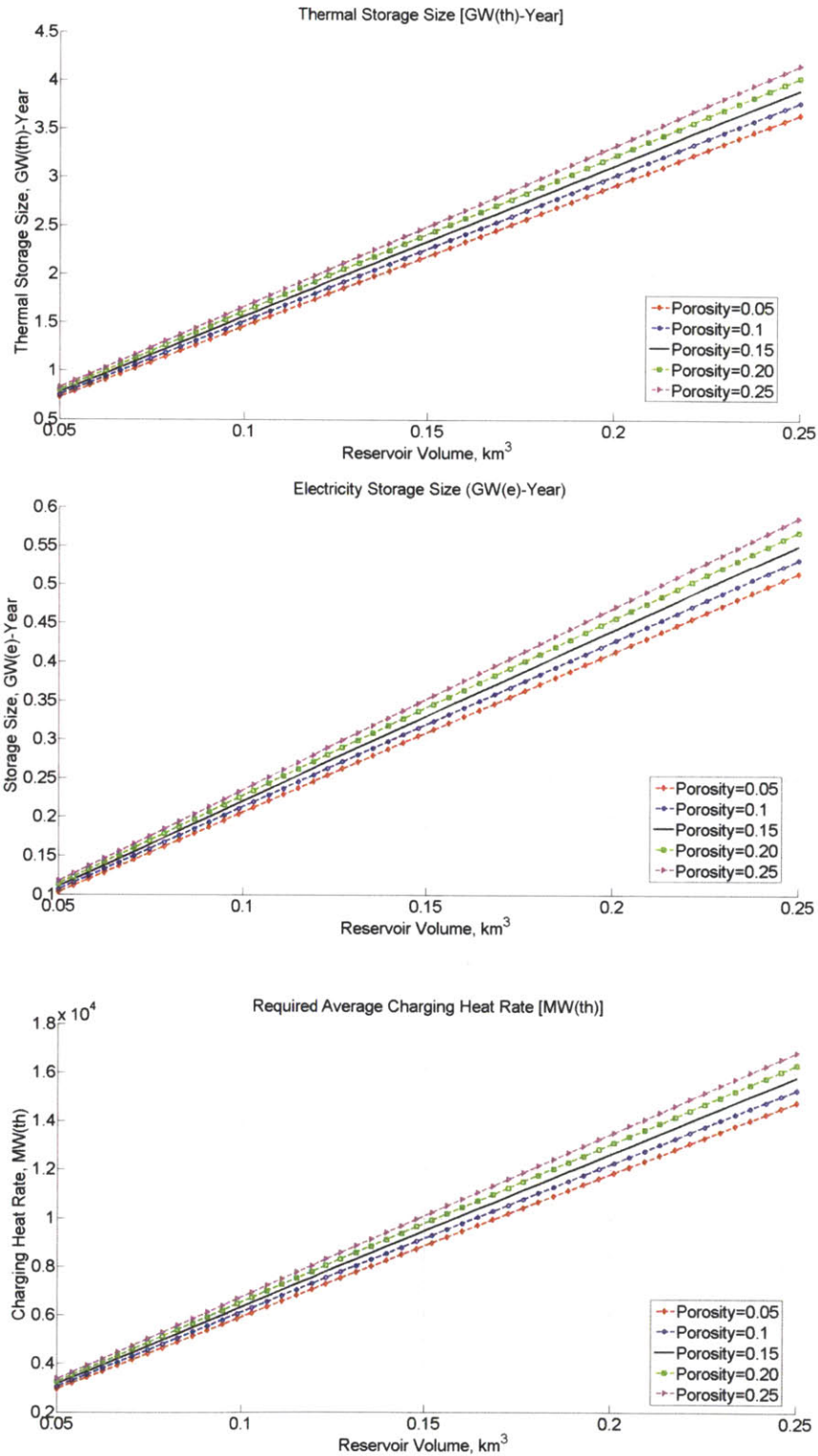
Fig.4-11 System Storage Performance Metrics with Varying Porosity (1) : Thermal Storage Size, Electricity Storage Size, Charging Heat Rate

4.3.2.4 Permeability effect

Permeability in a nuclear-EGS reservoir is artificially obtained by hydraulic fracture[26]. Unlike a conventional hydrothermal reservoir, a nuclear-EGS reservoir, in general, requires unusually high permeability, as geo-fluids flow rates are higher. As discussed in Chapter 2, a permeability of 2 Darcy is chosen to be the representative value. With the representative value being central, the lower bound of 0.5 Darcy and the upper bound of 3.5 Darcy are used for this sensitivity study[27].

Like the analysis of L/R effect case, the system storage performance metrics are insensitive to varying permeability. As discussed in Section 4.3.2.3, in this study, permeability is not related to porosity. Hence, varying permeability does not alter the relative ratio of rock to water, resulting in constant energy storage performance metrics. As an example, in Fig.4-12, thermal storage is essentially constant with varying permeability.

Permeability, however, does affect efforts for geo-fluid circulation and system efficiency significantly. Low permeability, by definition, increases pressure drop and pumping power as shown in Fig.4.12. It is worth noting that a reservoir permeability of 0.5 Darcy is not allowable as pressure gradient built up in a reservoir is so excessive that it can even potentially cause hydraulic fracturing. Such sensitivities are transferred to fraction of pumping power and average mass flow rate leakage ratio in Fig.4-13. Especially, mass flow rate leakage ratio far exceeds 10%, meaning that the economic energy production is not possible.

With all these effects, the round trip efficiency in Fig.4-13 demonstrates that reservoir permeability significantly affects system efficiency, hence economics, to a level that unsuitable permeability on its own can threaten the feasibility of the whole system. For instance, a permeability of 0.5 Darcy has almost 10% less round trip efficiency than the reference design with its Darcy value of 2. 10% reduction in system storage efficiency is likely to be unacceptable in terms of economics. Such an aspect is studied in detail in Chapter 5.

This sensitivity study leads to the conclusion that there is an unavoidable need for higher permeability for nuclear-EGS system reservoirs than conventional hydrothermal reservoirs: Simply, a nuclear-EGS system cannot work with the permeability typical of conventional reservoirs.

---

[26] In case of block cave mining, a packed bed pressure drop formulation is more appropriate than defining permeability

[27] 3.5 Darcy is assumed to be a potentially possible target permeability in the future while 0.5 Darcy can be regarded as a permeability of conventional hydrothermal reservoirs

Fig.4-12 System Storage and Geo-Fluid Circulation Effort Performance Metrics with Varying

Permeability (1) : Electricity Storage Size, Average Pressure Drop, and Average Pumping Power
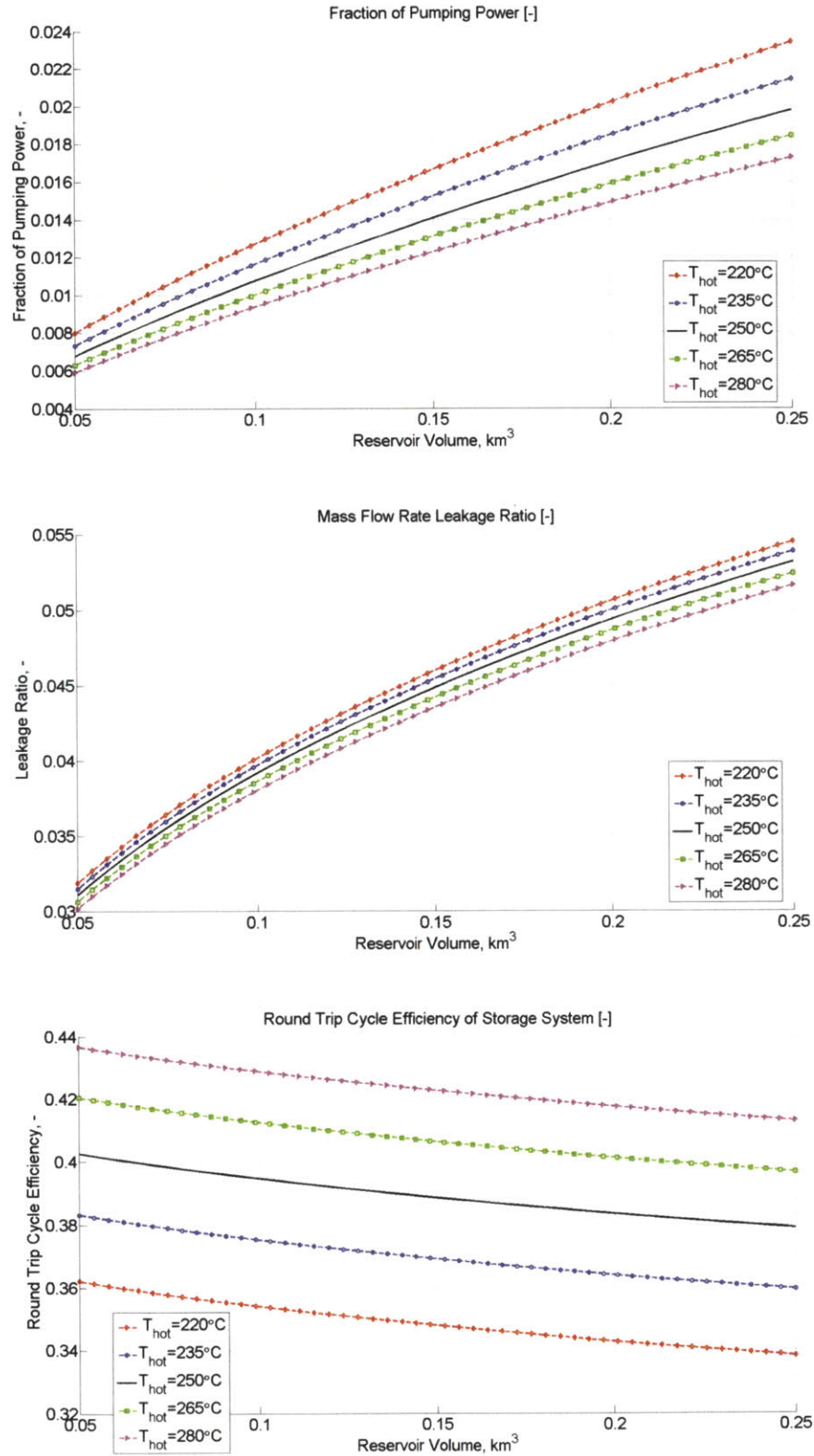
Fig.4-13 System Efficiency Performance Metrics with Varying Permeability (2): Fraction of Pumping Power, Mass Flow Rate Leakage Ratio, and Round Trip Cycle Efficiency of Storage System

4.3.2.5 Rock Volumetric Thermal Capacity Effect

Volumetric thermal capacity of rock - the ability of a given volume of a substance to store internal energy while undergoing a given temperature change, but without undergoing a phase change – can be obtained by multiplying density by the heat capacity of rock. With the reference volumetric thermal capacity, 2.21 MJ/m^3°C, being at center, ±50% of the reference values are taken to be upper bound and lower bound, respectively. Based on the discussions about rock thermal properties in Chapter 2, it is expected that the set range of rock volumetric thermal capacities can include any reasonable perturbations from the reference value.

As rock thermal capacity increases, storage size increases both for thermal and electric energy. Accordingly, charging heat rate increases to provide an increased storage requirement in a fixed cycle period. Such relations are linear as storage size is a linear function of the rock volumetric thermal capacity. Hence, as illustrated in Fig.4-14, the relative magnitudes for changes in the system storage performance metrics are the same with varying volumetric thermal capacities of rock.

Regarding system geo-fluid circulation effort performance metrics shown in Fig.4-15, more effort is needed to circulate water at a desired rate. This is because higher mass flow rate of water is required to store the increased amount energy while temperatures of water and volume are fixed. Such an increase in geo-fluid mass flow rate, in correspondence with increasing storage size, causes fluid velocity to increase, leading to a larger pressure drop. These two effects – increasing mass flow rate and velocity- are combined to further raise required pumping power at a faster rate. As can be seen in Figs.4-14 and 4-15, required pumping power increases faster than storage size with respect to increasing thermal capacity of the reservoir because of the combination of increasing mass flow rate and velocity effects on pumping power. As a result, fractional pumping power increases with increasing thermal capacity of rock, which causes round trip cycle efficiency of the storage system to decrease while mass flow rate leakage ratio remains essentially constant in Fig.4-16.

Interestingly, increasing thermal capacity of rock results in two competing phenomena as a whole: increasing storage size vs decreasing storage system efficiency. However, it can be seen in Figs.4-14 and 4-16, that the relative increase in storage size is far greater than the relative decrease in storage system efficiency for the same change in rock thermal capacity. In other words, the positive effect of increasing thermal capacity responds more sensitively to thermal capacity changes than the negative effect. Hence, if storage size is a concern in design, choosing a site of greater rock thermal capacity is a viable option.

134
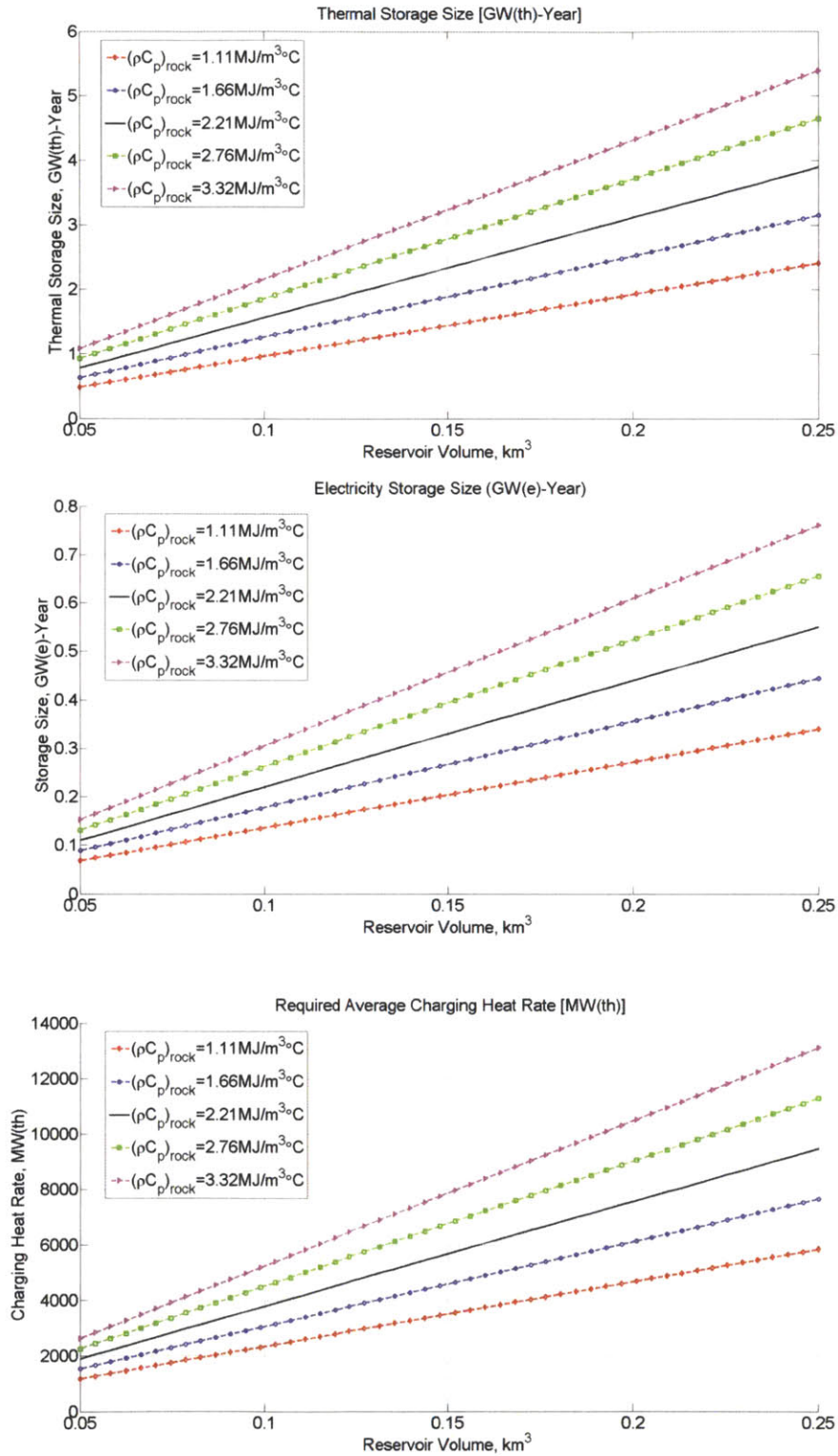
Fig.4-14 System Storage Performance Metrics with Varying Volumetric Thermal Capacity of Rock (1) :
Thermal Storage size, Electricity Storage Size, Charging Heat Rate
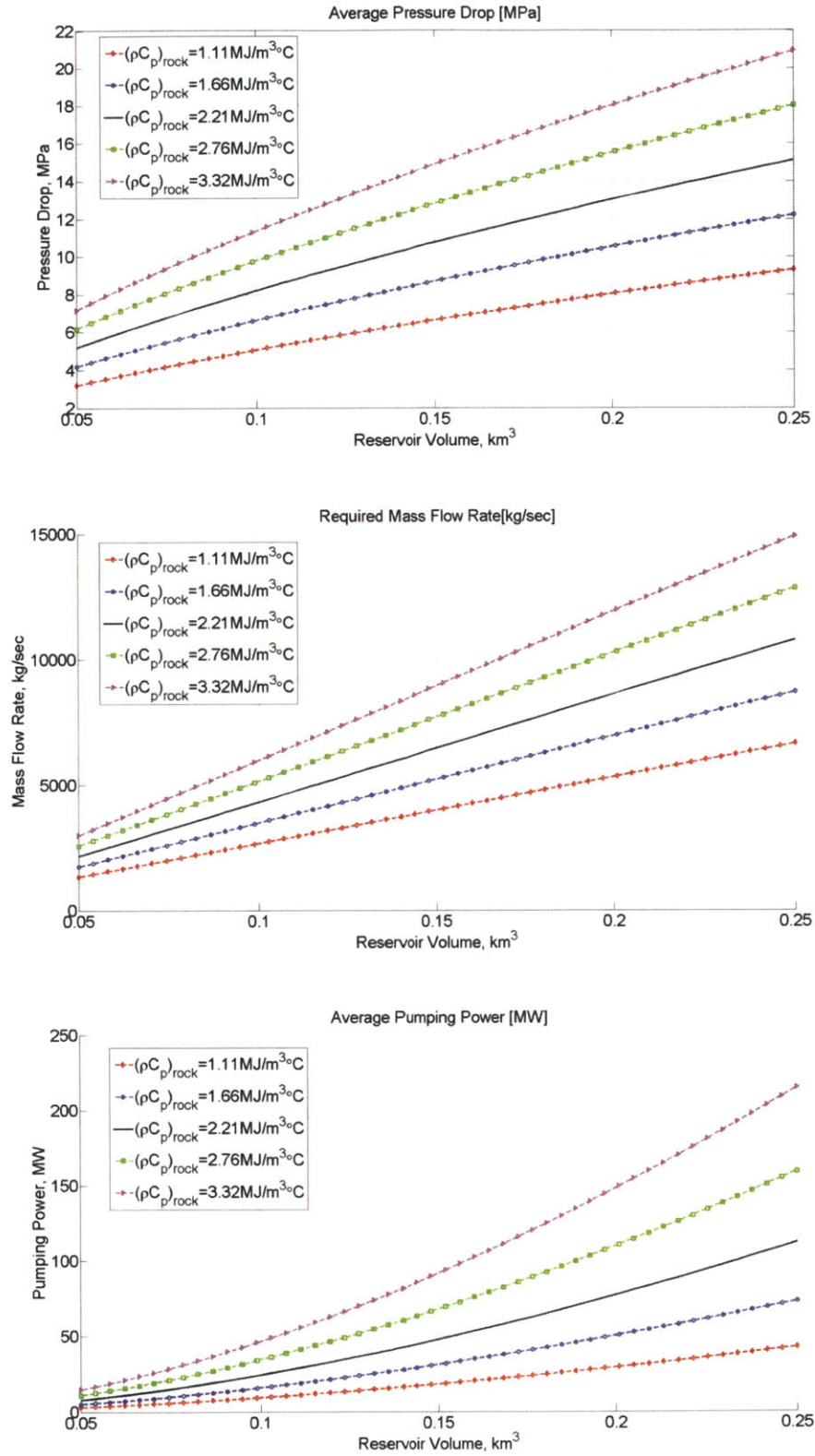
Fig.4-15 System Geo-Fluid Circulation Effort Performance Metrics with Varying Volumetric Thermal Capacity of Rock (2) : Average Pressure drop, Required Mass Flow Rate, Average Pumping Power
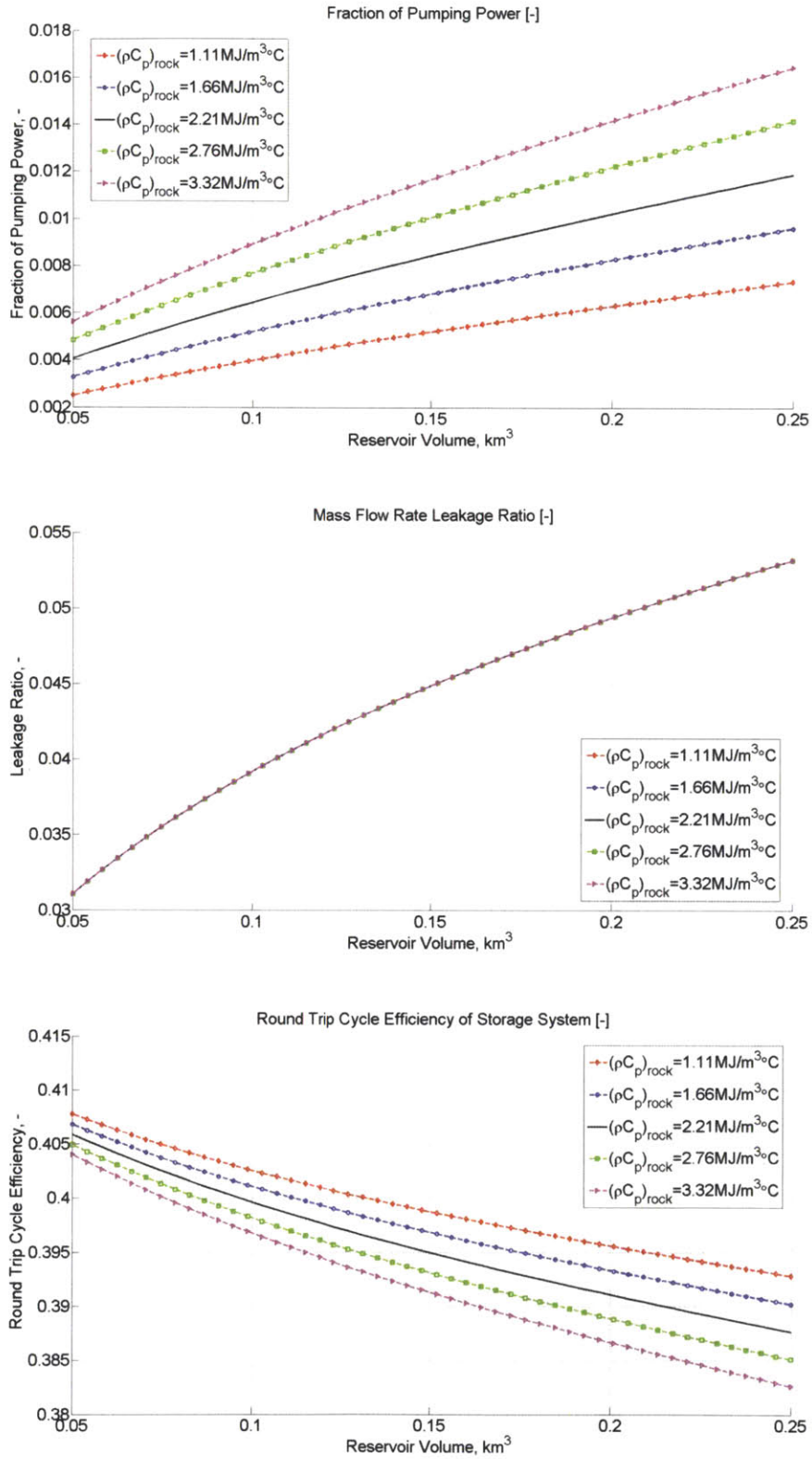
Fig.4-16 System Efficiency Performance Metrics with Varying Thermal Capacity of Rock (3) : Fraction of Pumping power, Mass Flow Leakage Ratio, Round Trip Cycle Efficiency of Storage System

4.3.2.6 Cycle Period Effect

It is worth noting that determining cycle period is an economic issue of a grid as it is, in principle, to be determined to cope with seasonal variations in electricity demand. Based on the length of peak and off-peak seasons and monetary profitability, cycle periods will be determined accordingly. Such cycle length determination based on economic analysis is discussed in Chapter 5.

The purpose of this section is to understand engineering aspects nuclear-EGS performance as a function of cycle periods. This is a critical issue for nuclear-EGS systems as it bridges to economic studies of the system and gives an important measure of compatibility of the system with given seasonal electricity demand characteristics of a grid. With 6 months (3 months of charging and 3 months of discharging) as the reference period, the upper bound of 10 months and the lower bound of 2months with equal lengths for charging and discharging are tested.

Like effects of L/R and permeability that are discussed in the previous sections, system storage performance sizes are not dependent on cycle period effects. They are dominantly functions of reservoir volume thermal capacity, so that it is implicitly assumed that the given storage size is to be charged and discharged within a set cycle period. Hence, mass flow rate and charging change accordingly, not the size of a reservoir. As illustrated in Fig.4-17, required charging rate increases with decreasing cycle period for the same reservoir volume because energy has to be charged faster to have the same amount of energy stored in a shorter time. Such a rapid charging accompanies an increase in mass flow rate, which results in increasing pressure drop and pumping power. An interesting observation is that such geo-fluid circulation efforts increase faster with decreasing cycle periods. For instance, the increase in average pumping power from 4months to 2months is substantially greater than that from 8 months to 4months. Such a trend is transferred to fractional pump in power, which is found to be increasingly sensitive to a shorter cycle period. While the relative mass flow leakage illustrated in Fig.4-18 remains constant with cycle periods, increasing fractional pumping power leads to decreasing round trip efficiency.

Therefore, in conclusion, shorter cycle periods make the storage system less efficient. In other words, a nuclear-EGS system performs better with a slowly varying electricity demand- characteristic suitable for large seasonal demand. Nuclear-EGS's unique function of storing a large amount of energy cannot be fully leveraged if such storage should occur rapidly. On the other hand, the shorter time period means more cycles in a given time, hence more chances for making profits if profit per unit energy storage is defined. For such a case, the nuclear-EGS storage system can operate with shorter time periods and accordingly low system efficiency but still making profits.
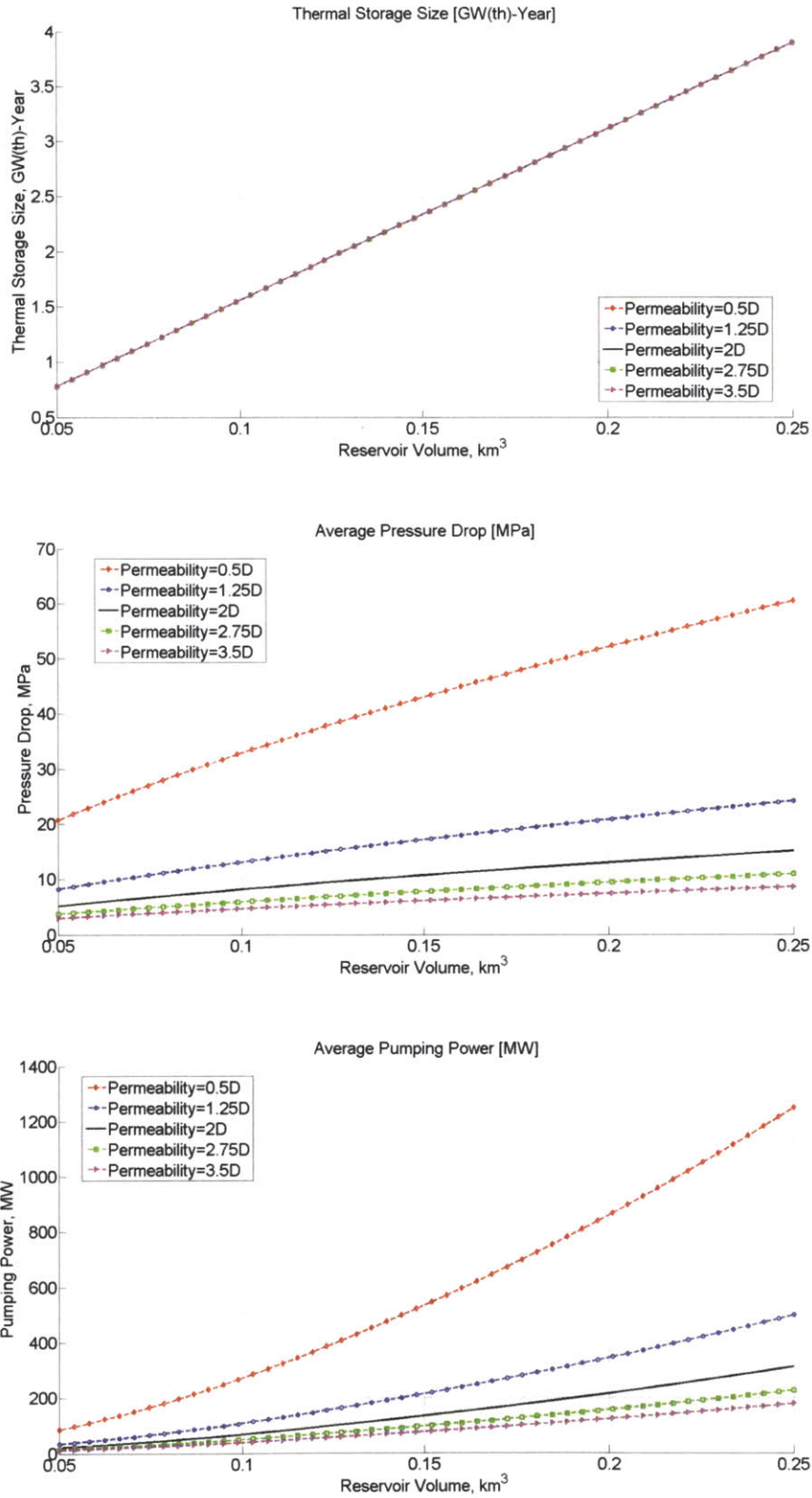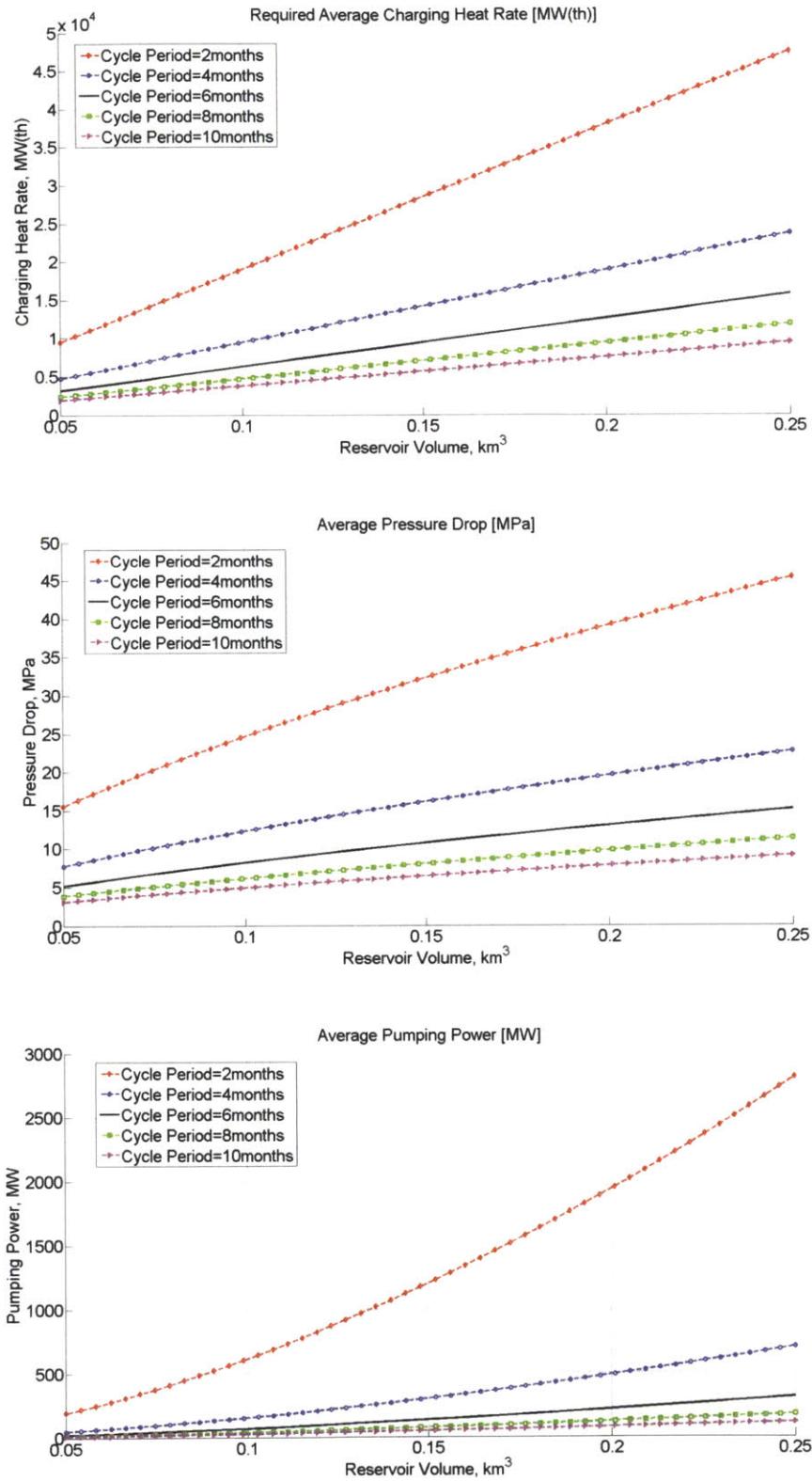
Fig.4-17 System Storage and Geo-Fluid Circulation Effort Performance Metrics with Varying Cycle
Period (1) : Electricity Storage Size, Average Pressure Drop, and Average Pumping Power
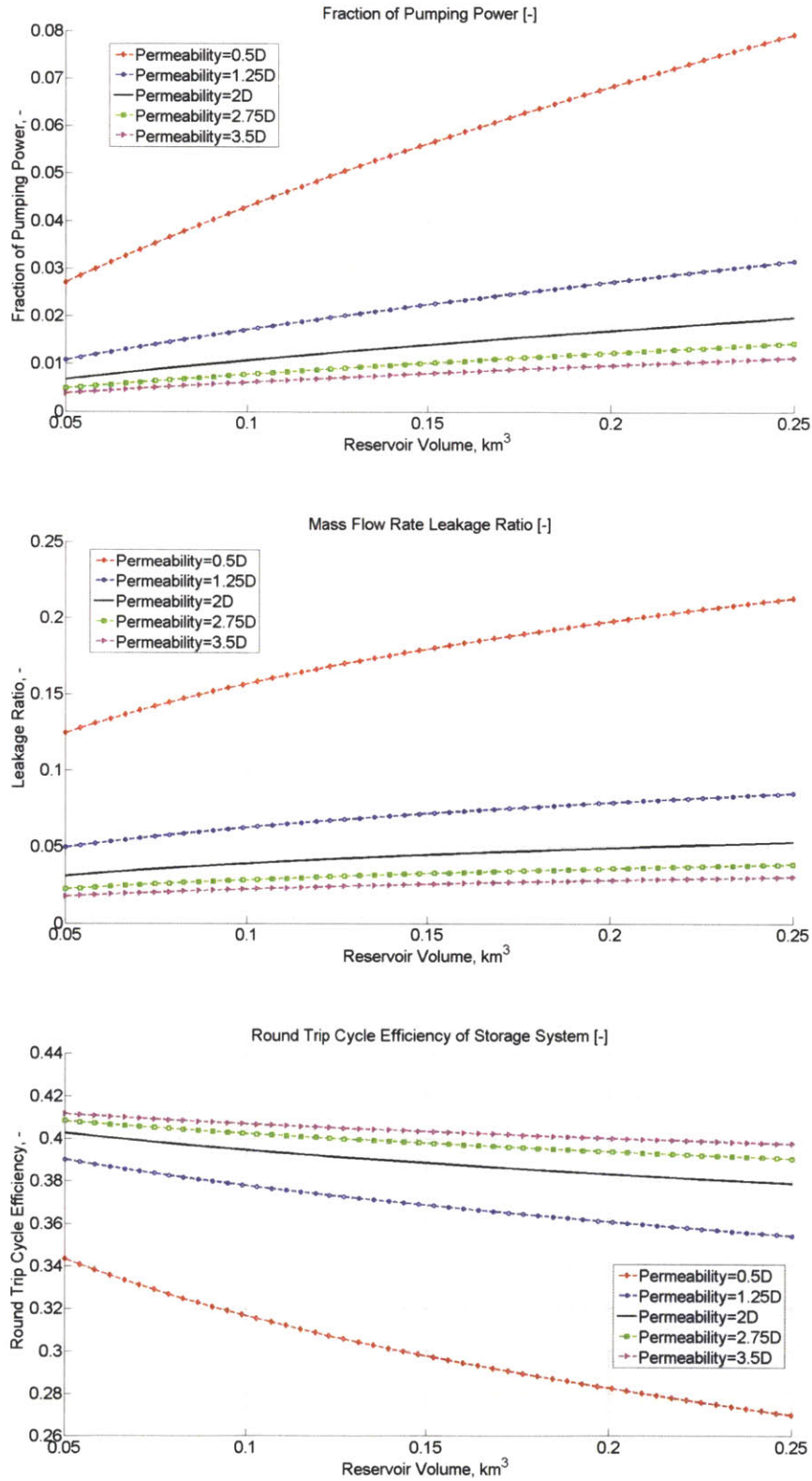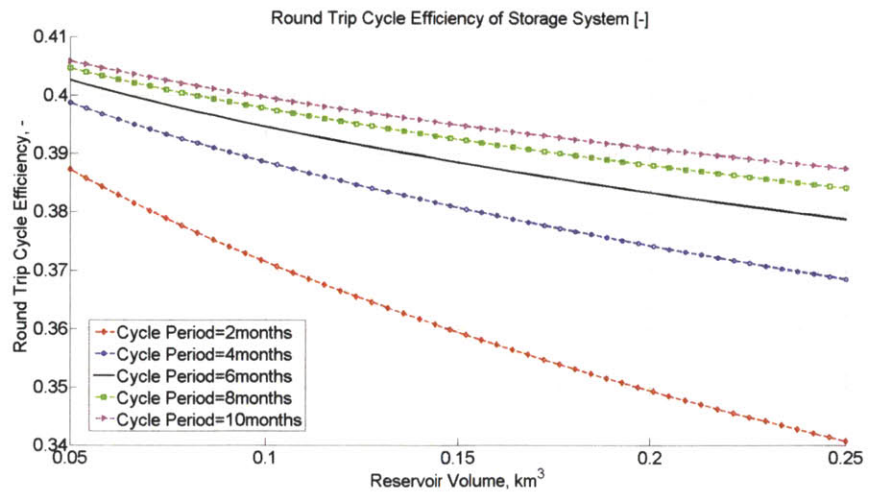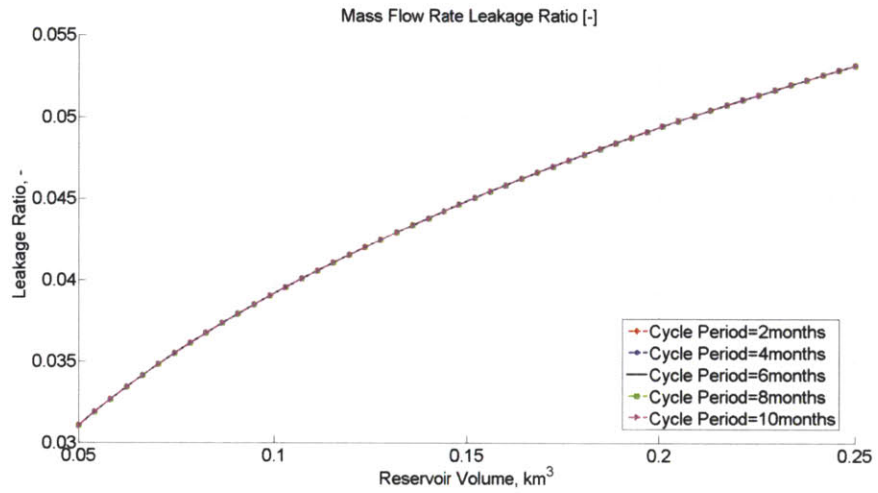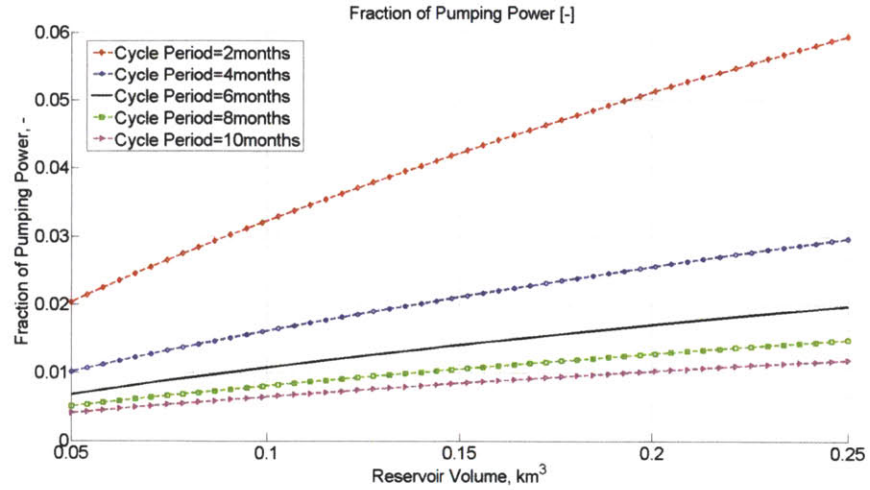
Fig.4-18 System Efficiency Performance Metrics with Varying Cycle Period (2): Fraction of Pumping Power, Mass Flow Rate Leakage Ratio, and Round Trip Cycle Efficiency of Storage System

140

4.4 Conclusion

In this Chapter, engineering design studies were performed in the context of design map and sensitivity studies. The following table summarizes the parameter space of nuclear-EGS energy storage systems.

Table 4-4 Summary of Design Variation Effects

	Design Parameters[28]						
	Volume	**L/R**	**T$_{hot}$[29],**	**Porosity**	**Permeability**	**Thermal capacity of Rock**	**Cycle Length**
Storage Size Maximization	Increase (high)	N/A	Increase (high)	Increase (low)	N/A	Increase (mid)	N/A
Storage Round-trip Efficiency Maximization	Decrease[30] (high)	Decrease[31] (medium)	Increase (high)	N/A	Increase (high)	Decrease[32] (low)	Increase (medium)

* Comments in parentheses represent the degree of effectiveness

* N/A indicates the design parameter has no appreciable influence

It was found that the performance metrics of a nuclear-EGS energy storage system can be categorized into two different criteria: storage size and storage round trip efficiency. Table 4-4 summarizes the parameter space and effectiveness of the design parameters for each performance criterion. Controlling reservoir volume is the most brute-force way of designing the system. However, it is not the omnipotent solution because it cannot simultaneously satisfy both storage size and round trip efficiency, and is likely to be limited spatially and economically. Increasing maximum temperature, however, is a way to achieve both storage size and round trip maximization with great effectiveness. This can be done through an improved heat exchanger design and better insulation of injection piping. For maximization of storage round trip

---

[28] Surrounding rock permeability and depth are not listed here as the former has already been discussed in detail since it is the single most dominant parameter for mass flow leakage rate.

[29] Maximum reservoir temperature works as effectively as the minimum reservoir temperature. Hence the column can also be replaced with T$_{cold}$ with "Increase" replaced by "Decrease".

[30] Larger sizes imply higher pumping losses through the larger reservoir. However, there is also a minimum size to avoid excessive heat conduction losses

[31] Starting with L/D >> 1

[32] A higher geo-fluid flow rate is needed for a larger storage capacity while the volume of the reservoir and the cycle length are assumed to be fixed. Higher flow rates increase pumping power and water-leakage faster than storage capacities.

efficiency, improved hydraulic fracture of the reservoir to achieve higher permeability is the most effective way. This implies that a block caved reservoir is likely to run at high round trip efficiency.

CHAPTER 5

Economic Analysis of Nuclear-EGS System

5.1   Introduction

This chapter is dedicated to the economic analysis of nuclear-EGS systems. Specifically, the sinusoidal characteristics of seasonal electricity grid demand, and electricity cost of nuclear-EGS are discussed. In addition, the economic benefits introduced by a nuclear-EGS system are assessed for various plausible grid situations. Electricity demand combined with engineering designs discussed in Chapter 4 focusing the connections are used as the basis for the economic analyses.

5.2   Grid Characteristics

It is necessary to understand some relevant real features of representative electricity grids and markets. Such data will not only be directly used in economic analysis but also provide general ideas and directions of nuclear-EGS performance. In this section, some important grid and market data are discussed, and modeling of the data is assessed.

In this study, it has been assumed that the seasonal electricity demand follows a sinusoidal curve. Sinusoidal modeling of electricity generation greatly facilitates economic analysis. However, it is questionable if a sinusoidal model is truly representative of the real case. If the sinusoidal model misses any crucial fact that cannot be ignored or approximated in the context of economic analysis of seasonal heat storage systems, then we are limited in using the model. Hence, it is important to confirm the validity of the sinusoidal model before discussing the economic characteristics of nuclear-EGS systems.

The U.S national electricity demand was taken as a reference example. Confirmation was carried out by comparing the best fit sinusoidal model with the total electricity net generation in the USA, 2007 through 2009 as illustrated in Fig. 5-1.
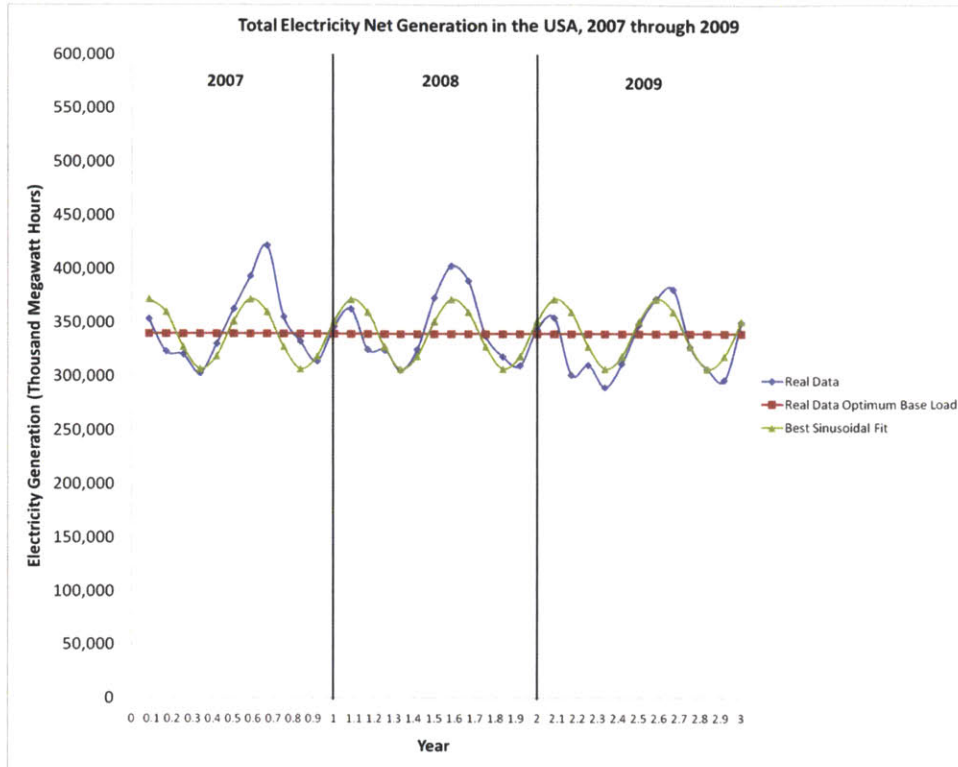
Fig.5-1 Total Electricity Net Generation in the USA 2007 through 2009
and Comparison with Sinusoidal Best Fit

The sinusoidal model that best fits the real data is found to be:

Net Electricity Generation[Thousand Megawatt Hours]= 339645.8+32802.3 Cos(4πτ-1.202)

Eq. 5-1

where τ represents fraction of a year. The sinusoidal model provides a reasonable model of demand although, as shown in Fig.5-1, the sinusoidal best fit slightly underestimates summer peaks and overestimates winter peaks. The real average value for net electricity generation, which is 'Real Data Optimum Base Load' in Fig.5-1 is practically the same as the sinusoidal average, 340 million megawatt hours.

However, it is important to note that the real capacity factor of peaking units is not accurately obtained if the sinusoidal model is used. The sinusoidal model gives approximately $1/\pi$ for the capacity factor of peaking units (nuclear-EGS) that are meant to provide electricity beyond optimum base load, whereas the real data gives 0.16, half of $1/\pi$. In addition, for peaking units (Gas turbine) that run on top of original base load, which is the lowest point of electricity generation in Fig.5-1, the sinusoidal model gives

144

approximately 0.5 for capacity factor whereas the real data gives 0.38. Considering the importance that capacity factor has on levelized electricity cost of peaking units, the sinusoidal model's tendency to exaggerate capacity factor is subject to further scrutiny, in the context of validation of the model for economic analysis of a seasonal heat storage system.

Indeed, it is found that the exaggerated capacity factor is neutralized by the decreasing amount of peaking electricity. Consequently, the sinusoidal model gives fairly equivalent results for the break-even electricity cost and other real data. Hence, it is concluded that the sinusoidal model bears no disqualifying limitation in its applicability, at least in the context of the economic analysis conducted in this study.

It is, however, worth noting that no decisive assessment of the aptness of the sinusoidal seasonal electricity demand can be made unless a real grid is examined. The total electricity net generation in the USA in Fig.5-1 is a mere exemplary case. In reality, a grid has a number of reasons that can potentially shape its seasonal demand curve, deviating from the sinusoidal model. Hence, in this case, New England Independent System Operator (ISO) is chosen as a real exemplary grid for analysis.

Based on New England ISO, Oloyede et al [1] have modeled demand, hence electricity generation as a cosine function as indicated in Eq.5-2 and Fig.5-2:

$$\text{Demand(MWe)} = P_0 + A\cos(4\pi\tau)$$

Eq. 5-2

Where P_0, A, τ are a new optimum base load when a lossless large energy storage system is deployed, peak power relative to base load and fraction of year, respectively.

145
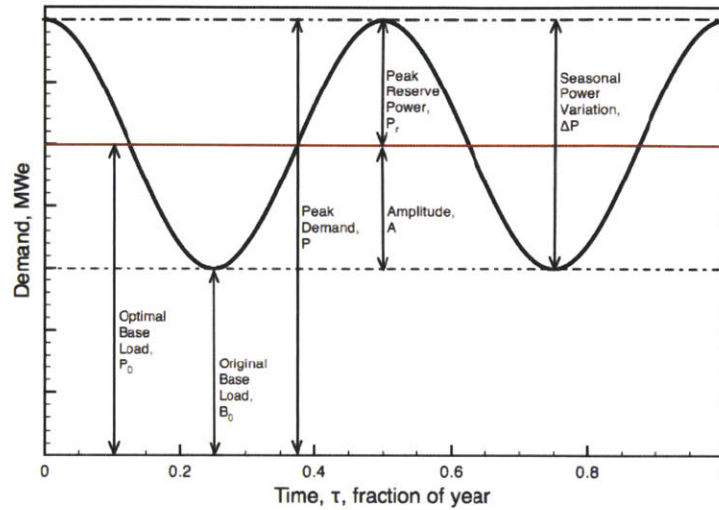
Demand Characteristics for Lossless ISO New England Demand Data

Mean Demand Characteristics	Evaluated Values			Relative Comparison		
	Hourly	Daily	Weekly[1]	Hourly	Daily	Weekly
Original Base Load, B_0 (MWe)	9,824	9,824	9,824	1.0	1.0	1.0
Peak Demand, P (MWe)	26,253	21,799	19,442	1.4	1.1	1.0
Optimal Base Load, P_0 (MWe)	15,418	15,418	15,419	1.0	1.0	1.0
Amplitude, A (MWe)	5,594	5,594	5,595	1.0	1.0	1.0
Seasonal Power Variation, ΔP (MWe)	16,429	11,975	9,618	1.7	1.2	1.0
Amplitude to Original Base Load Ratio, α	0.57	0.57	0.57	1.0	1.0	1.0
Peak Demand to Original Base Load Ratio, β	2.67	2.22	1.98	1.4	1.1	1.0
Peak Reserve Power, P_r	10,835	6,381	4,023	2.7	1.6	1.0
Peak Reserve Power to Original Base Load, φ	1.10	0.65	0.41	2.7	1.6	1.0
Peak Reserve Power to Optimal Base Load, γ	0.70	0.41	0.26	2.7	1.6	1.0

Fig.5-2 Sinusoidal Demand Curve with Period ½ Year of New England[33]

5.3 Electricity Price

The economic incentives to deploy Nuclear EGS are rooted in the electricity price difference between peak-power electricity and off-peak-power electricity. Beyond a certain price difference, deployment of a

---

[33] Peak power demands were analyzed three ways. Hourly implies using hourly data. Daily assumes each day has a constant power demand. In effect, the assumption is made that energy storage technologies such as pumped hydro levelize power demand each day. Weekly assumes that other energy storage technologies create level electricity demand for each week but each week has its own demand. Weekly data gives a perspective on seasonal storage requirements.

nuclear-EGS system will not only be justified but also starts to make profits. Figs.1-4 illustrates sector average monthly retail price of electricity in the USA, 2007 through 2009, and averaged retail price of all sectors.
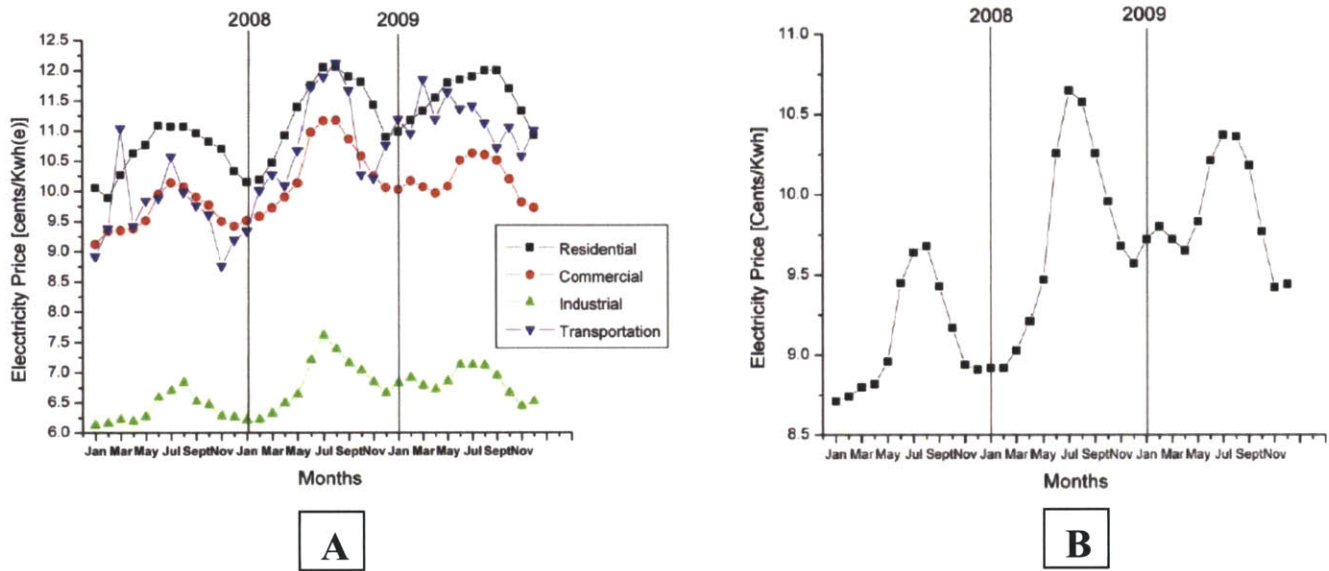
Fig. 2-2 Average Monthly Retail Price of Electricity in the USA, 2007 through 2009
(A: Different Sectors, B: All Sectors Averaged)

Fig.1-4 shows that retail electricity cost, in general, is quite constant over months as it is noted that the peak to off-peak price ratio is merely about 1.1. Apparently, such a fact may seem discouraging as one may be skeptic of about whether such a small difference in price could justify the deployment of a nuclear-EGS system. It is worth noting, however, that the price charged by a utility is affected by regulation, and hence does not necessarily represent the actual cost for the utility of generating electricity. Repeating the statement of the introduction Chapter.1,

"Such an electricity price difference between peak power electricity and off-peak power electricity is the economic basis of deployment of the nuclear geothermal system: Store energy when price is cheap, sell energy when the price is high. It is important to note that hourly electricity variation, which is not shown in Fig.4, is much more significant because its degree of demand fluctuation is greater and time to cope with such fluctuations is much shorter. Hence a well planned strategy of seasonal storage – charging at low price hours during low price seasons, selling at high price hours during high price seasons – could take advantage of both hourly and seasonal variations in electricity prices, ultimately leading to justifying the deployment of nuclear-geothermal energy storage systems.

147

However, basing the economic analysis of the nuclear-geothermal system on the retail price of peak electricity is not appropriate although it helps understand the economic incentive for the deployment of the system. This is because the retail price of electricity is a figure that is determined after taking into account regulations, pricing policy etc. In other words, the instantaneous retail price of electricity is a somewhat skewed or opaque reflection of actual instantaneous electricity demand. Thus, when quantifying economic effects upon the introduction of such a system in a grid, it is recommended to assess changes in electricity generation costs – not selling price. Hence in this study, economic studies are performed based on quantifying electricity cost."

The following section discusses the details of levelized cost of electricity which is relevant to a nuclear-EGS system.

5.4   Electricity Cost

Levelized electricity cost is a representative way of measuring and comparing economics of different power production technologies. In this section, levelized peaking electricity cost by an EGS is calculated. Peak power gas turbines are the ultimate competitor for an EGS peak power unit, assuming that in the future use of fossil fuel plants is constrained by increasing awareness of global warming and fuel cost. Considering this, the levelized cost of a peaking unit gas turbine is calculated for further comparisons relevant to feasibility analysis.

Levelized cost of a peaking EGS and a gas-turbine that includes capital related costs (plant + site work), operating and maintenance (O&M) costs were evaluated according to the following set of equations from [24]

Capital-Related Costs:

$$\frac{100\varphi}{8,766L}\left(\frac{I}{K}\right)_{-c}\left[1+\frac{x+y}{2}\right]^{c}$$

Plus Operating and Maintenance (O&M) Costs

$$+\frac{100}{8766L}\left(\frac{O}{K}\right)_{0}\left[1+\frac{yT}{2}\right]$$

Plus Fuel Costs

$$+(\text{Fossil})\left[\frac{0.0034 f_{0}}{\eta}\right]\left[1+\frac{yT}{2}\right]$$

Eq. 5-3

148

The definitions and values used for each term are summarized in Table 5-1.

	EGS	Geothermal Reference	Gas Turbine	Natural gas Reference
L (Plant Capacity)[34]	$1/\pi$	Sinusoidal Supply	0.5	Sinusoidal Supply
φ (Annual Fixed Charge Rate)	0.128/year	NREL Report 2007 [25]	0.128/year	$\varphi = x/(1-\tau)$
τ (Tax Fraction)	0.5058	Future of Geothermal Energy (MIT) [6]	*0.4	Sustainable Energy [24]
r_b (Rate of Return on Bonds)	0.064	Future of Geothermal Energy (MIT) [6]	0.08	CANES Report "Update on the Cost of Nuclear Power" 2009 [27]
r_s (Rate of Return on Equity)	0.17	Future of Geothermal Energy (MIT) [6]	0.12	CANES Report "Update on the Cost of Nuclear Power" 2009 [27]
b (Debt Fraction)	0.8	Future of Geothermal Energy (MIT) [6]	0.6	CANES Report "Update on the Cost of Nuclear Power" 2009 [27]
x	0.059	$x = (1-\tau)br_b + (1-b)r_s$	0.076	$x = (1-\tau)br_b + (1-b)r_s$
$\left(\frac{I}{K}\right)_{-c}$ (Overnight Specfic Captial Cost of Plant)	1377.2\$/KW for a 2-flash 100MW unit	Future of Geothermal Energy (MIT) [6]	850\$/KW for a 1000MWe Plant	CANES Report "Update on the Cost of Nuclear Power" 2009 [27]
	2 millions\$/well For depth 1.5km		650\$/KW for a conventional gas turbine	DOE/US Energy Information Administration Website. 2010 [28]
y (Annual Rate of Monetary Inflation)	0.04/year	Sustainable Energy [24]	0.04/year	Sustainable Energy [24]
c (Time required to construct plant)	2 years	Future of Geothermal Energy (MIT) [6]	2 years	CANES Report "Update on the Cost of Nuclear Power" 2009 [27]
T (Prescribed useful life of plant)	30 years	Future of Geothermal Energy (MIT) [6]	40 years	CANES Report "Update on the Cost of Nuclear Power" 2009 [27]
$\left(\frac{O}{K}\right)_0$ (Specific Operating and Maintenance Cost as of Start of Operation)	100\$/KW/Year	NREL Conference Paper. "The Status and Future of Geothermal Electric Power" Kutscher. 2000 [26]	13/Kw/year	CANES Report "Update on the Cost of Nuclear Power" 2009 [27]
η (Thermodynamic Efficiency)			0.35	Typical value for a natural gas plant
f_0 (Fossil Fuel Cost)			7\$/mmBTU	CANES Report "Update on the Cost of Nuclear Power" 2009 [27]

Table 5-1 Values Used for the Levelized Electricity Cost Evaluation

[34] The plant capacities are subject to changes depending on the grid portfolio. The values shown in the table are reference data

There are four important observations regarding the levelized electricity cost calculation. First, the reference capacity factors for the peak power EGS and gas turbine are different, as the former is about 0.32 whereas the latter is 0.5. This is because of the assumptions made for the grid portfolio. For simplicity, the grid was assumed to be only run by either the nuclear (base load)-EGS (peak load) with the round trip efficiency of unity or nuclear (base load)-gas turbine (peak power). Consequently the nuclear base load – EGS peak power combination runs with the raised base load at P_0 while the nuclear base load – gas turbine peak power combination runs with base load B_0 as illustrated in Fig.5-2, leading to the difference in the capacity factor. The capacity factor, however, can change if the grid portfolio changes or nuclear EGS round trip efficiency deviates from unity. Such effects are discussed in Section 5.5.

Second, it is worth looking in detail at how the site preparation cost and overnight plant were obtained. Site preparation cost consists of two items: drilling and underground stimulation. It is reported in the MIT study [6] that the underground stimulation cost is negligible compared to that of the drilling. Hence in this study, underground stimulation cost has been assumed to be zero.

$$\text{Underground Preparation Cost} = \text{Drilling} + \text{Underground Stimulation} \cong \text{Drilling}$$

Eq. 5-4

The MIT study [6] finds drilling cost as a function of depth as Fig.2-9 illustrates:

150
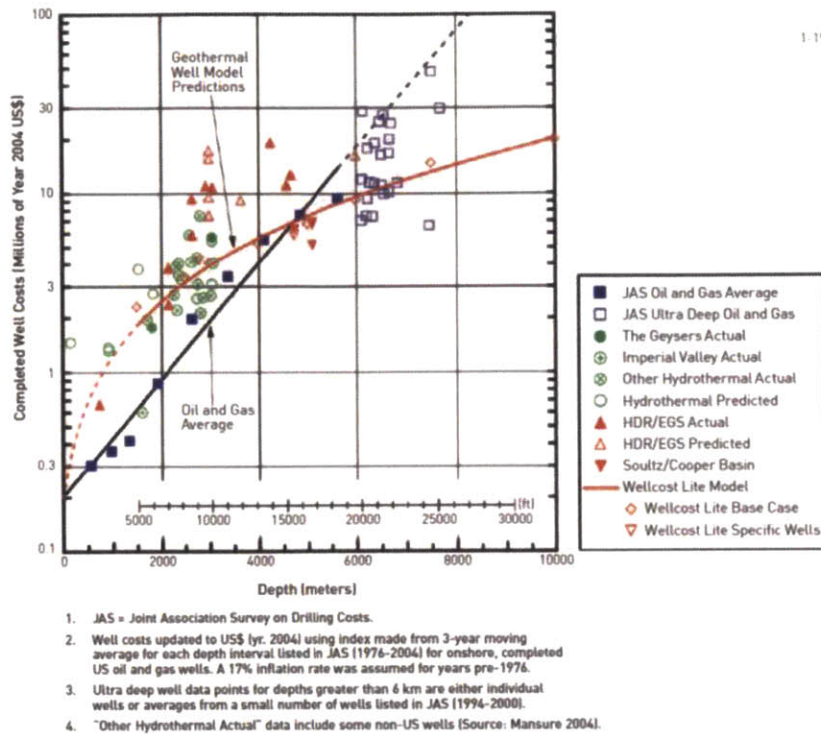
Fig.2-9 Completed Oil, Gas, and Geothermal Well Costs as a Function of Depth in 2004 US $

The engineering analysis in Chapters 2, 3, and 4 gives the depth of an EGS reservoir for a seasonal storage system as 1.5 km, which means 2 million $ /well according to Fig.2-9. Also the MIT study says that 1000kg/sec of mass flow rate is needed to achieve 100MW using a double flash plant, which is a typical cycle operating at the geo-fluid temperature of interest in a nuclear-EGS System (~240 °C). Also the study says the maximum tolerable flow rate for a single well in an EGS reservoir is 100 kg/sec. Another piece of necessary information is the ratio between injection wells and production wells. An NREL report [25] says that 3 production wells are needed for every injector in a typical EGS reservoir. Considering the fact that an EGS reservoir that is used for a seasonal heat storage system is quite different from typical EGS reservoirs, as the former is characterized by much greater stimulated reservoir permeability. Thus the numbers used here may be subject to changes as further research on reservoir modeling proceeds. However, for now, the numbers for the typical EGS were used, as it still gives a meaningful economic assessment of the Nuclear EGS system. Hence, overnight specific capital cost of drilling cost was evaluated as follows:

$$\left(\frac{I}{K}\right)_{-c}\left[\frac{\$}{KW}\right] = \text{Money for a single Well} \times \text{Number of Wells Needed per unit power}$$

$$= \frac{2\text{million}\$}{\text{Well}}_{@1.5\text{km}} \times \frac{1000\text{kg/sec}}{100\text{MW}}_{@\,240°\text{C,Double Flash Plant}} \times \frac{\text{Well}}{100\text{kg/sec}}$$

$$= \frac{2\text{million}\$}{\text{Well}}_{@1.5\text{km}} \times \frac{\frac{1000\text{kg}}{\text{sec}}}{100\text{MW}}_{@\,240°\text{C,Double Flash Plant}} \times \frac{\text{Well}}{\frac{100\text{kg}}{\text{sec}}}$$

$$= \frac{0.2\text{million}}{\text{MW}} = \frac{200\$}{\text{KW}} \text{ for injection wells}$$

Eq. 5-5

3 producers are needed for every injector in a typical EGS, hence 800$/KW is needed as a sum.

Overnight specific capital cost of the EGS plant was obtained using the formula developed in the MIT EGS study [6]:

$$C[\$/KW] = 750 + 1125\exp\left(-0.006115(\dot{W} - 5)\right)$$

Equation 5-6

Where C is the over-night specific capital cost of a binary flash EGS plant, and W is the rating of the power plant in MW. This formula accounts for both economy of scale and learning effects. A noticeable feature in this equation is that for large power plants, the cost approaches asymptotically to 750 $/KW. This limiting cost is the judgment based on experience with actual, recently constructed plants. Through personal correspondence with Prof. Tester at Cornell University, it was found that the maximum size of plants in an EGS system is highly likely to be no greater than 100MW. This gives 1377$/KW for overnight plant cost at 100MW. Nevertheless, it is worth keeping in mind that one can possibly reduce the capital cost associated with plants up to almost 60% if one can justify an EGS power plant several times larger than 100MW.

Third, it is important to note that the overnight capital costs of gas turbines are different from different references. This may be due to different design features. On the other hand, considering that reference years in Table 5-1 are different as for 2009 (850$/KW) and 2010 (650$/KW), a possible explanation could be that the large commodity price fluctuation in recent years has been built into the difference. For all that, since the cost of gas-turbine generation is highly dependent on the cost of fuel, the difference in capital cost is likely to bear small importance in levelized cost.

Fourth, a possible carbon tax duty on the gas-turbine was calculated. In the report "Update on the Cost of Nuclear Power"[27], carbon dioxide intensity per unit electricity produced is reported as 0.361kg CO_2/kWh and the carbon price is assumed to be $25/$tCO_2$. This gives 0.9cents/kWh additional cost to be added to the levelized peak power electricity cost of the gas turbine option.

Fig.5-3 illustrates levelized electricity cost of EGS and gas turbines at the reference capacity factors. In addition, comparing 1 and 2, and 3 and 4 of Fig.5-3 [35]reveals the sensitivity of electricity cost for the two technologies as a function of capacity factor. Given that the EGS is highly capital intensive, it is much more disadvantaged for the same marginal reduction in capacity factor, compared to a gas-turbine. Hence, as illustrated in number 1 and 2 of Fig.5-3, there is a large jump in levelized cost as the sinusoidal capacity factor 0.32 is reduced to half the value, which is more representative of the real capacity factor of the USA national grid, 0.16. This is because the built plant is less utilized as its idle time increases. On the contrary, the gas-turbine whose dominant cost component is fuel, is weakly affected by decreasing capacity factor, illustrating the typical inherent characteristic that peaking power technology conveys. The O&M cost is a significant portion of the total cost in the EGS system. If this cost can be appropriately reduced with increasing plant size in the context of economies of scale, a significant reduction in levelized EGS peak power cost is expected. The carbon tax imposed on the levelized cost of peaking gas turbines is quite negligible. This may be generally true for other peak power technologies, where high fuel costs are dominant.

It is evident that generally speaking the EGS peaking system's levelized cost is more expensive than that of a gas turbine, as it suffers from low capacity factor while such a condition is tolerable for gas-turbine peaking systems. Nevertheless, it is too early to conclude that a nuclear-EGS system has no economic competitiveness versus a Nuclear-gas turbine system before the assessment of the economic advantages that come with raising the original base load to the new level in the case of the nuclear-EGS system. In addition, a well-designed portfolio with both EGS and gas turbines can introduce synergistic effects in a grid. More details of such a grid portfolio study are discussed in the following section.

---

[35] The levelized electricity

153

1

Peak Power Electricity -Nuclear-EGS: Sinusoidal Capacity=0.32
(cents/kWh(e))

	Plant	O&M	Drilling*	Total
Nuclear Geothermal	6.96	5.73	3.85	16.54

2

Peak Power Electricity -Nuclear-EGS: Real Capacity=0.16
(cents/kWh(e))

	Plant	O&M	Drilling*	Total
Nuclear Geothermal	13.8	11.4	7.7	32.9

3

Peak Power Electricity -Nuclear-Gas Turbine: Sinusoidal Capacity=0.5
(cents/kWh(e))

	Plant	O&M	Fuel	Carbon Tax	Total
Nuclear_Natural Gas	2.78	0.53	12.24	0.9	16.45

4

Peak Power Electricity -Nuclear-Gas Turbine: Real Capacity=0.38
(cents/kWh(e))

	Plant	O&M	Fuel	Carbon Tax	Total
Nuclear_Natural Gas	3.7	0.76	12.2	0.9	17.56

Fig.5-3 Levelized Cost Break-Down of Two Different Capacity Factors for
EGS and Gas Turbines

154

5.5 Economic Benefits of Nuclear-EGS System

As discussed in the previous section, EGS is generally less suitable for meeting peak electricity demand compared to gas turbines because of the large portion of the capital cost in its levelized electricity cost. Hence, one is interested to consider a simple, yet representative, grid portfolio that consists of nuclear base load, EGS intermediate load, and gas turbine peak load as illustrated in Fig.5-4.
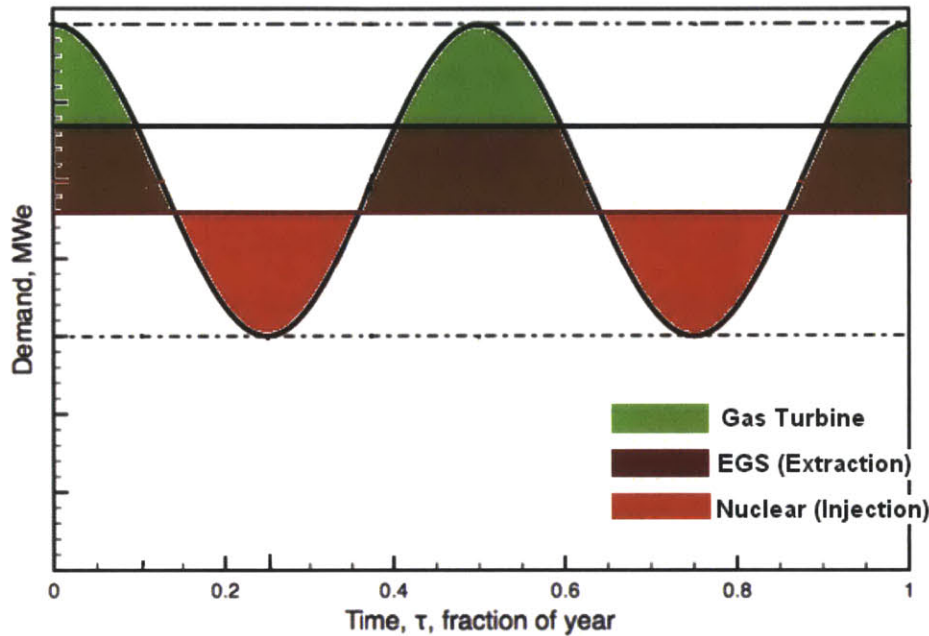
Fig.5-4 An Illustration for a Simplified Grid Portfolio of Nuclear, EGS and Gas Turbine

By using an EGS that is coupled with nuclear power plants via underground reservoirs for intermediate load, the grid can avoid running the capital intensive power technology (EGS) at a very low capacity factor. In other words, gas turbines can be strategically used for meeting the peak seasonal demand that cannot be effectively covered by EGS. Hence, should a nuclear-EGS energy storage system be realized, it will provide base and intermediate load. In that regard, the simplified grid portfolio that consists of nuclear, EGS and gas turbines is fairly representative for the purpose of preliminary economic studies as it includes the most pivotal power technologies for each definitive sector of grid demand. In this study, the economic benefits of the nuclear-EGS system are assessed based on its combination with gas turbines.

At what base load level would the economic benefits of a grid be maximized? Or is it better not to deploy nuclear-EGS systems at all? To answer these critical questions, calculations were made in the following sequence shown in Fig.5-5.

155
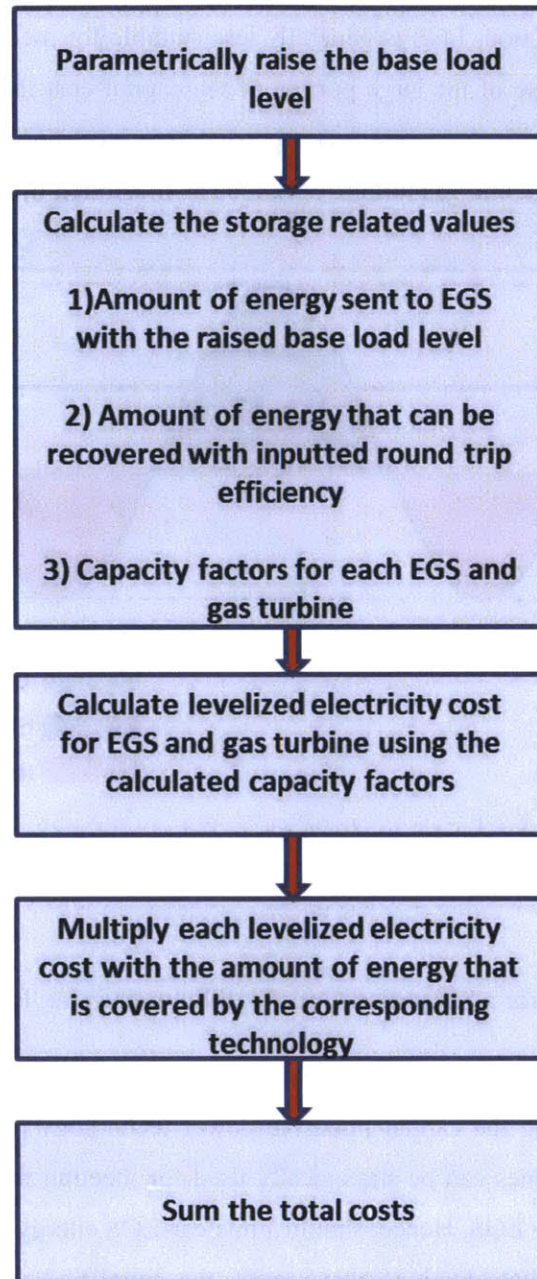
Fig.5-5 Calculation Procedure for the Total Costs for Different Base Load Levels

Storage requirements and capacity factors are evaluated for a raised base-load level. The levelized electricity cost is calculated using the obtained capacity factors and grid costs are obtained by multiplying each levelized electricity cost with the obtained storage requirements.

The New England ISO shown in Fig.5-2 is taken as a reference grid with the reference economic parameters shown in Table 5-1 except that the capacity factors may vary. A nuclear-EGS round trip efficiency of 0.46, which is obtained as the upper bound value of the reference nuclear-EGS system in Chapter 4, is used. Some important results are shown in Fig.5-6.

The base load of NE-ISO is 9900 MW(e). This is the starting point on the left for the various performance curves shown in Fig.5-6. Total cost to meet the required demand of the grid decreases upon the introduction of nuclear-EGS system. This is because cheap nuclear electricity is used to replace expensive peak power gas turbine electricity through storage. As the new base load level increases, the capacity factor of the EGS decreases because of its increasing use to meet higher peaking demand. The behavior continues until the new base load level reaches the minimum total cost point beyond which a marginal increase in base load leads to an increase in total cost. The minimum point exists because increasing levelized electricity cost of EGS due to a reduction in capacity factor with increasing base load level outweigh the benefits of increasing cheap nuclear. Base load electricity is not economically utilized because of excessive idle time of capital intensive geothermal power plants that are only used to meet peak load. This minimum point justifies the need for gas turbines in a grid which can serve the unique task of meeting extreme peak demand. If the system operates at its economic optimum point, it is possible that the NE grid can save about 2 billion dollars per year, which is a 14.3% reduction from its original cost. It is worth noting that the minimum point occurs actually quite distant from the original base load. This implies that the significant reduction in capacity factor of EGS takes place when the base load is significantly raised from its original base load because of the shape of the sinusoidal demand curve. The introduction of over approximately 5 GW(e) of additional nuclear base load capacity implies multiple EGS systems for an electricity grid size of NE-ISO.

The result for annual average electricity supply portfolio in Fig.5-6 shows the relative portion of each electricity provider. Nuclear is most benefited by the introduction of the storage system in terms of the grid dependence on the technology. With the raising nuclear base load, nuclear directly meets electricity demand that is otherwise covered by gas turbines as well as providing intermediate peak load through storage. The base load portion – nuclear– increases faster with increasing base load than EGS because of 1) the additional electricity demand that is directly met by nuclear and 2) the fact that EGS's electricity production is reduced by the factor of the round trip efficiency. For the same reason, gas turbines decrease faster than nuclear's increasing rate and such a difference is accommodate by nuclear. Results of the annual average electricity supply portfolio can be used to size each technology in the grid. The EGS electricity supply rate is a noticeable result as it provides the guideline for scaling geothermal power

157

plants. The result shows that no bigger than around 1 GW(e) of average geothermal electricity production capability is needed in the NE-ISO.

The storage size increases monotonically with the new base load level. 1 GW(e)-year of storage size is required for the economically optimum grid operation. In Chapter 4, the reference system design gives an uppermost storage size of 0.7 GW(e)-year. When limited by the average charging rate of 6000MW(th), the maximum individual site storage size reduces to 0.2GW(e). Although a grid and system design can deviate from the reference values, in general, a multiple number of storage sites are required to maximize the economic benefits of nuclear-EGS systems.
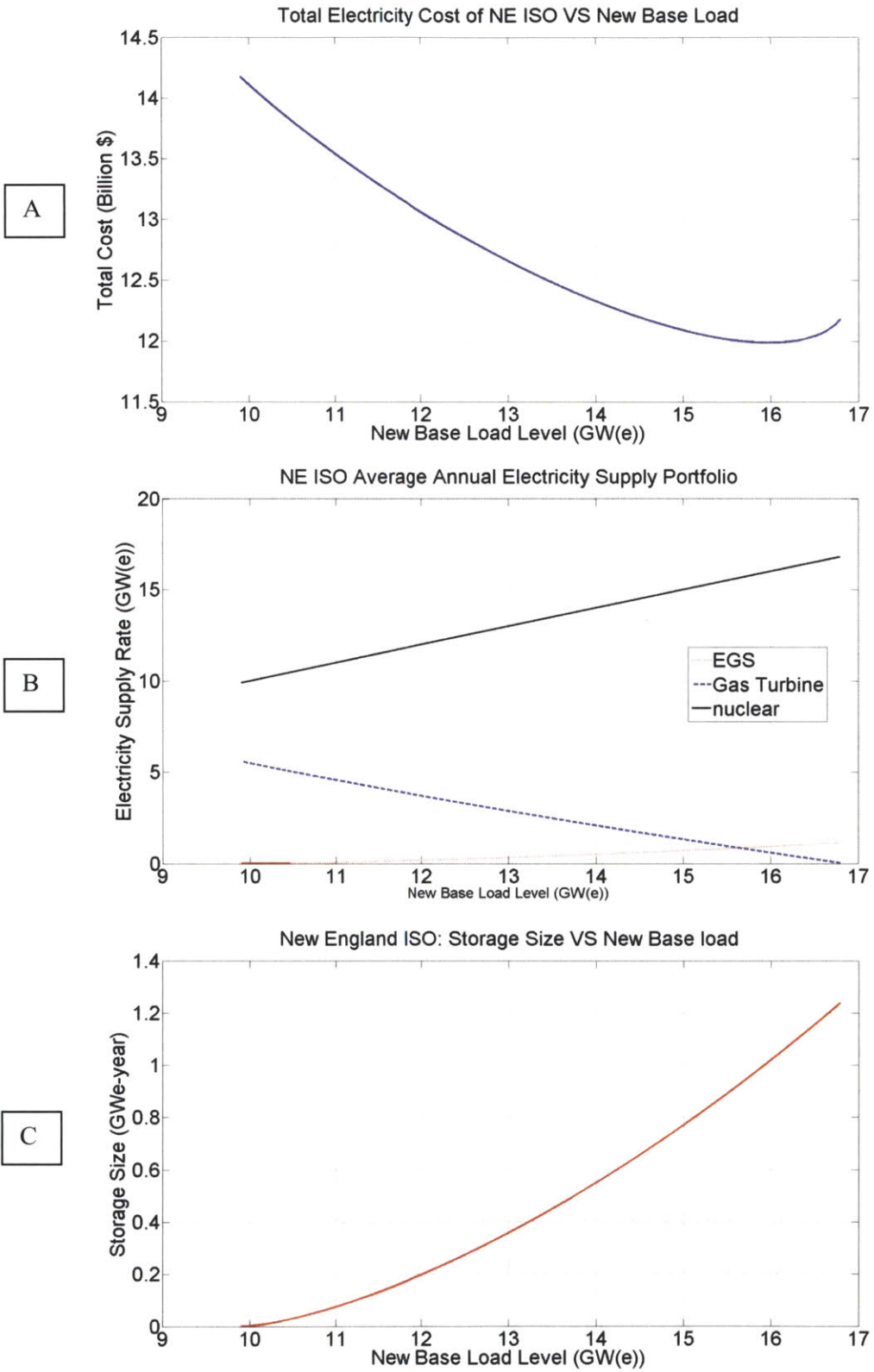
Fig.5-6 New England Grid Characteristics as a Function of New Base Load Level:
A-Total Electricity Cost, B-Annual Average Electricity Supply Portfolio, Electricity Storage Size

It is necessary to understand important factors that affect the economic benefits of nuclear-EGS systems. Key design parameters were parametrically changed to see their sensitivities on economic benefits. First, round trip efficiencies of 0.3, 0.46, and 0.7 were assessed. The round trip efficiency of 0.46 was obtained from the reference design in Chapter 4 in Table 4-2. Round trip efficiency is subject to changes with changes in geothermal efficiency and energy loss fraction. Should improvements of geothermal power plants be made followed by increasing size, the specific power output of geothermal power plants can significantly increase. As illustrated in Fig.5-7, however, changes in round trip efficiency would bring a noticeable difference only when the new base load is significantly raised, close to its maximum limit. Especially, for a limited degree of nuclear-EGS deployment in the grid, EGS provides only a small fraction of the electricity demand, which makes the round trip efficiency effects small. Another thing is that economic optimum points are pushed further from the original base load with decreasing round trip efficiency. This is because a system with lower round trip efficiency raises its base load higher as the stored thermal energy is utilized less effectively to provide peak power electricity; more thermal energy needs to be stored.

Besides round trip efficiency, cost components of the system are subject to changes upon improvements of technologies or economic situations. In this section, the most significant cost component of each technology is picked and tested with a reasonable envelope of possible variations. With the reference value (13.8 Cents/kWh(e)) being at center, the lower bound of 6.9 Cents/kWh(e) and the upper bound of 20.7 Cents/kWh(e) are used for this sensitivity study[36]. Equation 5.3 indicates that the levelized capital cost can be reduced through reducing the overnight plant cost. Such a reduction in the overnight plant cost can be possibly achieved as a result of scaling geothermal power plants to larger size. Figure B of 5-7 illustrates the result. Like the round trip efficiency case, changes in capital cost of EGS do not introduce significant differences for a limited deployment of nuclear-EGS systems in a grid. This is because EGS provides a small fraction of electricity at high capacity factor (hence, lower levelized electricity cost) in the total electricity demand for a small increase in the base load level. The difference, however, becomes evident near the economic optimum region because of the increasing importance of levelized cost of EGS in the overall grid cost. This is due to 1) increasing fraction of electricity from EGS and 2) low capacity factor of EGS that leads to a high levelized cost. One can read from Fig.5-7 that the importance of EGS round trip efficiency and capital cost are fairly comparable.

For gas turbine plants, natural gas cost is the cost component that is most subject to changes. Indeed, gas cost is more subject to transient changes than almost any other factor that affects the economics of a

---

[36] These levelized costs are the costs evaluated at the capacity factor of 0.16 for a fair comparison. The upper and lower bounds are ±50% of the reference cost.

nuclear-EGS system. Hence, understanding sensitivities of the economics of nuclear-EGS deployed in a grid with respect to changes in natural gas cost is not only worth understanding for the initial design of the system but also for the operational strategies of a grid as the grid will certainly experience changes in natural gas cost. With the reference value (7$/mmBTU) being at center, the lower bound of 5$/mmBTU and the upper bound of 9$/mmBTU are used for this sensitivity study. Fig.C of 5-7 illustrates the result. Opposite to the trend of EGS capital cost, the grid becomes less sensitive to changes in natural gas cost with increasing the base load level due to the diminishing natural gas portion associated with increasing the base load level. Such a fact implies that deployment of a nuclear-EGS system can also function to hedge any financial risks that come from natural gas cost fluctuations. In addition, if a grid operates below the economically optimum base load level for any reason, as charging rate limit, natural gas cost is a more important value to watch than either round trip efficiency or EGS plant cost. Last, it is worth noting that the total cost curve becomes flattened with decreasing natural gas cost. This means that the grid can operate at the cost close to its strictly minimum value even relatively distant from the optimum base load level. Such a characteristic implies flexibility of both grid portfolio optimization and design of electricity provision. Reduction in natural gas cost does introduce some auxiliary, yet important, benefits to a grid along with the grid cost reduction.

As mentioned previously in this section, nuclear is most benefited by the introduction of the storage system in terms of its increasing base load. Fig. D of 5-7 illustrates the sensitivity of changes in nuclear levelized electricity cost on the total grid cost. Nuclear cost significantly affects the grid cost as it provides the most electricity in the grid. The effect of changes in nuclear cost is by far the most significant as it determines the overall level of the grid cost. An important observation is that at the levelized nuclear cost of 10.5 cents/kWh(e), the grid cost curve is quite flat, implying that there are no strong economic incentives to deploy a nuclear-EGS system. This is because nuclear base load cost is high enough relative to natural gas peaking units that the economic incentive of replacing the peaking units with nuclear electricity is not significant. Hence, a careful watch should be made on the nuclear cost. Nuclear levelized electricity cost in reality, however, is less subject to cost fluctuations compared to natural gas cost.
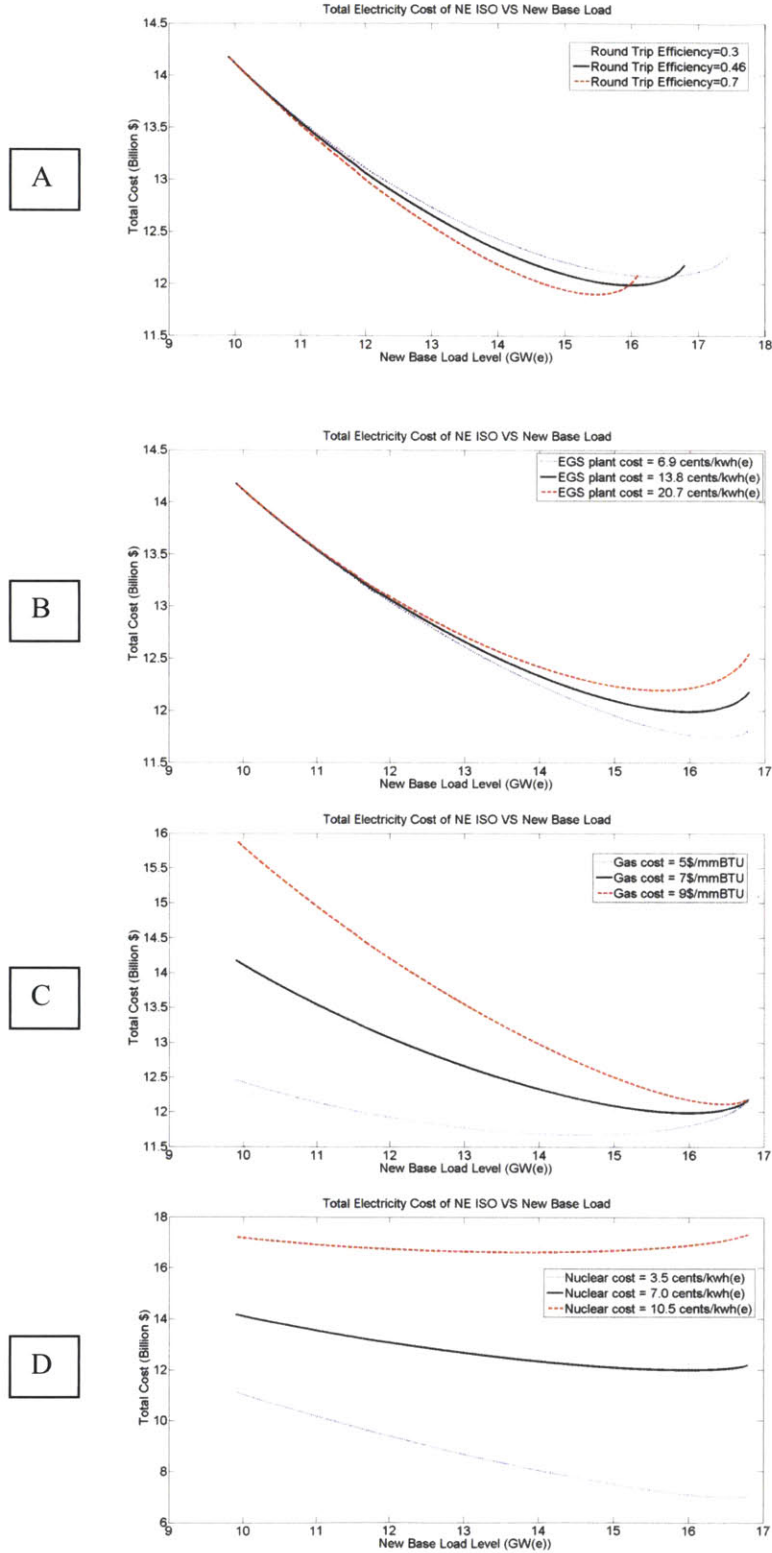
Fig.5-7 Sensitivity Studies of Economic Benefits of Nuclear-EGS System as a Function of:
A-Round Trip Efficiency, B-EGS Plant Cost, C-Gas Cost, D-Nuclear Cost

5.6 Conclusion

A grid that deploys a nuclear-EGS system will operate with three distinct electricity sectors: nuclear base load, EGS intermediate load, gas turbine peak power. The economic analysis of a nuclear-EGS system reveals (1) the fact that a grid (NE ISO, for example) can noticeably reduce (up to ~14% of the original cost) its electricity production cost by deploying nuclear-EGS storage systems (2) the importance of economics of nuclear technology for economics of a grid.

The importance of economic competitiveness of nuclear is in line with the function of the seasonal energy storage system – using energy of base load to provide peak load. Hence, economic competitiveness of nuclear technology is the key to the economic competitiveness of nuclear-EGS systems. Economics of geothermal power plants also matters, but it is evidently secondary to nuclear because it is a small portion of electricity supply. Nuclear cost, however, is likely to remain fairly unchanged. There are some other important factors that are more prone to fluctuations. Natural gas cost affects the economics of a nuclear-EGS deployed grid significantly. In addition to economic benefits to a grid, a reduction in natural gas cost introduces auxiliary gains such as flexibility in the grid portfolio optimization.

CHAPTER 6

Summary and Recommendations for Future Work

6.1 Summary of the Study

A wide range of technical options to fulfill the functional requirements of the nuclear geothermal system were addressed and the most promising options were identified, based on qualitative analyses. Table 6-1 summarizes the technical options and the chosen ones for further quantitative analyses.

As an essential prerequisite for the preliminary design study of nuclear-geothermal energy storage systems, models for the following list of pivotal design parameters and system performance metrics are established in Chapter 3.

- Thermal front velocity
- Storage size
- Cycle periods
- Conductive heat loss
- Pressure drop
- Water loss
- Geothermal power plant performance
- Operating conditions

Listed individual models are combined to identify a viable design space and to understand the nuclear-geothermal energy storage system in perspective through the comprehensive assessment of design trade-offs and sensitivity of performance metrics in Chapter 4.

In Chapter 4, engineering design studies were performed in the context of design maps and sensitivity studies. Table 6-2 summarizes the range of performance metrics of the reference design. It was found that the performance metrics of a nuclear-EGS energy storage system can be categorized into two different criteria: storage size and storage round trip efficiency. Table 6-3 summarizes the parameter space and

effectiveness of the design parameters for each performance criterion. Controlling reservoir volume is the most brute-force way of designing the system. However, it is not the omnipotent solution because it cannot simultaneously satisfy both storage size and round trip efficiency, and is likely to be limited spatially and economically. Reservoir permeability and geofluid temperature are found to be the most important design parameters that affect performance of nuclear-EGS storage systems.

Table 6-1 Summary of Technical Options for Nuclear Geothermal Energy Storage System

Technology	Options	Chosen Option	Constraint Imposed by the Chosen Option
Nuclear Power Plant	· LWRs – PWRs, BWRs · Advanced Reactors	LWRs-PWRs	Maximum geofluid temperature = 273°C
Geo-fluid	· Water · Steam · Carbon Dioxide	Water	Minimum Operating Pressure =5.7MPa
Nuclear-Reservoir Coupling	· Bypass flow line in the primary side of PWR · By pass flow line in the secondary side of PWR	By pass flow line in the primary side of PWR	Need for an intermediate heat exchanger(s)
Geothermal Power Plant	· Hydrothermal · Enhanced Geothermal (EGS)	Enhanced Geothermal (EGS)	Need for underground stimulation
Geothermal Power Cycle	· Flash Power Cycle · Binary Power Cycle	Binary Power Cycle	Efficiency
Geology	· Granite · Sandstone · Shale · Limestone	Sandstone	Rock properties Lithostatic pressure Permeability
Depth	· Ranges of possible depths	1km~1.5km	Adequate hydrostatic pressure; Known drilling cost
Underground Stimulation	· Hydraulic Fracture · Block Caving	Hydraulic Fracture	Maximum permeability of reservoir = 2Darcy

Table 6-2 Performance metrics of the reference nuclear-EGS energy storage systems

Representative Performance Metrics and design Parameters	Values	
	Unlimited charging rate	Limited charging rate 6000MWth
Reservoir Volume [km^3][37]	0.05 – 0.25	0.05 – 0.25
Minimum Reservoir Temperature [°C]	25-75°C	25-75°C
Thermal Storage Size [GW(th)-Year]	0.7 – 4.4	0.7 – 1.5
Electricity Storage Size [GW(e)-Year]	0.08-0.7	0.08- 0.2
Mass Flow Rate [kg/sec]	3.6E3 – 1.8E4	3.6E3-7.7E3
Charging Heat Rate [MW]	2.8E3-1.8E4	2.8E3-6.0E3
Average Pressure Drop [MPa]	4.1 - 19.5	4.1-9.3
Average Pumping Power [MW]	17.0 - 402.0	17.0-64.4
Fraction of Pumping Power [-]	0.006-0.023	0.006-0.01
Mass Flow Leakage Ratio [-]	0.03-0.05	0.03-0.04
Round Trip Efficiency [-]	0.33-0.46	0.34-0.46

---

[37] Reservoir volumes smaller than 0.05 km^3 are not regarded as design candidates because of small size of storage volume and excessive conductive heat loss fraction.

Table 6-3 Summary of design variation effects

	Design Parameters						
	Volume	Length/ Diameter	T_{hot}	Porosity	Permeability	Thermal capacity of Rock	Cycle Length
Storage Capacity Maximization	Increase (high)	N/A	Increase (high)	Increase (low)	N/A	Increase (mid)	N/A
Storage Round-trip Efficiency Maximization	Decrease[38] (high)	Decrease[39] (medium)	Increase (high)	N/A	Increase (high)	Decrease[40] (low)	Increase (medium)

*comments in parentheses represent the degree of effectiveness

* N/A indicates the design parameter has no appreciable influence

A grid that deploys nuclear-EGS systems will operate with three distinct electricity sectors: nuclear base load, EGS intermediate load, gas turbine peak power. The economic analysis of a nuclear-EGS system reveals 1) a grid (NE ISO, for example) can noticeably reduce (up to ~14% of the original cost) its electricity production cost by deploying nuclear-EGS storage system(s) 2) the importance of economics of nuclear technology for economics of a grid. EGS has higher capital costs but lower operating costs than gas turbines, thus the economics favors EGS use for intermediate demand and gas turbines for short duration peak demand. Economic competitiveness of nuclear technology is the key to the economic competitiveness of nuclear-EGS systems. Economics of geothermal power plants also matters, but it is evidently secondary to nuclear because of its small portion of electricity supply.

---

[38] Larger sizes imply higher pumping losses through the larger reservoir. However, there is also a minimum size to avoid excessive heat conduction losses

[39] Starting with L/D >>1

[40] A higher geo-fluid flow rate is needed for a larger storage capacity while the volume of the reservoir and the cycle length are assumed to be fixed. Higher flow rates increase pumping power and water-leakage faster than storage capacities.

6.2 Recommendations for Future Work

Follow on work is recommended in five areas

1. Improvement of Geothermal Power Plant

It is worth investigating augmentation of the size of conventional geothermal power plants (currently few tens of MW). Making the conventional geothermal power plant bigger is the key not only to the performance of the nuclear EGS system (through efficiency improvements) but also the economics of the system (economy of scale). Current geothermal power plants have low efficiencies, typically about 2/3 ~ 3/4 of a nuclear power plant for similar temperatures. There is no technical limit on the maximum geothermal power plant size as long as the reservoir size is big enough to support the discharging rate for a target time period. Hence, geothermal power plants for nuclear-EGS storage applications, freed from the natural reservoir size limit, can be made larger and potentially more efficient. The closest analogue to ta geothermal power plant are the multi-flash sea water distillation systems that produce fresh water from sea water. In those systems, the efficiency improves as plant capacity increases and the optimum number of stages increases. Similar effects may occur as geothermal plant size increases. Quantitative results for changes in geothermal power plant performance metrics, especially specific electric power output, can be fed into the system performance calculations in chapter.4.

2. Improvement of Reservoir Modeling

The cylindrical reservoir model characterized with a single porosity and permeability as used in this study is the simplest reservoir model that suffices for the analysis of the nuclear-EGS system. Although the general reservoir behavior discussed in this study still holds, detailed reservoir analysis and designs are subject to changes based on the use of different reservoir models. Researchers have conducted extensive studies on reservoir modeling taking into account well size, numbers, and detailed underground fracture geometries, etc. GEOCRACK is a code [17] that captures such parameters. As far as modeling reservoir geometry, various reservoir geometries (e.g rectangular) with a more detailed flow path can also be modeled. Among the number of possible improvements, it is recommended that the focus be primarily made on modeling well placement and detailed flow paths. It is important to note, however, that the benefit and cost of extensive reservoir modeling needs to be carefully assessed given the fact that the reservoir modeling is inherently limited in its exactness, and hence, applicability due to the empirical nature of underground conditions.

3. Improvement of Economic Studies

A more rigorous grid portfolio optimization can be performed with additional power providers (fossil fuels, renewables). In this study, the economic effect of the introduction of the nuclear-EGS system is studied in terms of the cost to a grid operator. Economic profitability of a utility that runs the nuclear-EGS system, with inclusion of more sophisticated grid management strategies, can be analyzed to make the economic study more comprehensive.

4. Water-Rock Chemistry and Structural Mechanics of Reservoir

Unlike the typical geothermal reservoir, storage reservoirs for nuclear-EGS storage application continuously experience extreme temperature fluctuations over their lifetime. The temperature fluctuations may change water-rock chemistry mechanisms and precipitation formation. Also, structural analysis primarily focusing on thermal fatigue of reservoir structure due to the temperature fluctuation is recommended.

5. Improved Methods of Reservoir Construction

The requirements for the EGS reservoir are different than any existing application. Our analysis used a traditional approach to create the reservoir based on geothermal technologies. There are however alternatives to create void spaces from cave-block mining to use of heavy oil fields after heavy oil extraction [16]. These are not options for a traditional geothermal plant but are options for a nuclear-EGS. There has been a very little examination of these options.

REFERENCES

[1] I. Oloyede and C. Forsberg, "Implications of Gigawatt-Year Electric Storage Systems on Future Baseload Nuclear Electricity Demand", International Congress on Advances in Nuclear Power Plants (ICAPP), 2010.

[2] Y. Lee and C. Forsberg, et al., "Options for Nuclear-Geothermal Gigawatt-Year Peak Electricity Storage Systems", International Congress on Advances in Nuclear Power Plants (ICAPP), 2010.

[3] C. Forsberg and D. Solis, "A Nuclear-Geothermal Heat Storage System for Daily, Weekly, and Seasonal Peak Electricity Production", American Nuclear Society Winter Meeting ;210302, 2009.

[4] American Physical Society (APS), "Challenges of Electricity Storage Technologies – A Report from the APS Panel on Public Affairs Committee on Energy and Environment", APS Panel on Public Affairs, 2007.

[5] U.S Energy Information Administration EIA, website, www.eia.doe.gov ,2010.

[6] J. W. TESTER et al., "The Future of Geothermal Energy", Massachusetts Institute of Technology, 2006.

[7] N. Todreas and M. Kazimi, "Nuclear Systems 1", Taylor & Francis, New York and London, 1990.

[8] H.C.H, Armstead and J.W. Tester, "Heat Mining", E. & F.N. Spon Ltd., London and New York, 1987.

[9] R. DiPippo, "Geothermal Power Plants: Principles, Applications and Case Studies", Elsevier Advanced Technology, Oxford, England 2005.

[10] Schlumberger,website, www.sbc.slb.com, 2010.

[11] Alternate forms of energy, http:// http://alternateformsofenergy.com, 2010.

[12] Y. Guéguen and V. Palciauskas, "Introduction to the Physics of Rocks", Princeton University Press, Princeton, New Jersey, 1994.

[13] Center for Environment, Commerce & Energy, Website, http://cenvironment.blogspot.com, 2010.

[14] Global INFOMINE, website, http://technology.infomine.com/reviews/Blockcaving/welcome.asp, 2010.

[15] INCROPERA et al., "Fundamentals of Heat and Mass Transfer", WILEY, New Jersey, 200.

[16] C Forsberg et al., "Nuclear Energy for Low-Carbon Heavy-Oil Recovery and Gigawatt-Year Heat Storage for Peak Electricity Production", Center for Advanced Nuclear Energy Systems, Department of Nuclear Science and Engineering, Massachusetts Institute of Technology, 2010.

[17] D. Swenson et al., "GEOCRACK", Department of Mechanical & Nuclear Engineering, Kansas State University, http://www.mne.ksu.edu/~geocrack/, 2010.

[18] G. Frosch et al., "Probing the Pore Space of Geothermal Reservoir Sandstones by Nuclear Magnetic Resonance", Geothermics, 29: 671-687, 2000

[19] FLUENT Inc, FLUENT manual, Lebanon New Hampshire, 2005.

[20] du Toit CG et al., "The Porous Structure of an Annular Pebble Bed Reactor", Final paper 9123, Tokyo, Japan: ICAPP; 2009. May 10–14, 2009.

[21] D. Winterbone, "Advanced Thermodynamics for Engineers", Arnold, London, Sydney and Auckland, 1997.

[23] G. Björnsson and G. Bodvarsson, "A Survey of Geothermal Reservoir Properties", Geothermics, 19:17-27, 1990

[24] J. Tester et al., "Sustainable Energy: Choosing among Options", The MIT Press, Cambridge Massachusetts, London, England, 2005.

[25] J. McVeigh et al., "Preliminary Technical Risk Analysis for the Geothermal Technologies Program", National Renewable Energy Laboratory (NREL), Technical Report NREL/TP-640-41156, 2007

[26]C. Kutscher, "The status and Future of Geothermal Electric Power", National Renewable Energy Laboratory (NREL), Presented at the American Solar Energy Society (ASES) Conference, 2000.

[27]Y. Du and J. Parsons, "Update on the Cost of Nuclear Power", Center for Energy and Environmental Policy Research (CEEPR), Massachusetts Institute of Technology, 2009.

[28] DOE/US Energy Information Administration Website, http://www.eia.doe.gov/, 2010

APPENDIX A: MATLAB Script for Engineering Map Calculations

```matlab
clear all;
close all;

Ref=50;
v=linspace(0.05*10^9,0.25*10^9,Ref);
T_Ref=linspace(25+273.15,75+273.15,Ref);
[X,Y] = meshgrid(v,T_Ref);

Ratio=4; %(L/R)
R=(X./(Ratio*pi)).^(1/3);
L=X./(pi.*R.^2);
T_hot=250+273.15;
porosity=0.15;
rho_rock=2600;
cp_rock=850;
K=1.9738*10^-12;
K_surr=0.01*K;
Area=pi.*R.^2;
depth=1500;

L_cycle=3*30*24*60*60;
cp_water_hot=2823.042+11.8307*T_hot-0.03506*T_hot^2+(3.602*10^-5)*T_hot^3;
cp_water_cold=2823.042+11.8307.*Y-0.03506.*Y.^2+(3.602*10^-5).*Y.^3;
rho_water_hot=741+1.9557*T_hot-0.0037*T_hot^2;
rho_water_cold=741+1.9557.*Y-0.0037.*Y.^2;
mu_water_hot=1205000*T_hot^-3.73045;
mu_water_cold=1205000.*Y.^-3.73045;
avg_mu_water=(mu_water_hot+mu_water_cold)./2;
avg_cp_water=(cp_water_cold+cp_water_hot)./2;
avg_rho_water=(rho_water_hot+rho_water_cold)./2;
m=((X.*(porosity.*avg_rho_water.*avg_cp_water+(1-
porosity)*rho_rock*cp_rock))./(avg_cp_water.*L_cycle));
Sp_turbine=123.5.*((1-(Y./523.15).^0.5)./0.214).*((523.15-Y)./200);
Turbine=(m.*Sp_turbine)./(10.^3); %MW

storage=X.*(1-porosity).*rho_rock.*cp_rock.*(T_hot-
Y)+X.*porosity.*avg_rho_water.*avg_cp_water.*(T_hot-Y);
contourf(X./10^9,Y-273.15,storage./(3.1536*10^16),100);
title('Thermal Storage Size (GW(th)-Year)');
ylabel('Minimum Reservoir Temperature(C)');
xlabel('Reservoir Volume, km^3');
colorbar;
grid on;
shading flat;

max_thermalstorage=max(max(storage./(3.1536*10^16)))
min_thermalstorage=min(max(storage./(3.1536*10^16)))

pressuredrop=(avg_mu_water.*m.*L)./(avg_rho_water.*Area.*K);
figure
contourf(X./10^9,Y-273.15,pressuredrop./10^6,100);
title('Pressure Drop (Mpa)');
ylabel('Minimum Reservoir Temperature(C)');
```

```matlab
xlabel('Reservoir Volume, km^3');
colorbar;
grid on;
shading flat;

max_avgpressuredrop=max(max(pressuredrop./10^6))
min_avgpressuredrop=min(max(pressuredrop./10^6))

figure
contourf(X./10^9,Y-273.15,m,100);
title('Mass Flow Rate');
ylabel('Minimum Reservoir Temperature(C)');
xlabel('Reservoir Volume, km^3');
colorbar;
grid on;
shading flat;

max_flowrate=max(max(m))
min_flowrate=min(min(m))

figure
pumpingpower=pressuredrop.*Area.*(m./(avg_rho_water.*Area));
contourf(X./10^9,Y-273.15,pumpingpower./10^6,100);
title('Average Pumping Power (MW)');
ylabel('Minimum Reservoir Temperature(C)');
xlabel('Reservoir Volume, km^3');
colorbar;
grid on;
shading flat;

max_avgpumpingpower=max(max(pumpingpower./10^6))
min_avgpumpingpower=min(min(pumpingpower./10^6))

figure
e_production=Turbine;%-(pumpingpower./10^6);%MW
contourf(X./10^9,Y-273.15,(e_production.*L_cycle)./(31536000.*10.^3),100);
title('Electricity Storage Size (GW(e)-Year)');
ylabel('Minimum Reservoir Temperature(C)');
xlabel('Reservoir Volume, km^3');
colorbar;
grid on;
shading flat;

max_avgpumpingpower=max(max((e_production.*L_cycle)./(31536000.*10.^3)))
min_avgpumpingpower=min(min((e_production.*L_cycle)./(31536000.*10.^3)))

figure
Max_pressuredrop=(mu_water_cold.*m.*L)./(rho_water_cold.*Area.*K);
Max_pumpingpower=Max_pressuredrop.*Area.*(m./(rho_water_cold.*Area));
contourf(X./10^9,Y-273.15,Max_pumpingpower./10^6,100);
title('Maximum Required Pumping Power');
ylabel('Minimum Reservoir Temperature(C)');
xlabel('Reservoir Volume, km^3');
colorbar;
grid on;
```

```matlab
shading flat;

max_maxpumpingpower=max(max(Max_pumpingpower./10^6))
min_maxpumpingpower=min(min(Max_pumpingpower./10^6))

m_pumpingpower=ones(Ref,Ref);

for u=1:Ref

    for o=1:Ref;

        if Max_pumpingpower(u,o)/10^6 > 400

            m_pumpingpower(u,o)=0;

        else

            m_pumpingpower(u,o)=1;

        end;


    end;

end;

figure
contourf(X./10^9,Y-273.15,m_pumpingpower,1);
title('Maximum Required Pumping Power');
ylabel('Minimum Reservoir Temperature(C)');
xlabel('Reservoir Volume, km^3');
grid on;
shading flat;

figure
chargingrate=storage./L_cycle;
contourf(X./10^9,Y-273.15,chargingrate./10^6,100);
title('Charging Heat Rate (MW(th))');
ylabel('Minimum Reservoir Temperature(C)');
xlabel('Reservoir Volume, km^3');
colorbar;
grid on;
shading flat;

max_chargingrate=max(max(chargingrate./10^6))
min_chargingrate=min(min(chargingrate./10^6))

L_chargingrate =ones(Ref,Ref);

for i=1:Ref

    for j=1:Ref;
```

```matlab
        if chargingrate(i,j)/10^6 > 6000

            L_chargingrate(i,j)=0;

        else

             L_chargingrate(i,j)=1;

        end;


    end;

end;


figure
contourf(X./10^9,Y-273.15,L_chargingrate,1);
title('Charging Heat Rate (MW(th))');
ylabel('Minimum Reservoir Temperature(C)');
xlabel('Reservoir Volume, km^3');
colorbar;
grid on;
shading flat;


figure;
leak_ratio=((avg_rho_water.*L)./(2.*depth.*avg_mu_water)).*((pi.*2.*R.*L)./(p
i.*R.^2)).*(K_surr/K).*((mu_water_cold./rho_water_cold)+(mu_water_hot./rho_wa
ter_hot));
contourf(X./10^9,Y-273.15,leak_ratio,100);
shading flat;
title('Mass Flow Rate Leakage Ratio');
ylabel('Minimum Reservoir Temperature(C)');
xlabel('Reservoir Volume, km^3');
colorbar;
grid on;
shading flat;
max_leakratio=max(max(leak_ratio))
min_leakratio=min(min(leak_ratio))


figure;
ratio=pumpingpower./chargingrate;
contourf(X./10^9,Y-273.15,ratio,100);
shading flat;
title('Fraction of Pumping Power (Pumping Power/Charging Heat Rate)');
ylabel('Minimum Reservoir Temperature(C)');
xlabel('Reservoir Volume, km^3');
colorbar;
grid on;
shading flat;

max_pumpingratio=max(max(ratio))
min_pumpingratio=min(min(ratio))
```

```matlab
figure;
Cycyle_eff1=((e_production.*L_cycle)./(31536000.*10.^3)).*(1-
leak_ratio)./((storage./(3.1536*10^16)).*0.333);
contourf(X./10^9,Y-273.15,Cycyle_eff1,100);
shading flat;
title('Round Trip Cycle Efficiency');
ylabel('Minimum Reservoir Temperature(C)');
xlabel('Reservoir Volume, km^3');
colorbar;
grid on;
shading flat;


figure;
Cycyle_eff2=(1-
leak_ratio).*((e_production.*L_cycle)./(31536000.*10.^3))./((storage./(3.1536
*10^16)).*0.333+(pumpingpower./10^6).*(L_cycle)./(31536000.*10.^3));
contourf(X./10^9,Y-273.15,Cycyle_eff2,100);
shading flat;
title('Round Trip Cycle Efficiency Parasatic Pumping(During Charging)
Considered');
ylabel('Minimum Reservoir Temperature(C)');
xlabel('Reservoir Volume, km^3');
colorbar;
grid on;
shading flat;

max_Roundtrip=max(max(Cycyle_eff2))
min_Roundtrip=min(min(Cycyle_eff2))
```

APPENDIX B: MATLAB Script for Design Parameter Sensitivity Tests

```matlab
clear all;
%close all;

Ref=50;
v=linspace(0.05*10^9,0.25*10^9,Ref);
T_Ref=linspace(25+273.15,75+273.15,Ref);
[X,Y] = meshgrid(v,T_Ref);

Ratio=4; %(L/R)
R=(X./(Ratio*pi)).^(1/3);
L=X./(pi.*R.^2);
T_hot=250+273.15;
porosity=0.15;
rho_rock=2600 ;
cp_rock=850;
Darcy=3.5;
K=(9.869*10^-13)*Darcy;
K_surr=(9.869*10^-13)*0.02;
Area=pi.*R.^2;
depth=1500;

L_cycle=3*30*24*60*60;%%%%%%%%%%%%%%%%%%%%%%%%%%%%
cp_water_hot=2823.042+11.8307*T_hot-0.03506*T_hot^2+(3.602*10^-5)*T_hot^3;
cp_water_cold=2823.042+11.8307.*Y-0.03506.*Y.^2+(3.602*10^-5).*Y.^3;
rho_water_hot=741+1.9557*T_hot-0.0037*T_hot^2;
rho_water_cold=741+1.9557.*Y-0.0037.*Y.^2;
mu_water_hot=1205000*T_hot^-3.73045;
mu_water_cold=1205000.*Y.^-3.73045;
avg_mu_water=(mu_water_hot+mu_water_cold)./2;
avg_cp_water=(cp_water_cold+cp_water_hot)./2;
avg_rho_water=(rho_water_hot+rho_water_cold)./2;
m=((X.*(porosity.*avg_rho_water.*avg_cp_water+(1-
porosity)*rho_rock*cp_rock))./(avg_cp_water.*L_cycle));
Sp_turbine=123.5.*((1-(Y./T_hot).^0.5)./0.214).*((T_hot-Y)./200);
Turbine=(m.*Sp_turbine)./(10.^3); %MW

figure(1)
storage=X.*(1-porosity).*rho_rock.*cp_rock.*(T_hot-
Y)+X.*porosity.*avg_rho_water.*avg_cp_water.*(T_hot-Y);
plot(v./10^9,storage(25,1:50)/(3.1536*10^16),'m-->','LineWidth',2.5);%%%%%%%
ylabel('\fontsize{25}Thermal Storage Size, GW(th)-Year');
xlabel('\fontsize{25}Reservoir Volume, km^3');
grid on;
title('\fontsize{25} {Thermal Storage Size [GW(th)-Year]}');
%Legend('\fontsize{25}
L/R=1','L/R=2.5','L/R=4','L/R=5.5','L/R=7','location','best');%%%%%
%Legend('\fontsize{25}
T_h_o_t=220\circC','T_h_o_t=235\circC','T_h_o_t=250\circC','T_h_o_t=265\circC
','T_h_o_t=280\circC','location','best')
%Legend('Porosity=0.05','Porosity=0.1','Porosity=0.15','Porosity=0.20','Poros
ity=0.25','location','best');
%Legend('Permeability=0.5D','Permeability=1.25D','Permeability=2D','Permeabil
ity=2.75D','Permeability=3.5D','location','best');
```

```matlab
Legend('Cycle Period=2months','Cycle Period=4months','Cycle
Period=6months','Cycle Period=8months','Cycle
Period=10months','location','best');
%Legend('(\rhoC_p)_r_o_c_k=1.11MJ/m^3\circC','(\rhoC_p)_r_o_c_k=1.66MJ/m^3\ci
rcC','(\rhoC_p)_r_o_c_k=2.21MJ/m^3\circC','(\rhoC_p)_r_o_c_k=2.76MJ/m^3\circC
','(\rhoC_p)_r_o_c_k=3.32MJ/m^3\circC','location','best');
set(gca,'FontSize',25);

figure(2);
pressuredrop=(avg_mu_water.*m.*L)./(avg_rho_water.*Area.*K);
plot(v./10^9,pressuredrop(25,1:50)/(10^6),'m--> ','LineWidth',2.5);
ylabel('\fontsize{25} Pressure Drop, MPa');
xlabel('\fontsize{25}Reservoir Volume, km^3');
grid on;
title('\fontsize{25} {Average Pressure Drop [MPa]}');
%Legend('L/R=1','L/R=2.5','L/R=4','L/R=5.5','L/R=7','location','best');
%Legend('\fontsize{25}
T_h_o_t=220\circC','T_h_o_t=235\circC','T_h_o_t=250\circC','T_h_o_t=265\circC
','T_h_o_t=280\circC','location','best')
%Legend('Porosity=0.05','Porosity=0.1','Porosity=0.15','Porosity=0.20','Poros
ity=0.25','location','best');
%Legend('Permeability=0.5D','Permeability=1.25D','Permeability=2D','Permeabil
ity=2.75D','Permeability=3.5D','location','best');
Legend('Cycle Period=2months','Cycle Period=4months','Cycle
Period=6months','Cycle Period=8months','Cycle
Period=10months','location','best');
%Legend('(\rhoC_p)_r_o_c_k=1.11MJ/m^3\circC','(\rhoC_p)_r_o_c_k=1.66MJ/m^3\ci
rcC','(\rhoC_p)_r_o_c_k=2.21MJ/m^3\circC','(\rhoC_p)_r_o_c_k=2.76MJ/m^3\circC
','(\rhoC_p)_r_o_c_k=3.32MJ/m^3\circC','location','best');
set(gca,'FontSize',25);

figure(3)
plot(v./10^9,m(25,1:50),'m--> ','LineWidth',2.5);
ylabel('\fontsize{25}Mass Flow Rate, kg/sec');
xlabel('\fontsize{25}Reservoir Volume, km^3');
grid on;
title('\fontsize{25} {Required Mass Flow Rate[kg/sec]}');
%Legend('L/R=1','L/R=2.5','L/R=4','L/R=5.5','L/R=7','location','best');
%Legend('\fontsize{25}
T_h_o_t=220\circC','T_h_o_t=235\circC','T_h_o_t=250\circC','T_h_o_t=265\circC
','T_h_o_t=280\circC','location','best')
%Legend('Porosity=0.05','Porosity=0.1','Porosity=0.15','Porosity=0.20','Poros
ity=0.25','location','best');
%Legend('Permeability=0.5D','Permeability=1.25D','Permeability=2D','Permeabil
ity=2.75D','Permeability=3.5D','location','best');
%Legend('Cycle Period=2months','Cycle Period=4months','Cycle
Period=6months','Cycle Period=8months','Cycle
Period=10months','location','best');
%Legend('(\rhoC_p)_r_o_c_k=1.11MJ/m^3\circC','(\rhoC_p)_r_o_c_k=1.66MJ/m^3\ci
rcC','(\rhoC_p)_r_o_c_k=2.21MJ/m^3\circC','(\rhoC_p)_r_o_c_k=2.76MJ/m^3\circC
','(\rhoC_p)_r_o_c_k=3.32MJ/m^3\circC','location','best');
set(gca,'FontSize',25);

figure(4)
pumpingpower=pressuredrop.*Area.*(m./(avg_rho_water.*Area));
plot(v./10^9,pumpingpower(25,1:50)/10^6,'m--> ','LineWidth',2.5);
```

```matlab
ylabel('\fontsize{25}Pumping Power, MW');
xlabel('\fontsize{25}Reservoir Volume, km^3');
grid on;
title('\fontsize{25} Average Pumping Power [MW]');
%Legend('L/R=1','L/R=2.5','L/R=4','L/R=5.5','L/R=7','location','best');
%Legend('\fontsize{25}
T_h_o_t=220\circC','T_h_o_t=235\circC','T_h_o_t=250\circC','T_h_o_t=265\circC
','T_h_o_t=280\circC','location','best')
%Legend('Porosity=0.05','Porosity=0.1','Porosity=0.15','Porosity=0.20','Poros
ity=0.25','location','best');
%Legend('Permeability=0.5D','Permeability=1.25D','Permeability=2D','Permeabil
ity=2.75D','Permeability=3.5D','location','best');
%Legend('Cycle Period=2months','Cycle Period=4months','Cycle
Period=6months','Cycle Period=8months','Cycle
Period=10months','location','best');
%Legend('(\rhoC_p)_r_o_c_k=1.11MJ/m^3\circC','(\rhoC_p)_r_o_c_k=1.66MJ/m^3\ci
rcC','(\rhoC_p)_r_o_c_k=2.21MJ/m^3\circC','(\rhoC_p)_r_o_c_k=2.76MJ/m^3\circC
','(\rhoC_p)_r_o_c_k=3.32MJ/m^3\circC','location','best');
set(gca,'FontSize',25);


figure(5)
e_production=Turbine;%-(pumpingpower./10^6);%MW
plot(v./10^9,e_production(25,1:50)*L_cycle/(31536000*10^3),'m-->
','LineWidth',2.5);
ylabel('\fontsize{25} Storage Size, GW(e)-Year');
xlabel('\fontsize{25}Reservoir Volume, km^3');
grid on;
title('\fontsize{25} {Electricity Storage Size (GW(e)-Year)}');
%Legend('L/R=1','L/R=2.5','L/R=4','L/R=5.5','L/R=7','location','best');
%Legend('\fontsize{25}
T_h_o_t=220\circC','T_h_o_t=235\circC','T_h_o_t=250\circC','T_h_o_t=265\circC
','T_h_o_t=280\circC','location','best')
%Legend('Porosity=0.05','Porosity=0.1','Porosity=0.15','Porosity=0.20','Poros
ity=0.25','location','best');
%Legend('Permeability=0.5D','Permeability=1.25D','Permeability=2D','Permeabil
ity=2.75D','Permeability=3.5D','location','best');
%Legend('Cycle Period=2months','Cycle Period=4months','Cycle
Period=6months','Cycle Period=8months','Cycle
Period=10months','location','best');
Legend('(\rhoC_p)_r_o_c_k=1.11MJ/m^3\circC','(\rhoC_p)_r_o_c_k=1.66MJ/m^3\cir
cC','(\rhoC_p)_r_o_c_k=2.21MJ/m^3\circC','(\rhoC_p)_r_o_c_k=2.76MJ/m^3\circC'
,'(\rhoC_p)_r_o_c_k=3.32MJ/m^3\circC','location','best');
set(gca,'FontSize',25);


figure(6)
Max_pressuredrop=(mu_water_cold.*m.*L)./(rho_water_cold.*Area.*K);
Max_pumpingpower=Max_pressuredrop.*Area.*(m./(rho_water_cold.*Area));
plot(v./10^9,Max_pumpingpower(25,1:50)/10^6,'m--> ','LineWidth',2.5);
ylabel('\fontsize{25} Pumping Power, MPa');
xlabel('\fontsize{25}Reservoir Volume, km^3');
grid on;
title('\fontsize{25} {Maximum Required Pumping Power [MPa]}');
%Legend('L/R=1','L/R=2.5','L/R=4','L/R=5.5','L/R=7','location','best');
%Legend('\fontsize{25}
T_h_o_t=220\circC','T_h_o_t=235\circC','T_h_o_t=250\circC','T_h_o_t=265\circC
','T_h_o_t=280\circC','location','best')
```

```matlab
%Legend('Porosity=0.05','Porosity=0.1','Porosity=0.15','Porosity=0.20','Poros
ity=0.25','location','best');
%Legend('Permeability=0.5D','Permeability=1.25D','Permeability=2D','Permeabil
ity=2.75D','Permeability=3.5D','location','best');
%Legend('Cycle Period=2months','Cycle Period=4months','Cycle
Period=6months','Cycle Period=8months','Cycle
Period=10months','location','best');
%Legend('(\rhoC_p)_r_o_c_k=1.11MJ/m^3\circC','(\rhoC_p)_r_o_c_k=1.66MJ/m^3\ci
rcC','(\rhoC_p)_r_o_c_k=2.21MJ/m^3\circC','(\rhoC_p)_r_o_c_k=2.76MJ/m^3\circC
','(\rhoC_p)_r_o_c_k=3.32MJ/m^3\circC','location','best');
set(gca,'FontSize',25);

figure(7)
chargingrate=storage./L_cycle;
plot(v./10^9,chargingrate(25,1:50)/10^6,'m--> ','LineWidth',2.5);
ylabel('\fontsize{25} Charging Heat Rate, MW(th)');
xlabel('\fontsize{25}Reservoir Volume, km^3');
grid on;
title('\fontsize{25} {Required Average Charging Heat Rate [MW(th)]}');
%Legend('L/R=1','L/R=2.5','L/R=4','L/R=5.5','L/R=7','location','best');
%Legend('\fontsize{25}
T_h_o_t=220\circC','T_h_o_t=235\circC','T_h_o_t=250\circC','T_h_o_t=265\circC
','T_h_o_t=280\circC','location','best')
%Legend('Porosity=0.05','Porosity=0.1','Porosity=0.15','Porosity=0.20','Poros
ity=0.25','location','best');
%Legend('Permeability=0.5D','Permeability=1.25D','Permeability=2D','Permeabil
ity=2.75D','Permeability=3.5D','location','best');
%Legend('Cycle Period=2months','Cycle Period=4months','Cycle
Period=6months','Cycle Period=8months','Cycle
Period=10months','location','best');
%Legend('(\rhoC_p)_r_o_c_k=1.11MJ/m^3\circC','(\rhoC_p)_r_o_c_k=1.66MJ/m^3\ci
rcC','(\rhoC_p)_r_o_c_k=2.21MJ/m^3\circC','(\rhoC_p)_r_o_c_k=2.76MJ/m^3\circC
','(\rhoC_p)_r_o_c_k=3.32MJ/m^3\circC','location','best');
set(gca,'FontSize',25);

figure(8)
leak_ratio=((avg_rho_water.*L)./(2.*depth.*avg_mu_water)).*((pi.*2.*R.*L)./(p
i.*R.^2)).*(K_surr/K).*((mu_water_cold./rho_water_cold)+(mu_water_hot./rho_wa
ter_hot));
plot(v./10^9,leak_ratio(25,1:50),'m--> ','LineWidth',2.5);
ylabel('\fontsize{25} Leakage Ratio, -');
xlabel('\fontsize{25}Reservoir Volume, km^3');
grid on;
title('\fontsize{25} {Mass Flow Rate Leakage Ratio [-]}');
%Legend('L/R=1','L/R=2.5','L/R=4','L/R=5.5','L/R=7','location','best');
%Legend('\fontsize{25}
T_h_o_t=220\circC','T_h_o_t=235\circC','T_h_o_t=250\circC','T_h_o_t=265\circC
','T_h_o_t=280\circC','location','best')
%Legend('Porosity=0.05','Porosity=0.1','Porosity=0.15','Porosity=0.20','Poros
ity=0.25','location','best');
Legend('Permeability=0.5D','Permeability=1.25D','Permeability=2D','Permeabili
ty=2.75D','Permeability=3.5D','location','best');
%Legend('Cycle Period=2months','Cycle Period=4months','Cycle
Period=6months','Cycle Period=8months','Cycle
Period=10months','location','best');
```

```matlab
%Legend('(\rhoC_p)_r_o_c_k=1.11MJ/m^3\circC','(\rhoC_p)_r_o_c_k=1.66MJ/m^3\ci
rcC','(\rhoC_p)_r_o_c_k=2.21MJ/m^3\circC','(\rhoC_p)_r_o_c_k=2.76MJ/m^3\circC
','(\rhoC_p)_r_o_c_k=3.32MJ/m^3\circC','location','best');
set(gca,'FontSize',25);


figure(9)
ratio=pumpingpower./chargingrate;
plot(v./10^9,ratio(25,1:50),'m--> ','LineWidth',2.5);
ylabel('\fontsize{25} Fraction of Pumping Power, -');
xlabel('\fontsize{25}Reservoir Volume, km^3');
grid on;
title('\fontsize{25} {Fraction of Pumping Power [-]}');
%Legend('L/R=1','L/R=2.5','L/R=4','L/R=5.5','L/R=7','location','best');
%Legend('\fontsize{25}
T_h_o_t=220\circC','T_h_o_t=235\circC','T_h_o_t=250\circC','T_h_o_t=265\circC
','T_h_o_t=280\circC','location','best')
%Legend('Porosity=0.05','Porosity=0.1','Porosity=0.15','Porosity=0.20','Poros
ity=0.25','location','best');
%Legend('Permeability=0.5D','Permeability=1.25D','Permeability=2D','Permeabil
ity=2.75D','Permeability=3.5D','location','best');
%Legend('Cycle Period=2months','Cycle Period=4months','Cycle
Period=6months','Cycle Period=8months','Cycle
Period=10months','location','best');
%Legend('(\rhoC_p)_r_o_c_k=1.11MJ/m^3\circC','(\rhoC_p)_r_o_c_k=1.66MJ/m^3\ci
rcC','(\rhoC_p)_r_o_c_k=2.21MJ/m^3\circC','(\rhoC_p)_r_o_c_k=2.76MJ/m^3\circC
','(\rhoC_p)_r_o_c_k=3.32MJ/m^3\circC','location','best');
set(gca,'FontSize',25);


figure(10)
Cycyle_eff2=(1-
leak_ratio).*((e_production.*L_cycle)./(31536000.*10.^3))./((storage./(3.1536
*10^16)).*0.333+(pumpingpower./10^6).*(L_cycle)./(31536000.*10.^3));
plot(v./10^9,Cycyle_eff2(25,1:50),'m--> ','LineWidth',2.5);
ylabel('\fontsize{25} Round Trip Cycle Efficiency, -');
xlabel('\fontsize{25}Reservoir Volume, km^3');
grid on;
title('\fontsize{25} {Round Trip Cycle Efficiency of Storage System [-]}');
%Legend('L/R=1','L/R=2.5','L/R=4','L/R=5.5','L/R=7','location','best');
%Legend('\fontsize{25}
T_h_o_t=220\circC','T_h_o_t=235\circC','T_h_o_t=250\circC','T_h_o_t=265\circC
','T_h_o_t=280\circC','location','best')
%Legend('Porosity=0.05','Porosity=0.1','Porosity=0.15','Porosity=0.20','Poros
ity=0.25','location','best');
Legend('Permeability=0.5D','Permeability=1.25D','Permeability=2D','Permeabili
ty=2.75D','Permeability=3.5D','location','best');
%Legend('Cycle Period=2months','Cycle Period=4months','Cycle
Period=6months','Cycle Period=8months','Cycle
Period=10months','location','best');
%Legend('(\rhoC_p)_r_o_c_k=1.11MJ/m^3\circC','(\rhoC_p)_r_o_c_k=1.66MJ/m^3\ci
rcC','(\rhoC_p)_r_o_c_k=2.21MJ/m^3\circC','(\rhoC_p)_r_o_c_k=2.76MJ/m^3\circC
','(\rhoC_p)_r_o_c_k=3.32MJ/m^3\circC','location','best');
set(gca,'FontSize',25);
```

APPENDIX C: MATLAB Script for Economic Benefit Calculations for NE-ISO

```matlab
clear all;

% Constants

%EGS Cost
EGS_Capital=13.8;%for 0.16
EGS_OM=11.4;%for 0.16
EGS_Drilling=7.7;%for 0.16

%Natural Gas Cost
GAS_Capital=3.7; %for 0.38
GAS_OM=0.76; %for 0.38
Carbon_Tax=0.9;
%GAS_Fuel=10.49; %6$/mmBTU
%GAS_Fuel=15.74; %9$/mmBTU
GAS_Fuel=12.24; %7$/mmBTU
%GAS_Fuel=8.74; %5$/mmBTU

%Nuclear Cost
Nu_C=7;

%Cosine Curve
P_0=15500;
%P_n=10000:2:15000;

A=5600;

eff=0.46; %set g=6900
%eff=0.7; %set g=6200
%eff=0.3; %set g=7600

g=6900;

for i=1:g

    P_n=9900+i*0.999;

    P_n_data(i)=P_n;

    Peak_nuclear=P_n_data-(P_0-A);

    % Step 1
    t_1=(acos((P_n-P_0)/A))/(4*pi);


    %Step 2
    t_2=0.5-t_1;

    %Step 3
```

```matlab
    S_area(i)=P_n*(t_2-t_1)-P_0*(t_2-t_1)-(A/(4*pi))*(sin(4*pi*t_2)-
sin(4*pi*t_1));


    %Step 4

    P_EGS=linspace(P_n,P_0+A,10000);
    t_1_star=(acos((P_EGS-P_0)./A))./(4.*pi);
    t_2_star=0.5-t_1_star;
    temp=P_EGS.*(t_2_star-t_1_star)-P_n.*(t_2-t_1)+P_0.*(t_2-
t_1)+(A./(4.*pi)).*(sin(4.*pi.*t_2)-sin(4.*pi.*t_1))-(P_0.*(t_2_star-
t_1_star)+(A./(4.*pi)).*(sin(4.*pi.*t_2_star)-sin(4.*pi.*t_1_star)));
    temp_1=eff*S_area(i)-((P_EGS-P_n).*0.5-temp);

    j=1;

    while temp_1(j)>0

        data(i)=P_EGS(j);
        data_2(i)=t_1_star(j);
        j=j+1;



    end;

    Peak_EGS=data-P_n_data;
    Peak_GAS=(P_0+A)-data;
end;

Portion_GAS=4*(P_0.*data_2+(A./(4.*pi)).*sin(4.*pi.*data_2)-data.*data_2);




%Step 5

Capacity_EGS=(2.*S_area.*eff)./(data-P_n_data);

%Step 6

numerator=4.*(P_0.*data_2-data.*data_2+(A./(4.*pi)).*sin(4.*pi.*data_2));

denominator=(P_0+A)-data;

Capacity_GAS=numerator./denominator;


%step 7

L_C_EGS=(EGS_Capital+EGS_OM+EGS_Drilling).*(0.16./Capacity_EGS);
```

```matlab
L_C_GAS=((GAS_Capital+GAS_OM).*(0.38./Capacity_GAS))+Carbon_Tax+GAS_Fuel;

Total=Nu_C.*P_n_data+2.*S_area.*eff.*L_C_EGS+L_C_GAS.*numerator;

minimum=0;
f=1;

while Total(f)>Total(f+1)

    minimum=f+1;

    f=f+1;

end;

ratio=Peak_nuclear./Peak_EGS;
ratio2=Peak_EGS./Peak_GAS;
ratio3=(S_area*2)./Portion_GAS;

storage_size=S_area./10^3;

%subplot(3,1,1);
plot((P_n_data)./(10^3),(Total.*365.*24.*10^3)./(100*10^9),'k','LineWidth',3);
title('\fontsize{24} Total Electricity Cost of NE ISO VS New Base Load');
xlabel('\fontsize{24} New Base Load Level (GW(e))');
ylabel('\fontsize{24} Total Cost (Billion $)' );
grid on;
%Legend('Round Trip Efficiency=0.3','Round Trip Efficiency=0.46','Round Trip
Efficiency=0.7','location','best');
%Legend('Gas cost = 5$/mmBTU','Gas cost = 7$/mmBTU','Gas cost =
9$/mmBTU','location','best');
%Legend('Nuclear cost = 3.5 cents/kwh(e)','Nuclear cost = 7.0
cents/kwh(e)','Nuclear cost = 10.5 cents/kwh(e)','best');
Legend('EGS plant cost = 6.9 cents/kwh(e)','Nuclear cost = 13.8
cents/kwh(e)','Nuclear cost = 20.7 cents/kwh(e)','best');
set(gca,'FontSize',24);

%subplot(3,1,2)
%plot(P_n_data./(10^3),(eff.*S_area*2)./(10^3),'r','lineWidth',2);
%hold;
%plot(P_n_data./(10^3),Portion_GAS./(10^3),'b','lineWidth',2);
plot(P_n_data./10^3,P_n_data./10^3,'k','lineWidth',2);
title('Annual Electricity Supply by EGS and Gas-Turbine');
xlabel('New Base Load Level (GW(e))');
ylabel('Electricity Supply (GW(e))' );
legend('EGS','Gas Turbine','nuclear');

%subplot(3,1,3)
%plot(P_n_data./(10^3),S_area./10^3);
%title('New England ISO: Storage Size VS New Base load');
%xlabel('New Base Load Level (GW(e))');
%ylabel('Storage Size (GWe-year)');
```